TECHNISCHE UNIVERSITÄT MÜNCHEN

Wissenschaftszentrum Weihenstephan für Ernährung, Landnutzung und Umwelt

Lehrstuhl für Siedlungswasserwirtschaft

Insights into anaerobic degradation of benzene and naphthalene

Xiyang Dong

Vollständiger Abdruck der von der Fakultät Wissenschaftszentrum Weihenstephan für Ernährung, Landnutzung und Umwelt der Technischen Universität München zur Erlangung des akademischen Grades eines Doktors der Naturwissenschaften genehmigten Dissertation.

Vorsitzende(r):	Prof. Dr. Wolfgang Liebl
Prüfer der Dissertation:	1. Priv.-Doz. Dr. Tillmann Lueders
	2. Prof. Dr. Siegfried Scherer
	3. Prof. Dr. Rainer Meckenstock

Die Dissertation wurde am 03.07.2017 bei der Technischen Universität München eingereicht und durch die Fakultät Wissenschaftszentrum Weihenstephan für Ernährung, Landnutzung und Umwelt am 18.08.2017 angenommen.

天道酬勤

God rewards those who work hard

Abstract

Aromatic hydrocarbons, e.g. benzene and naphthalene, have toxic, mutagenic and/or carcinogenic properties. Fortunately, these compounds can be degraded in environmental systems by indigenous microorganisms. Especially under anaerobic conditions, the physiology and ecology of the microbes involved are still poorly understood. In this thesis, important knowledge gaps are addressed in this field using microbiological approaches combined with “omics tools” (metagenomics and metaproteomics). A novel “reverse stable isotope labelling” approach is also introduced to investigate biodegradation activities.

Firstly, the enrichment culture BPL was studied, which can degrade benzene coupled with sulfate reduction. It is dominated by an organism of the genus *Pelotomaculum*. Members of this genus are usually known to be fermenters, undergoing syntrophy with anaerobic respiring microorganisms or methanogens. It remains unclear if *Pelotomaculum* identified here (namely, *Pelotomaculum* candidate BPL) could perform both benzene degradation and sulfate reduction. By using a metagenomic approach, a high-quality genome was reconstructed for it. Interestingly, the genome has all the genes for a complete sulfate reduction, similar as in other Gram-positive sulfate-reducing bacteria. The proteome analysis revealed that the essential enzymes for sulfate reduction were all expressed during growth with benzene. The proteogenomic data also suggested: (1) anaerobic benzene degradation was activated by a yet unknown mechanism for conversion of benzene to benzoyl-CoA; (2) the central benzoyl-CoA degradation pathway involved reductive dearomatization by a class II benzoyl-CoA reductase followed by hydrolytic ring cleavage and modified β-oxidation; (3) the oxidative acetyl-CoA pathway was utilized for complete oxidation to CO_2. All these data indicate that, besides its potential to anaerobically degrade benzene, *Pelotomaculum* candidate BPL is the first member of the genus that can perform sulfate reduction.

Secondly, the functional role of environmental Spirochaetes was investigated. Such microbes are frequently detected in anaerobic hydrocarbon- and

organohalide-contaminated environments, but their function remains unclear. For insights into their roles in such systems, a sulfate-reducing, naphthalene-degrading enrichment culture was taken as an example. It comprises sulfate-reducing *Deltaproteobacteria* and the spirochaete *Rectinema cohabitans*. Genome sequencing and proteome analysis suggested that the Spirochaete is an obligate fermenter that catabolizes proteins and carbohydrates resulting in acetate, ethanol, and hydrogen production. Physiological experiments showed that H_2 derived from fermentation by *R. cohabitans* was used as reductant for sulfate respiration by the *Deltaproteobacteria*. Differential proteomics and physiological experiments revealed that *R. cohabitans* in turn utilizes biomass (proteins and carbohydrates) released from cell lysis. Further comparative genome analyses indicated that *Rectinema* species are widespread in contaminated environments and adapted to a hydrogenogenic fermentative lifestyle similar to *R. cohabitans*. Together, this indicates that environmental Spirochaetes thrive in highly toxic contaminated habitats by scavenging detrital biomass concomitant with production of hydrogen. The reductants produced can in turn fuel biomass formation by other hydrogenotrophic microorganisms in the ecosystem. Thus, environmental Spirochaetes might constitute a critical component of a microbial loop central to nutrient cycling in subsurface environments.

Finally, a sensitive approach to monitor biodegradation was introduced using reverse stable isotope labelling (RIL) via dissolved inorganic carbon (DIC). Microbial mineralization of organic compounds in laboratory microcosms is preferably assessed by adding ^{14}C or ^{13}C-labelled substrates and following the release of labelled CO_2. Labelled compounds, however, are usually expensive or not commercially available. The biodegradation assay used here contains unlabeled organic contaminants and ^{13}C-labelled DIC with ^{13}C atom fractions ($x(^{13}C)_{DIC}$) clearly above natural abundance (typically 2-50%). The CO_2 produced during incubation ($x(^{13}C) \approx 1.11\%$) gradually dilutes the initial $x(^{13}C)_{DIC}$ allowing to quantify microbial mineralization using mass-balance calculations. For ^{13}C-enriched CO_2 samples, a newly-developed Isotope Ratio Mid-Infrared Spectrometer was shown to have a precision of $x(^{13}C) < 0.006\%$. As proof-of-principle, measured CO_2 production was close to the theoretical stoichiometry for anaerobic naphthalene degradation in a sulfate-reducing enrichment culture.

Furthermore, the method was used to measure aerobic degradation of dissolved organic carbon (DOC) adsorbed to granular activated carbon in a drinking water production plant. This process cannot be investigated using ^{13}C-labelled substrates. Thus, the RIL approach can be applied to sensitively monitor biodegradation of various organic compounds (e.g. benzene and naphthalene) as well as complex substrate mixtures, which are not available with ^{13}C-labelling.

Zusammenfassung

Aromatische Kohlenwasserstoffe, wie z.B. Benzol und Naphthalin, haben toxische, mutagene und/oder karzinogene Eigenschaften. Diese Substanzen können jedoch glücklicherweise in der Umwelt von natürlich vorkommenden Mikroorganismen beseitigt werden. Über die Physiologie und Ökologie dieser Mikroben ist bisher vor allem unter anaeroben Bedingungen wenig bekannt. In dieser Doktorarbeit befasse ich mich mit wichtigen Wissenslücken auf diesem Gebiet indem ich mikrobiologische Ansätze mit „omics"-Techniken (Metagenomik und Metaproteomik) verbinde. Außerdem stelle ich eine neue Methode umgekehrter stabiler Isotopenmarkierung zur Messung biologischer Abbauaktivitäten vor.

Zunächst wurde die Anreicherungskultur BPL, die Benzol mit Sulfat als Elektronenakzeptor abbauen kann, untersucht. Diese Kultur wird von einem Organismus aus der Gattung *Pelotomaculum* dominiert. Die Mitglieder dieser Gattung sind normalerweise als Fermentierer bekannt, die in syntropher Beziehung mit anaeroben Mikroorganismen oder Methanogenen leben. Unklar ist jedoch, ob jener *Pelotomaculum* aus dieser Studie (nämlich *Pelotomaculum* candidate BPL) in der Lage ist, sowohl Benzol abzubauen als auch Sulfat zu reduzieren. Für diesen Organismus wurde mit Hilfe von Metagenomik ein qualitativ hochwertiges Genom rekonstruiert. Interessanterweise enthält das Genom alle Gene, die für eine vollständige Sulfatreduktion nötig sind, ähnlich der Genome anderer gram-positiver, sulfatreduzierender Bakterien. Die Proteomanalyse zeigte, dass die für die Sulfatreduktion essentiellen Enzyme alle während des Wachstums auf Benzol exprimiert wurden. Die proteogenomischen Daten zeigten außerdem: (1) Anaerober Benzolabbau wurde durch einen bisher unbekannten Mechanismus für die Umsetzung von Benzol zu Benzoyl-CoA aktiviert; (2) der zentrale Benzoyl-CoA Abbauweg ging mit der reduktiven Dearomatisierung durch eine Benzoyl-CoA-reduktase der Klasse II einher, die wiederum von einer hydrolytischen Ringspaltung und einer modifizierten β–Oxidation gefolgt wurde; (3) für die vollständige Oxidation zu CO_2 wurde der oxidative Acetyl-CoA Abbauweg verwendet. All diese Daten zeigen, dass *Pelotomaculum* candidate BPL nicht nur

das Potenzial für anaeroben Benzolabbau besitzt, sondern auch das erste Mitglied dieser Gattung ist, das Sulfat reduzieren kann.

Zweitens wurde die funktionelle Bedeutung von Umwelt-Spirochäten untersucht. Diese Mikroben werden häufig in anoxischen Milieus gefunden, die Kohlenwasserstoffe enthalten und mit Organohaliden verunreinigt sind, doch ihre Funktion ist bisher unbekannt. Um Einblick in ihre Funktion zu bekommen, wurde eine sulfatreduzierende und naphthalinabbauende Anreicherungskultur als Beispiel genommen. Diese Kultur enthält sulfatreduzierende Deltaproteobakterien und den Spirochäten *Rectinema cohabitans*. Genomsequenzierung und Proteomanalyse deuteten darauf hin, dass der Spirochät ein obligater Fermentierer ist, der Proteine und Kohlenwasserstoffe abbaut und dabei Azetat, Ethanol und Wasserstoff produziert. Physiologische Experimente zeigten, dass das H_2, welches bei der Fermentation durch *R. cohabitans* entsteht, von den Deltaproteobakterien als Reduktionsmittel für die Sulfatatmung genutzt wurde. Verschiedene proteomische und physiologische Experimente zeigten, dass *R. cohabitans* wiederum die Biomasse (Proteine und Kohlenwasserstoffe) verwendet, die durch Zelllyse entstehen. Weitere vergleichende Genomanalysen deuteten darauf hin, dass *Rectinema*-Arten in verunreinigten Milieus weit verbreitet sind und, ähnlich wie *R. cohabitans*, an einen wasserstoffproduzierenden, fermentativen Lebensstil angepasst sind. All dies zeigt, dass Umwelt-Spirochäten in besonders toxischen, kontaminierten Milieus gedeihen indem sie tote Biomasse abbauen und dabei Wasserstoff produzieren. Die entstehenden Reduktionsmittel können wiederum die Synthese von Biomasse durch andere Umwelt-Mikroorganismen befeuern, die Wasserstoff konsumieren. Umwelt-Spirochäten sind also möglicherweise ein wichtiger Bestandteil eines mikrobiellen Kreislaufs, der für den unterirdischen Nährstoffkreislauf von zentraler Bedeutung ist.

Schließlich wurde ein sensitives Verfahren zur Messung von biologischem Abbau mit Hilfe umgekehrter stabiler Isotopenmarkierung von gelöstem anorganischem Kohlenstoff vorgestellt. Die mikrobielle Mineralisierung organischer Substanzen wird vorzugsweise in Labor-Experimenten durch Zugabe von ^{14}C- oder ^{13}C-markierten Substraten und der Messung von entstandenem, markiertem CO_2 untersucht. Markierte Substrate sind in der Regel jedoch teuer oder kommerziell

nicht erhältlich. Die Methode, die hier verwendet wurde, enthält nicht-markierten, organischen Kontaminationsstoff und ^{13}C-markierten anorganischen Kohlenstoff mit einem höheren ^{13}C-Anteil, als er natürlicherweise vorkommt. Das produzierte CO_2 verdünnt allmählich den ursprünglichen ^{13}C-Anteil, was eine Quantifizierung der mikrobiellen Mineralisierungsrate mittels Berechnung der Massenbilanz erlaubt. Ein neu entwickeltes Isotopenverhältnis-Mittelinfrarotspektrometer ermöglichte das Messen von ^{13}C-Anteilen von weniger als 0.006%. Die gemessene CO_2-Produktion war nahe der theoretisch ermittelten Stöchiometrie für anaeroben Naphthalinabbau in einer sulfatreduzierenden Anreicherungskultur. Außerdem wurde die Methode verwendet, um aeroben Abbau von gelöstem organischen Kohlenstoff zu messen, der an granulare Aktivkohle in einer Anlage zur Trinkwassergewinnung gebunden war. Dieser Prozess kann nicht mit Hilfe von ^{13}C-markierten Substraten gemessen werden. Das Verfahren umgekehrter stabiler Isotopenmarkierung kann also verwendet werden den biologischen Abbau verschiedenster organischer Substanzen (z.B. Benzol und Naphthalin) sowie komplexer Substratmischungen, die nicht mit ^{13}C markiert werden können, empfindlich zu messen.

Table of Contents

List of Figures

List of Tables

Abbreviations

Abc	Anaerobic benzene carboxylase
APS	Adenosine-5’-phosphosulfate
BAC	Biologically active carbon
BCRs	Benzoyl-CoA reductases
Bss	Benzylsuccinate synthase
CRDS	Cavity ring-down spectroscopy
CSIA	Compound-specific isotope analysis
CTAB	Hexadecyltrimethylammonium bromide
DAPI	4’, 6-diamidino-2-phenylindole
DIC	Dissolved inorganic carbon
DOC	Dissolved organic carbon
DsrABC	Dissimilatory sulfite reductase cytoplasmic subunits
DsrMk	transmembrane dissimilatory sulfite reductase complex
FISH	Fluorescent in situ hybridization
GAC	Granular activated carbon
GC-MS	Gas chromatography–mass spectrometry
IRMS	Isotope ratio mass spectrometry
IRIS	Isotope ratio infrared spectroscopy
MCR	Methyl coenzyme M reductase
m/z	Mass-to-charge ratios
Nod	Nitric oxide dismutase
OTU	Operational taxonomic unit

PAHs	Polycyclic aromatic hydrocarbons
QmoAB	Quinone-interacting membrane-bound oxidoreductase
qPCR	Quantitative polymerase chain reaction
RIL	Reverse stable isotope labelling analysis
SIP	Stable isotope probing

1. Introduction

1.1. Anaerobic benzene and naphthalene degradation with various electron acceptors

Aromatic hydrocarbons, e.g. benzene and naphthalene, have toxic, mutagenic, and/or carcinogenic properties (Samanta et al. 2002). They can be released into groundwater due to leakages from pipelines, oil tanks or gas stations and other improper treatments, thus posing a hazardous risk to drinking water resources. But fortunately, these compounds can be removed by microorganisms which exist in nature.

Due to their limited chemical reactivity, these compounds were considered to be degraded only in the presence of free oxygen for many decades (Widdel and Rabus 2001). However, because of the low oxygen solubility in water (8 mg/L = 250 µM at 25 ^{o}C) and high carbon loads of aromatic hydrocarbons, the saturated systems rapidly turn anoxic even when they are exposed to small carbon loads (e.g. 33 µM benzene) (Meckenstock and Mouttaki 2011). Thus, anaerobic degradation of these compounds is of outstanding interest. Up to date, it has been shown that Fe(III), nitrate, sulfate, perchlorate and electrodes can be utilized by anaerobic microorganisms as terminal electron acceptors during the degradation of benzene and naphthalene (Meckenstock et al. 2016).

From a thermodynamic point of view, the redox potential of electron acceptors determines not only the biochemical strategies of anaerobic degradation pathways, but also the amount of potential energy the microorganisms can gain (Table 1). Normally, in case of acetate as the substrate, more energy can be theoretically provided for cell growth per mole of acetate for microorganisms when nitrate or ferric iron are used as electron acceptors, compared to the acceptors sulfate and carbon dioxide. Enigmatically, previous studies showed that anaerobic benzene degradation under various electron acceptors is against the energetic rule as shown in Table 1. One possible clue is that lower biomass yield under nitrate-reducing condition was produced than that under methanogenic conditions (Vogt et al. 2011). Additionally, anaerobic naphthalene degradation is

demonstrated so far only reliably to occur under sulfate- and ferric-reducing conditions (Kleemann and Meckenstock 2011, Musat et al. 2009). Nitrate-dependent naphthalene degradation is never reproduced or can only be stimulated by a non-fermentable substrate (Mittal and Rockne 2008), even though the oxidation of naphthalene with nitrate should be more feasible compared to with sulfate and ferric (Philipp and Schink 2012).

Table 1. Standard free energy changes and calculated possible synthesis of ATP associated with complete mineralization of 1 mol benzene and naphthalene with different electron acceptors.

	Electron acceptors (oxidized/reduced)[b]	Stoichiometric equation	$\Delta G^{0'}$ (KJ)[a]	Estimated ATP (mol)[c]
Benzene	CO_2/CH_4	$C_6H_6 + 10.5H_2O + 3.75CO_2 \rightarrow 6HCO_3^- + 3.75CH_4 + 6H^+$	-106	1.5
	SO_4^{2-}/H_2S	$C_6H_6 + 3H_2O + 3.75SO_4^{2-} \rightarrow 6HCO_3^- + 3.75HS^- + 2.25H^+$	-186	2.7
	Ferrihydrite/Fe^{2+}	$C_6H_6 + 30Fe(OH)_3 \rightarrow 6HCO_3^- + 30Fe^{2+} + 18H_2O + 54OH^-$	-525~-1104	7.5~15.8
	MnO_2/Mn^{2+}	$C_6H_6 + 15MnO_2 + 24H^+ \rightarrow 6HCO_3^- + 15Mn^{2+} + 12H_2O$	-2104	30.1
	NO_3^-/N_2	$C_6H_6 + 6NO_3^- \rightarrow 6HCO_3^- + 3N_2$	-2978	42.5
Naphthalene	CO_2/CH_4	$C_{10}H_8 + 18H_2O + 6CO_2 \rightarrow 10HCO_3^- + 6CH_4 + 10H^+$	-157	1.2
	S^0/HS^-	$C_{10}H_8 + 30H_2O + 24S \rightarrow 24\ HS^- + 10HCO_3^- + 34H^+$	-40	0.6
	SO_4^{2-}/H_2S	$C_{10}H_8 + 6SO_4^{2-} + 6H_2O \rightarrow 10HCO_3^- + 6HS^- + 4H^+$	-286	4.1
	Ferrihydrite/Fe^{2+}	$C_{10}H_8 + 48Fe(OH)_3 \rightarrow 10HCO_3^- + 48Fe^{2+} + 28H_2O + 86OH^-$	-828~-1754	11.9~25.1
	MnO_2/Mn^{2+}	$C_{10}H_8 + 24MnO_2 + 38H^+ \rightarrow 10HCO_3^- + 24Mn^{2+} + 18H_2O$	-3355	47.9
	NO_3^-/N_2	$C_{10}H_8 + 1.2H_2O + 9.6NO_3^- \rightarrow 10HCO_3^- + 0.4H^+ + 4.8N_2$	-4752	67.9

Table 1 was modified from Meckenstock et al. (2016). [a] The Gibbs free energy of formation for naphthalene, 2-methylnaphthalene, phenanthrene are obtained from Mavrovouniotis (1990), Dean (1987), and McFarland and Sims (1991), respectively. The Gibbs free energy of formation for other substances are obtained from Madigan et al. (2008). Note that the calculation of energy yield is based on reduction potential differences when ferrihydrite is used as the electron acceptor (Madigan et al. 2008). [b] The standard redox potential for ferrihydrite/Fe^{2+} is -0.1 V~+0.1 V (Straub et al. 2001). [c] The energy required to synthesize ATP is taken as 70 KJ/mol, assuming the intracellular pH in anaerobic bacteria as 7.0 (Jackson and McInerney 2002).

1.2. Multiple possible activation mechanisms for anaerobic benzene degradation

Unlike oxygenase-dependent reactions involved in aerobic degradation, anaerobic microorganisms have to employ alternative biochemical pathways to mineralize these compounds in the absence of molecular oxygen. For anaerobic degradation of benzene, three types of initial activation reactions have been proposed: methylation to toluene, hydroxylation to phenol and direct carboxylation to benzoate (Figure 1).

Methylation of benzene to toluene was proposed from the recovery of labeled toluene using compound-specific isotope analyses (Aburto-Medina and Ball 2014, Meckenstock and Mouttaki 2011, Vogt et al. 2011). But hitherto benzylsuccinate, the key product of further anaerobic toluene activation, has never been detected in benzene-degrading cultures. Although Taubert et al. (2012) found two proteins that might be involved in putative β-oxidation pathway of benzylsuccinate using protein-based stable isotope probing (protein-SIP) in a benzene-degrading, sulfate-reducing enrichment culture, they only showed a low homology (~30% identity) to BbsA and BbsB of *Thauera aromatica*.

Evidence favoring hydroxylation of benzene to phenol as initial activation reaction was found for *Geobacter metallireducen* which metabolizes benzene with Fe(III) citrate as the electron acceptor (Zhang et al. 2012, Zhang et al. 2013). This scenario was supported by the production of ^{18}O-labelled phenol during growth with $H_2{}^{18}O$, and the loss of capacity for benzene degradation due to deletion of genes encoding subunits of two phenol catabolic enzymes (Zhang et al. 2013). Subsequently, Gmet 0231 and 0232 were identified as genes specific for benzene rather than phenol oxidation (Zhang et al. 2014). Nevertheless, unless further investigation is performed on the gene products, these findings should be taken with great caution.

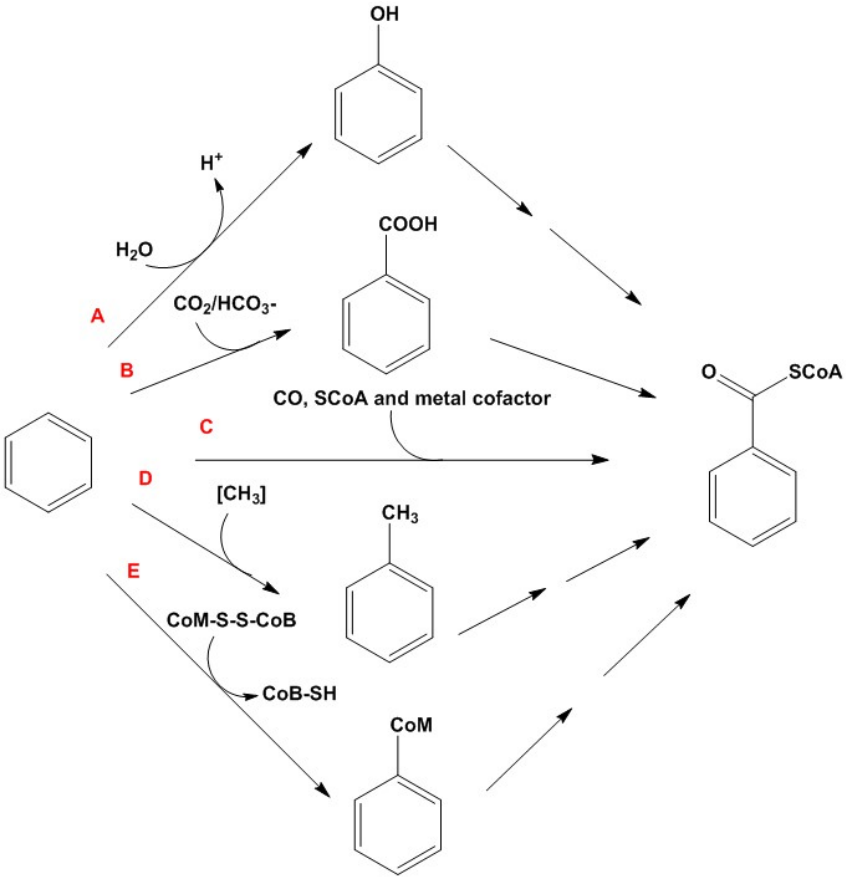

Figure 1. Possible activation mechanisms for initial steps of anaerobic benzene degradation. A) Hydroxylation into phenol; B) carboxylation into benzoate; C) Wood-Ljungdahl-type carbonylation; D) methylation to toluene; E) forming of CoM-mimic molecules via coenzyme M-like reductases. Modified from Abu Laban et al. (2010).

Compared to methylation and hydroxylation, more literatures are in favor of direct carboxylation of benzene into benzoate as the first step. The best investigated examples comprise a Fe(III)-reducing enrichment culture BF (Abu Laban et al. 2010), a hyperthermophilic archaeon *Ferroglobus placidus* (Holmes et al. 2011), and a nitrate-reducing enrichment culture (Luo et al. 2014). Combined genomic and proteomic studies of culture BF revealed that gene products of ORFs 137 and 138 were probably two subunits of putative anaerobic benzene carboxylase (Abc), i.e., AbcD and AbcA, respectively (Abu Laban et al. 2010). The metatranscriptome of a nitrate-reducing enrichment culture during the metabolism of benzene versus benzoate suggested that members of the family *Peptococcaceae* were responsible for initial benzene activation. It showed 97% similarity in 16S rRNA gene sequences with the culture BF (Luo et al. 2014). In that case, two benzene-specific

genes similar to *abcD* and *abcA* were also highly transcribed. Consequently, these two benzene-induced genes might be used as a biomarker for anaerobic benzene degradation in contaminated sites. However, for field application, benzene carboxylation activity still needs to be confirmed in vitro. In a pure archaeal culture, the transcript abundance of Ferp_1630 with homology to *abcA* was higher in benzene-grown cells compared to acetate- and benzoate-grown cells. However, other genes encoding for carboxylase proteins could not be found in the proximity of Ferp_1630 (Holmes et al. 2011). Recently, van der Waals et al (2017) detected a high abundance of the benzene carboxylase gene (*abcA*) in a denitrifying biofilm reactor for benzene degradation dominated by members of the *Peptococcaceae* and *Ananerolineaceae*.

However, there is no direct biochemical evidence for any of these three reactions, so far. For some benzene-degrading cultures, it has been shown that their ability to degrade benzoate, toluene or phenol is not as high as expected, especially for sulfate-reducing and methanogenic cultures (Abu Laban et al. 2009, Devine 2013). On the one side, this fact limits the potential to perform a differential experiment using proteomics or transcriptomics. On the other side, other possible mechanisms for initial benzene activation might be possible. Laso-Pérez et al. (2016) proposed that an enzyme similar to methyl coenzyme M reductase (MCR) is responsible for initial butane cleavage in *Candidatus Syntrophoarchaeum*. It can activate butane to butyl–CoM, followed by an unknown step for conversion of the intermediate butyl–CoM to butyl–CoA (Figure 1). If this is the case, the benzene-degrading microbes should harbor genes for both reverse methanogenesis and e.g. sulfate reduction. Only in this way it can make the hydrocarbon activation process thermodynamically favorable in one single cell (Laso-Pérez et al. 2016, Ragsdale 2016). Another possible mechanism was proposed by Devine (2013): a so-called Wood-Ljungdahl-type carbonylation pathway for conversion of benzene to benzoyl-CoA. In this process, a metal-centered cofactor might allow for a simultaneous addition of CO and CoA to form benzoyl-CoA (Figure 1).

In contrast to the above-mentioned mechanisms, *Alicycliphilus denitrificans* strain BC and *Dechloromonas aromatica* strain RCB, which grow on benzene with chlorate and nitrate as the electron acceptors, respectively, are suggested to

adopt cryptic aerobic pathways. They possibly use molecular oxygen produced intracellularly during reduction of chlorate or nitrate (Oosterkamp et al. 2013, Salinero et al. 2009, Weelink et al. 2008). Under nitrate-reducing conditions, oxygen can be produced by nitric oxide dismutase (Nod) via NO dismutation into N_2 and O_2. Recently, Zhu et al. (2017) found that *nod* genes exist in contaminated aquifers in high diversity and abundance.

1.3. Syntrophic biodegradation of benzene and naphthalene

Syntrophy is a term used to describe microbial cross-feeding, more specifically the tight interdependency between producer and consumer (Dolfing 2014). It is of importance for degradation of organic compounds at methanogenic conditions where electron acceptors are limited or absent. Fermenting bacteria convert complex substrates to small molecules, such as acetate, formate and H_2. But the accumulation of end products (e.g. hydrogen) makes the fermentation process energetically unfavorable. Methanogenic archaea can maintain those end products at low concentrations making the whole reaction exergonic (Morris et al. 2013). This example emphasizes the need of thermodynamic rational for microbial interdependency in the concept of syntrophy. But syntrophic interactions can also occur in the presence of electron acceptors (e.g. sulfate, nitrate, or ferric iron) without participation of methanogens (Gieg et al. 2014). At such a situation, the relationship might be not as tight as methanogenic conditions.

1.3.1 Methanogenic degradation of benzene and naphthalene

Methanogenic hydrocarbon degradation is important in hydrocarbon-contaminated environments, as electron acceptors are often not available due to the high carbon load (Jiménez et al. 2016, Sieber et al. 2012). However, due to slow-growth and the syntrophic nature of this process, laboratory-enriched methanogenic cultures have been rarely reported for benzene and naphthalene degradation. And most observations come from experiments based on stable isotope probing, molecular analysis and omics techniques including metagenomics, metatranscriptomics and metaproteomics (Jiménez et al. 2016).

Luo et al. (2016) monitored a long-term benzene-degradation experiment using different types of techniques, including 16S rRNA gene sequencing, metagenome sequencing and quantitative polymerase chain reaction (qPCR). They showed that members belonging to the new genus *Deltaproteobacterium* ORM2 initiated anaerobic benzene attack. Hydrogenotrophic methanogen (*Methanoregula*, *Methanospirillum*, *Methanocella*, *Methanolinea* or *Methanobacterium*) and acetoclastic *Methanosaeta* were supposed to maintain low concentrations of hydrogen and acetate generated from benzene fermentation. Berdugo-Clavijo et al. (2012) tested if a crude oil-degrading methanogenic enrichment culture can be used for naphthalene degradation but they couldn't find substantial methane production. Siegert et al. (2011) reported a similar observation when ^{13}C labeled naphthalene was the only substrate added into microcosms containing Zeebrugge sediment.

1.3.2 Syntrophic benzene degradation

For syntrophy in the presence of electron acceptors such as nitrate, Fe(III), or sulfate, members of Gram-positive *Peptococcaceae* from the order *Clostridiales* are frequently reported as primary degraders of hydrocarbons like benzene (Lueders 2017) (Figure 2b). The family *Peptococcaceae* encompasses the genera *Peptococcus*, *Cryptanaerobacter*, *Dehalobacte*r, *Desulfitibacter*, *Desulfitispora*, *Desulfitobacterium*, *Desulfonispora*, *Desulfosporosinus*, *Desulfotomaculum*, *Desulfurispora*, *Pelotomaculum*, *Sporotomaculum*, *Syntrophobotulus*, and *Thermincola* (Stackebrandt 2014). Members of this family are physiologically heterogeneous with several types of metabolic features, including chemoorganotroph, chemolithoheterotroph, chemolithoautotroph, or syntrophy with hydrogenotrophs (Ezaki 2015, Stackebrandt 2014).

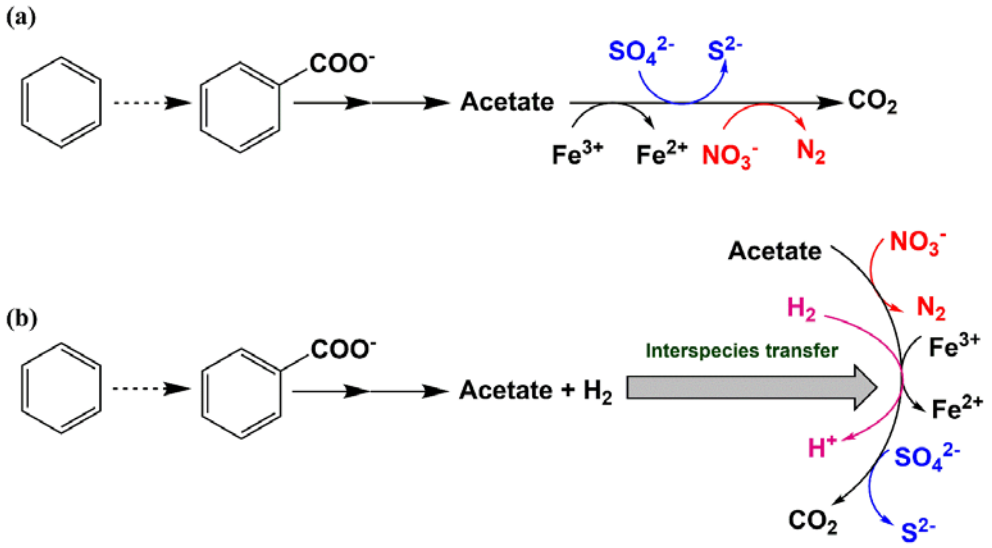

Figure 2. Two working scenarios for *Peptococcaceae* as primary degraders in the presence of electron acceptors such as nitrate, Fe(III), or sulfate. (a) Complete degradation coupled with reduction of electron acceptors is performed by a single cell process; (b) *Peptococcaceae* are responsible for fermentation of hydrocarbons and share electrons in the form of e.g. acetate and hydrogen with other respiring bacteria. Modified from Gieg et al. (2014).

In a denitrifying benzene-degrading enrichment culture (van der Zaan et al. 2012), addition of hydrogen inhibited anaerobic degradation of benzene presumably performed by *Peptococcaceae* based on results from DNA-stable isotope probing with ^{13}C-labelled benzene. But they did not give clear evidence for who was the other denitrifying partner responsible for H_2 scavenge. In a study performed on another denitrifying enrichment culture (Luo et al. 2014), a benzene-degrading *Peptococcaceae* strain worked together with a benzoate-degrading denitrifying *Azoarcus* strain for the complete mineralization of benzene. But in a stricter interpretation of syntrophy, such an interaction is only to share work together but not because of the thermodynamic reason as for methanogenic conditions. Similar interactions were also reported for iron-reducing and sulfidogenic benzene-degrading enrichment cultures dominated by *Peptococcaceae* with evidence derived from DNA-SIP experiments (Herrmann et al. 2010, Kunapuli et al. 2007). They all proposed that electrons from benzene degradation could be transferred to either co-existing sulfate or iron reducers. But none of them could exclude the possibility that *Peptococcaceae* themselves could be directly involved with sulfate

or iron reduction. Therefore, it is still likely that benzene can be mineralized by a single organism without syntrophic interactions (Figure 2a).

1.4. Besides key players, who else is there and what are they doing?

While it is important to have key players for activation of hydrocarbons and/or reduction of electron acceptors, it has become clear that more subtle and complex microbial interactions are also critical for complete removal of hydrocarbons in situ. Thus, besides a focus on the key players, it is relevant to understand who else is there and why they are there. Molecular surveys of anaerobic hydrocarbon-degrading enrichment cultures have revealed a majority of microbial species in the subsurface do not show a clear correlation to the geochemical processes observed.

Spirochaetes. *Sphaerochaeta pleomorpha* strain Grapes and *Sphaerochaeta globosa* strain Buddy were obtained during enriching trichloroethene (TCE)-dehalo-respiring anaerobes (Caro-Quintero et al. 2012, Ritalahti et al. 2012). They are members of the phylum Spirochaetes based on 16S rRNA gene sequences and whole-genome level phylogenies, but they never display a helical morphology or motility during laboratory cultivation. This was further confirmed by genome sequencing showing the lack of genes encoding a flagellar apparatus (Caro-Quintero et al. 2012, Ritalahti et al. 2012). To date, the roles of these organisms in this enrichment have remained enigmatic. In addition, Spirochaetes are also abundant in microbial communities degrading other hydrocarbon compounds such as terephthalate (Nobu et al. 2015), trichloroethene (Caro-Quintero et al. 2012, Ritalahti et al. 2012), and other organohalides (Duhamel and Edwards 2006). But the function of the Spirochaetes in these cultures has remained unresolved.

Epsilon-*proteobacteria*. Epsilon-*proteobacteria* are frequently found in hydrocarbon-degrading, sulfate-reducing enrichment cultures (Lueders 2017). For example, they were detected in a benzene-degrading, sulfate-reducing microbial community but not supposed to be essential for benzene degradation (Keller et al. 2015, Starke et al. 2016). Metagenomics, metaproteomics and pulsed $^{13}C_2$-acetate protein-stable isotope labelling suggested that they were responsible for acetate

capture and polysulfide cycling (Keller et al. 2015, Starke et al. 2016). The oxidation of sulfide could avoid the toxicity of polysulfide to other microorganisms.

Parcubacteria (OD1). Members belong to uncultivated Parcubacteria (OD1) were found in a methanogenic benzene-degrading enrichment culture but their abundance was not directly linked to benzene consumption (Luo et al. 2016). A similar role in sulfur cycling as for Epsilon-*proteobacteria* was proposed for OD1, in agreement with usage of ferrous sulfide in the medium (Luo et al. 2016). In contrast, a nearly complete genome for an organism from Parcubacteria (OD1) derived from an oil reservoir suggested that it is an obligate fermenter (Hu et al. 2016). Therefore, the function of OD1 in hydrocarbon degradation can be diverse.

Chloroflexi and Chlorobi. Stable isotope probing of two benzene-degrading cultures suggested that specific members of the phyla Chloroflexi (mainly *Anaerolineae*) and Chlorobi (mainly *Ignavibacteria*) were unlikely involved in direct benzene degradation, even though they were at relatively high abundances (Taubert et al. 2012, van der Zaan et al. 2012). However, they might thrive on dead biomass (Taubert et al. 2012, van der Zaan et al. 2012).

Caldiserica (formerly candidate division OP5). In a methanogenic reactor treating terephthalate-containing wastewater, metagenomics revealed that members of the candidate division OP5 could not degrade terephthalate or its metabolites (e.g. acetate and butyrate) (Lykidis et al. 2011). Instead, they were proposed to use CO_2 and H_2 from terephthalate fermentation for anaerobic autotrophic butyrate production. The produced butyrate would fuel other syntrophs like *Syntrophus*, *Thermotogae* and WWE1 in the system.

1.5. The importance of microbial H_2 metabolism in the subsurface system

Hydrogen is an important energy source in lithoautotrophic microbial ecosystems when organic compounds are limited or absent (Greening et al. 2016). Bagnoud et al. (2016) introduced high hydrogen concentrations to deep Opalinus Clay rock formation. Based on metaproteomics they found that it can greatly fuel sulfate reducers belonging to the family Desulfobulbaceae, which thereby fixes inorganic carbon. These generated organic carbons then become necromass, which can be

used by other microorganisms, sustaining the microbial metabolic web in this system. Hernsdorf et al. (2017) took samples from groundwater at depths of 140-250 m below the surface and they found that a majority of microorganisms in this system rely on hydrogen consumption based on the detection of genes encoding oxidative [NiFe] hydrogenases and electron-bifurcating [FeFe] hydrogenases. Like Bagnoud et al., they also proposed that the oxidation of hydrogen will contribute to carbon fixation, which is important for closing the carbon loop in this oligotrophic ecosystem.

For ecosystems rich in organic carbons, genes encoding hydrogenases also exist in large quantities and high diversities (Greening et al. 2016). Wrighton et al. (2014) used metagenomics and proteomics to understand microbial interdependencies in an aquifer, which was fed with acetate aiming to elevate carbon loads. The results show that members from Candidate Phyla Radiation (CPR) (Hug et al. 2016) were responsible for fermentation and their products e.g. hydrogen could be further consumed by other respiratory organisms in this system, e.g. sulfate reducers. This emphasizes the importance of hydrogen exchange for linking fermentation and respiratory metabolisms. In hydrocarbon–contaminated system, sulfate reducers can not only feed on a variety of organic pollutants, but also use the fermentation products such as hydrogen, acetate and fatty acids (Wasmund et al. 2017). But so far little is known about how they can affect the bioremediation process.

1.6. Using ^{13}C isotopes to quantify anaerobic hydrocarbon degradation

One of the most important steps in understanding microbial degradation processes is to quantify the extent of biodegradation. The direct measurement of concentrations of contaminants, in most cases, is not practical. On one hand, the biodegradation rate is usually very slow and it can only lead to very small change in the concentration, most probably below the reproducibility of the measurements; on the other hand, most compounds are volatile and can strongly adsorb to sediments in situ or stoppers in laboratory microcosm studies. In this context, people turn to using the powerful stable isotope tools to reliably assess pollutant biodegradation. There are two main stable isotope tools in this perspective: (i)

analysis of natural abundance changes of stable isotopes for one specific compound based on the isotopic fractionation effects during the biodegradation process; (ii) determination of incorporation of stable isotopes to the degradation intermediates and/or mineralization products derived from a labelled compound (Figure 3). These two tools rely on (iii) the development of very precise and accurate stable isotope analytical techniques (Figure 3). Here the three aspects are summarized as below with focus on the ^{13}C stable isotopes.

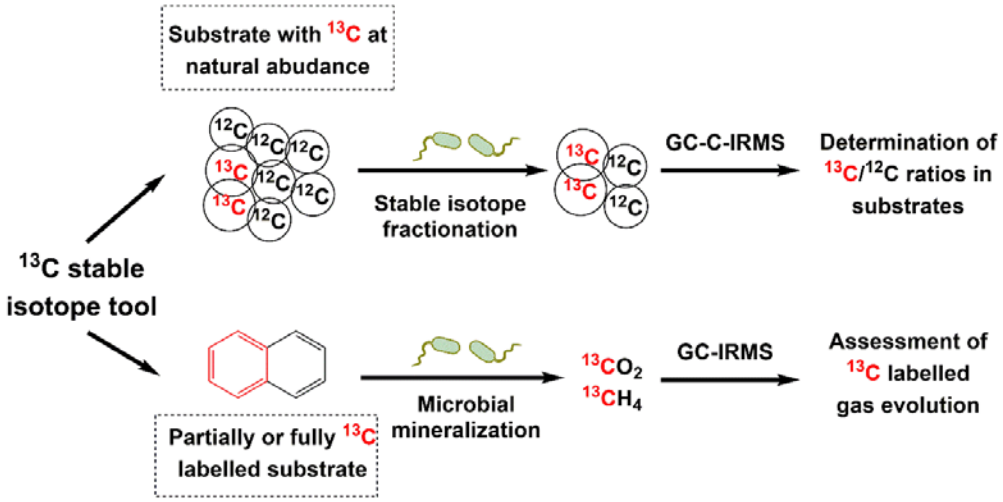

Figure 3. Application of ^{13}C stable isotope tools to quantify the extent of anaerobic hydrocarbon degradation.

1.6.1 Stable isotope fractionation

In biochemical reactions, lighter isotopes (e.g. ^{12}C and ^{1}H) react faster, which results in a relative enrichment of heavier isotopes (e.g. ^{13}C and ^{2}H) in the nonbiodegraded, residual fraction of the substrates (e.g. benzene and naphthalene). The shifts in stable isotope ratios (e.g. $^{13}C/^{12}C$, $^{2}H/^{1}H$) of organic contaminants can be measured by means of compound-specific isotope analysis using mainly gas chromatography-isotope ratio mass spectrometry, and therefore can be employed for qualitative and even quantitative determination of anaerobic degradation of benzene and PAHs (Elsner 2010, Meckenstock and Richnow 2010, Schmidt and Jochmann 2012, Thauer et al. 1977). The stable isotope ratios are expressed in δ notations as $\delta^{13}C$ values (‰) for carbon with Vienna Pee Dee

Belemnite as the standard, and δ^2H values (‰) for hydrogen with Vienna Standard Mean Ocean Water as the standard (Coplen 2011).

For quantification of in situ biodegradation, the stable isotope fractionation factor α needs to be determined in the laboratory first. For field applications, the Rayleigh equation is then used to estimate the extent of contaminant biodegradation based on stable isotope ratio shifts and corresponding isotope fractionation factors (Hunkeler 2008, Meckenstock and Richnow 2010). Based on $^{13}C/^{12}C$ fractionation data, Griebler et al. (2004) calculated that decreasing benzene concentrations in a contaminated aquifer were almost exclusively due to biodegradation. Fischer et al. (2008) could quantitatively connect the stable isotope fractionation of a mixture of ring-deuterated (d_5) and completely (d_8) deuterium-labeled toluene injected into a contaminated aquifer, with the release of deuterium from toluene mineralization. However, variations in fractionation factors for different microorganisms and biochemical reactions have to be taken into account (Bergmann et al. 2011b, Fischer et al. 2008, Griebler et al. 2004, Mancini et al. 2008). Griebler et al. (2004) also obtained $^{13}C/^{12}C$ isotope fractionation factors for anaerobic degradation of naphthalene and 2-methylnaphthalene using the sulfate-reducing enrichment culture N47. However, Morasch et al. (2011) could not find significant stable isotope shifts to evidence the occurrence of methylnaphthalenes. The study indicated the limitation of carbon isotope fractionation for molecules larger than 11 carbon atoms such as 2-methylnaphthalene. The extent of observable isotope fractionation is diluted with an increasing number of carbon atoms (Elsner 2010, Kummel et al. 2015). This makes an accurate detection of biodegradation impossible using compound-specific isotope analysis for higher-molecular-weight PAHs, e.g. molecules with more than 11 carbon atoms.

Analysis of hydrogen stable isotope ratios, however, might be useful for higher-molecular-mass PAHs as the number of hydrogen atoms per molecule only slightly increases for larger PAHs and hydrogen stable isotope fractionation effects can be very strong. Bergmann et al. (2011b) demonstrated that hydrogen isotope enrichment factors were remarkably large during anaerobic degradation of naphthalene by the sulfate-reducing cultures N47 and NaphS2. This indicated that

hydrogen stable isotope fractionation might be employed to qualitatively and quantitatively assess microbial degradation of PAHs in the field.

1.6.2 Stable isotope labelling

Complete oxidation of hydrocarbons to CO_2 and CH_4 is the final goal of bioremediation leading to complete removal of contaminants without toxic intermediates. In terms of monitoring complete mineralization, one of the best ways is to use stable isotope-based methods by either fully or partially labelling the target contaminant with ^{13}C. If the compound is biodegraded, it will be converted to $^{13}CO_2$ or $^{13}CH_4$. Changes in $^{13}C/^{12}C$ carbon isotope ratios therefore indicate the mineralization rate of the target compound. This method is quite useful to assess the biodegradation potential in laboratory microcosms of enrichment cultures or pure isolates. Besides the data from evolution profiles of $^{13}CO_2$ or $^{13}CH_4$, further evidence should be provided to demonstrate a reliable mineralization of pollutants such as the consumption of electron acceptors (e.g. sulfate or nitrate) and the accumulation of biomass (Bolliger et al. 1999).

Stable isotope labelling has been successfully used to assess biodegradation of recalcitrant organic compounds such as benzene and polycyclic aromatic hydrocarbon (Fischer et al. 2016). For example, Nijenhuis et al. (2007) sufficiently proofed anaerobic mineralization of $^{13}C_6$-monochlorobenzene in laboratory microcosms indicated by the production of $^{13}CO_2$ even at very small portions of degraded contaminant. But with stable isotope fractionation analysis, they failed to provide clear evidence demonstrating the high sensitivity of stable isotope labelling tools. Morasch et al. (2007) and Fischer et al. (2016) followed the production of $^{13}CO_2$ from ^{13}C-labelled polycyclic aromatic hydrocarbons (e.g. naphthalene) by isotope-ratio mass spectrometry (IRMS) providing in situ biodegradation evidence via the high sensitivity and reproducibility of $^{13}C/^{12}C$ stable isotope analysis.

However, this method has at least two disadvantages: (1) usually in field experiments people have to deal with a mixture of compounds which is impossible to be labelled; (2) this method is less applicable for higher-molecular compounds

because the ^{13}C-labelled contaminants usually need special syntheses; and thus, they are very expensive or even not commercially available.

1.6.3 Stable isotope techniques

Stable isotope methods rely on highly accurate and precise techniques for determination of $^{13}C/^{12}C$ carbon isotope ratios. Isotope ratio mass spectrometry (IRMS) is the method of choice for highly accurate determinations (Zanasi et al. 2006, Zare et al. 2009). But the IRMS instrument requires a relatively large space in a temperature-controlled laboratory and professional experts for operation and maintenance. Besides, they are costly and not portable. Recently, the development of optical-based technologies has provided more options for the determination of carbon isotope ratios in e.g. CH_4 and CO_2. The most attractive one is referred to as isotope ratio infrared spectroscopy (IRIS) relying on infrared laser absorption. These instruments are smaller in size and less expensive. Moreover, they can be installed in the field allowing for high-resolution and real-time in situ measurements which IRMS cannot perform (van Geldern et al. 2014).

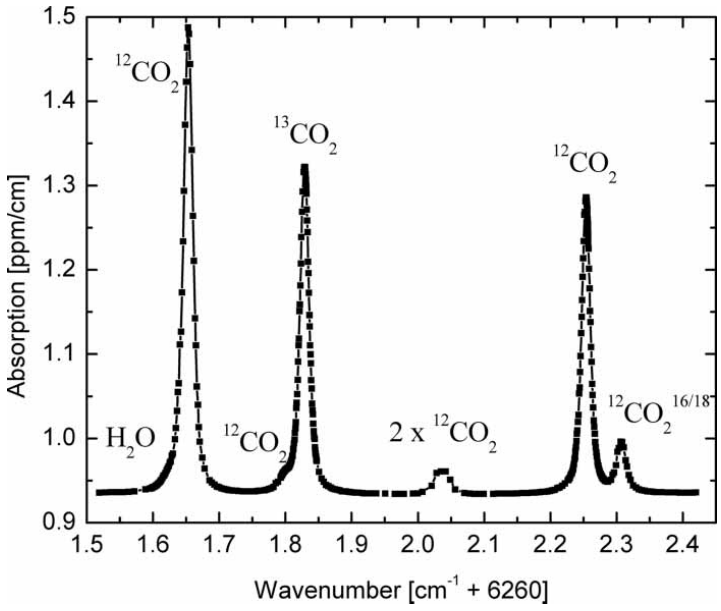

Figure 4. Near-infrared spectrum of 5% carbon dioxide at 6.7 kPa operating pressure, showing three different isotopes. Taken from Wahl et al. (2006).

Different molecules have different absorption lines at specific wavelengths due to the quantum mechanical rotational and vibrational states. This principle is also

applied to the same molecule but with different isotopic species. For example, if ^{12}C in CO_2 is replaced by ^{13}C, the absorption wavelengths change (Crosson et al. 2002, Wahl et al. 2006) (Figure 4). Therefore, shifts in different absorption peaks allow to quantify the respective abundances of different isotopologues following Beer's law. As we can see from Figure 4, the spectral features are quite narrow and therefore special techniques are needed to distinguish between closely spaced wavelengths of light. The method used to achieve this goal is called tunable diode laser absorption using the continuous wave for such a high selectivity (Bowling et al. 2003, Fischer et al. 2016). Meanwhile this technique uses multi-pass cells to have an enhanced path length for high resolution (Bowling et al. 2003, Fischer et al. 2016).

So far, the most frequently-used commercial IRIS instruments are Cavity ring-down spectroscopy (CRDS) (Crosson et al. 2002) and Delta Ray (van Geldern et al. 2014) based on tunable laser direct absorption in the near-infrared and mid-infrared wavelength regions, respectively. These instruments have a comparable accuracy for determination of $^{13}C/^{12}C$ in CO_2 at natural abundance to conventional IRMS (Crosson et al. 2002, Flores et al. 2017). Moreover, they can be used to roughly estimate CO_2 concentrations (Bowling et al. 2003). IRMS has been shown that it is not suitable for microbial labeling experiments as highly enriched samples cannot be measured (Reinsch and Ambus 2013). In contrast, IRIS instruments can be applied for labelled samples as long as the concentration of e.g. CO_2 is not high enough. But compared to IRMS, so far, the application of IRIS in compound-specific isotope analysis (CSIA) is still at its infancy. One pioneering work done by Zare et al. (2009) integrated a CRDS instrument, a chromatographic separation technique, and a combustor into one system (GC-C-CRDS). With this setting, they successfully measured the $^{13}C/^{12}C$ isotope ratios in organic compounds, such as ethane and propane.

1.7. Objectives of this thesis

This thesis has two objectives. Firstly, I aimed to employ omics techniques (metagenomics and metaproteomics) and physiological experiments to understand the ecology of anaerobic hydrocarbon degradation performed by slow-growing

bacteria. Secondly, I planned to develop a novel reverse stable isotope labelling method for monitoring microbial mineralization rates of organic compounds. In detail, they are divided into three parts in this thesis as below.

Part I Reconstructing metabolic pathways of a member of the genus *Pelotomaculum* suggesting its potential to oxidize benzene to carbon dioxide with direct reduction of sulfate (Chapters 2.1.1, 2.2.1, 2.3.1, 2.4.1, 2.6, 3.1 and 4.1)

Genomic information, usually combined with transcriptomics or proteomics, has the potential to directly and comprehensively unravel the metabolic potential and physiology of cultures that have the capability for anaerobic mineralization of benzene. The enrichment culture BPL used in this part is able to degrade benzene under sulfate-reducing conditions (Abu Laban et al. 2009). Previous community analysis based on 16S rRNA gene sequencing and Fluorescent in situ hybridization (FISH) revealed the dominant member (~95%) in this community was the Gram positive bacterial genus *Pelotomaculum*. However, members of the genus *Pelotomaculum* are mostly obligate syntrophs that need methanogens as syntrophic partners to oxidize propionate, alcohols, or aromatic compounds (Imachi et al. 2002, Stams and Plugge 2009). The aim of Part I is to understand who is responsible for benzene degradation and sulfate reduction using a combination of genomic and proteomics.

Part II Fermentative Spirochaetes drive nutrient cycling by a subsurface microbial loop in hydrocarbon-contaminated habitats (Chapters 2.1.2, 2.2.2, 2.3.2, 2.3.3, 2.4.2, 2.6, 3.2 and 4.2)

Under sulfate-reducing conditions, naphthalene can be anaerobically mineralized to CO_2 by the stable enrichment culture N47 (Meckenstock et al. 2000). Based on 16S rRNA gene sequence analysis, ~93% of the culture comprises a sulfate-reducing deltaproteobacterium that has been shown genetically and biochemically to be responsible for naphthalene degradation. The remainder of the enrichment can be assigned to representatives of the phylum Spirochaetes (Bergmann et al. 2011a, Selesi et al. 2010). To date, the roles of these organisms in this enrichment have remained enigmatic. The aim of Part II is to gain insights into its function in

this enrichment using combination of physiological, genomic, and proteomic analyses.

<u>Part III</u> Monitoring microbial mineralization using reverse stable isotope labelling analysis by mid-infrared laser spectroscopy (Chapters 2.1.3, 2.5, 2.6, 2.7, 2.8, 3.3 and 4.3)

A crucial step in studying microbial degradation of organic compounds is using microcosm experiments to prove the degradation ability and to obtain degradation rates. Of special interest here is to assess if the compounds are totally mineralized to CO_2 or if they are just transformed to metabolites which might be even more toxic in some cases (Fischer et al. 2016). A preferred method is to prove mineralization of the compound of interest by the development of labelled CO_2 in airtight containers. To this end, target compounds are either labelled with stable (^{13}C) or radioactive (^{14}C) carbon isotopes and the evolution of $^{13}CO_2$ or $^{14}CO_2$ is measured over time, providing a very sensitive way for detection of low substrate turnover compared to residual substrate concentration measurements (Bahr et al. 2015, Berry et al. 2017, Fischer et al. 2016, Johnsen et al. 2013). Compared to radioactive labelling, stable isotope methods are a preferred alternative in recent years, because the compounds are easier to handle and less expensive. However, this method is less applicable for higher-molecular weight compounds, because the ^{13}C-labelled substrates usually require special synthesis, and are thus very expensive or even not commercially available. Furthermore, complex substrates such as dissolved organic carbon (DOC) or crude oil cannot be synthesized or labelled. To address the above-mentioned issue, in Part III I aimed to develop a new method for quantitatively assessing biodegradation of organic compounds to CO_2, namely reverse stable isotope labelling (RIL).

2. Materials and Methods

2.1. Cultivation of anaerobic cultures

2.1.1 Cultivation of the enrichment culture BPL

The anaerobic sulfate-reducing culture BPL was enriched from soil at a former coal gasification site in Gliwice, Poland, and was cultivated in bicarbonate-buffered (30 mM) freshwater medium as described earlier (Abu Laban et al. 2009). Benzene (0.5 mM) (Sigma-Aldrich, Steinheim, Germany) was added as sole electron donor and sulfate (10 mM) as electron acceptor. The enrichment culture was transferred in 1:10 (vol/vol) dilutions and the metabolic activity was monitored by consumption of sulfate (Abu Laban et al. 2009).

2.1.2 Cultivation of the enrichment culture N47 and its pure isolate

The naphthalene-degrading, sulfate-reducing enrichment culture N47 was cultivated in bicarbonate-buffered freshwater medium as described previously (Selesi et al. 2010). Three mL of 1.5% naphthalene dissolved in 2,2,4,4,6,8,8-heptamethylnonane (Sigma-Aldrich, Steinheim, Germany) were added to each cultivation bottle after autoclaving. The highly enriched Deltaproteobacteria N47 culture (without Spirochaetes) (Bergmann et al. 2011a, Selesi et al. 2010) performs sulfate reduction and naphthalene oxidation. It was obtained from the enrichment culture N47 by serial dilution in agar roll tubes and cultivated in the same way as the enrichment culture N47. *Rectinema cohabitans* strain HM isolated from the enrichment culture N47 (Koelschbach et al. 2017) was cultivated in bicarbonate-buffered freshwater medium (pH 7.0), which was reduced with a final concentration of 0.5 mM sodium sulfide and amended with 10 mM glucose and 0.1% yeast extract. All culture bottles were incubated at 30 °C in the dark.

To test if *R. cohabitans* can utilize dead biomass of highly enriched Deltaproteobacteria as carbon source, we first harvested cells of highly enriched Deltaproteobacteria from 150 ml cultures by centrifugation at 3214 × *g* (30 min), suspended them in 2.5 mL anoxic fresh medium (without substrate and yeast extract), and autoclaved them in a closed serum bottle three times at 121 °C for

20 min. We then transferred 0.5 mL dead biomass of highly enriched Deltaproteobacteria to serum bottles filled with 30 ml fresh medium and inoculated 3 mL starter cultures of *R. cohabitans*. For control experiments, we incubated fresh media with the same amount of starter cultures of *R. cohabitans* without biomass of highly enriched Deltaproteobacteria or dead biomass without the inoculation of *R. cohabitans*. To investigate if *R. cohabitans* can gain carbon sources from the supernatant of highly enriched Deltaproteobacteria cultures, we transferred 3 mL starter cultures of *R. cohabitans* to serum bottles filled with 30 ml centrifuged supernatant of highly enriched Deltaproteobacteria cultures, which was in addition filtered through 0.22 µm pore-size filter membrane (Sarstedt, Germany). For control experiments, we incubated 30 ml filtered supernatant of highly enriched Deltaproteobacteria without *R. cohabitans*.

2.1.3 Cultivation of bacterial cultures for RIL experiments

Thauera aromatica strain K172 (DSM 6984) and *Geobacter metallireducens* strain GS-15 (ATCC 53774/DSM 7210) were purchased from the Deutsche Sammlung von Mikroorganismen und Zellkulturen (DSMZ, Braunschweig, Germany). Both strains were cultivated as described before under anoxic conditions in a carbonate-buffered freshwater mineral medium at pH of 7.2 to 7.4 spiked with ~0.8 mM pure toluene (Sigma-Aldrich, Steinheim, Germany) (Widdel and Bak 1992) and amended with 5 mM nitrate or 50 mM ferric citrate as electron acceptors, respectively. The sulfate-reducing enrichment culture N47 was cultivated as described in Chapter 2.1.2 but with addition of 1 mL of 1.5% 2-methylnaphthalene or 3 mL of 1.5% naphthalene dissolved in 2,2,4,4,6,8,8-heptamethylnonane (Sigma-Aldrich, Steinheim, Germany) to each cultivation bottle after autoclaving.

The uncharacterized iron-reducing, naphthalene-degrading enrichment culture SN was enriched from Pitch Lake in Trinidad and Tobago (Meckenstock et al. 2014) with ferrihydrite as electron acceptor according to previously described methods (Kleemann and Meckenstock 2011). It was transferred to freshwater mineral medium every 3-4 months when significant production of ferrous iron was indicated by the presence of black iron oxides. The culture was maintained in the lab for more than three years before our experiment, leading to a stable and

sediment-free, iron-reducing culture (Figure 5). For the RIL experiment, 3 mL of 1.5% naphthalene dissolved in 2,2,4,4,6,8,8-heptamethylnonane were added to each cultivation bottle after autoclaving.

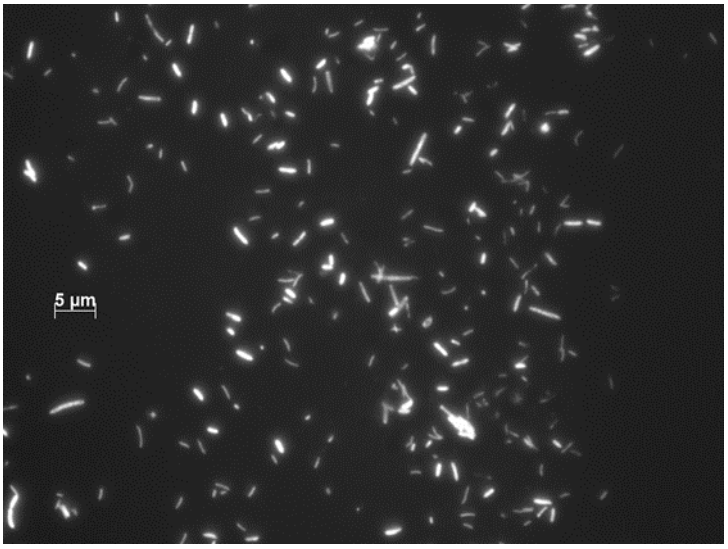

Figure 5. Epifluorescence microscopy images of naphthalene-degrading, iron-reducing enrichment cultures after six months' cultivation stained with 4', 6-diamidino-2-phenylindole (DAPI).

For every culture, RIL experiments were performed using five separate 250 mL serum bottles first filled with 135 mL of fresh medium without bicarbonate buffer and flushed with CO_2/N_2 (20:80, v/v). The $NaH^{13}CO_3$ (Sigma-Aldrich Co.) and $NaH^{12}CO_3$ (Sigma-Aldrich Co.) were injected separately through the stopper from filter-sterilized stock solutions (1 M each, headspace briefly flushed with N_2) to produce a mixture of 30 mM bicarbonate in the medium. Considering the linearity range of IRMS/IRIS, we shifted the added labelled bicarbonate ratios from 50 to 10%. Afterwards, substrates stated before were injected through the stoppers. Then, three bottles were inoculated with 15 mL parent cultures whereas the other two were inoculated with triple-autoclaved cultures serving as controls. All culture bottles were incubated at 30 ^{o}C in the dark.

2.2. Metagenomic and genomic analyses

2.2.1 Binning draft genomes from the BPL metagenome

Genomic DNA was extracted from a 1200-mL BPL culture when ~2 mM sulfate was reduced using the modified CTAB (hexadecyltrimethylammonium bromide) method (Zhou et al. 1996). Whole metagenome sequencing was performed with a 454 GS FLX Titanium system (Roche, Penzberg, Germany) in two different runs. The resulting reads were co-assembled into contigs with the Newbler v2.7 assembly software. The automated assembly of the sequences was checked manually by mapping the raw 454 reads against the contigs with Mosaik v2.2.3 (Lee et al. 2014) followed by visual inspection with Tablet v1.14 (Milne et al. 2013). The assembled contigs were submitted to IMG-M 4.530 (Project ID: Gp0111374) (Markowitz et al. 2014) for automated gene calling and annotation. Automatic annotations were manually curated for genes described in this study by bioinformatics tools in the IMG platform (e.g. KEGG and BLAST) (Markowitz et al. 2014).

All contigs from the BPL metagenome were annotated taxonomically without length restriction with taxator-tk v1.3.0e using default settings and the refpack (microbial_20150430) provided by the authors (Droge et al. 2015). Additionally, we screened all contigs for (partial) marker genes (5S, 16S, 18S, and thirty-one conserved genes) (Wu and Scott 2012) and classified them taxonomically, both using PhyloPythiaS+ v1.4 (Gregor et al. 2016). The two assignment methods provided similar results. Then, we validated the results by checking i. their consistency with the taxonomic profiles obtained from both independent 16S rRNA gene amplicon sequencing data and the contigs-extracted SSU (16S) sequences data for the same community, ii. the read coverage and iii. the GC content of contigs assigned to the same clades.

Finally, we identified the major taxa based on the taxonomic annotations and used them to extract sample-specific training data for the training stage of the composition-based taxonomic classifier PhyloPythiaS+ using default settings. By considering the taxonomic annotation, GC content, and average read coverage, we divided the metagenome contigs into four genome bins.

2.2.2 Sequencing and reconstruction of Spirochaetes genomes

For comparative genomic analyses, three draft genomes were used: *R. cohabitans*, uncultured Spirochaetes bacterium bdmA 4 and uncultured Spirochaetes bacterium SA-8. The draft genome of uncultured Spirochaetes bacterium SA-8 was derived from the metagenome of a terephthalate-degrading community TA, which is available on IMG/M as taxon object ID 3300001095 (Nobu et al. 2015). The draft genome of uncultured Spirochaetes bacterium bdmA 4 was reconstructed from the metagenome of another sulfate-reducing, naphthalene-degrading enrichment culture (designated Sob). Culture Sob was enriched from a creosote-contaminated wood preservation facility located in Soběslav, south of Bohemia (Czech Republic), as described by Kummel et al (2015). The shotgun sequencing information and followed-up assembly and binning process for the (meta)genomes for *R. cohabitans* and enrichment culture Sob are described as below.

Construction and sequencing of paired-end DNA libraries. DNA (30 to 250 ng) was sonicated to a 100- to 800-bp size range on the E210 Covaris instrument (Covaris, Inc., USA). Fragments were end-repaired, then 3'-adenylated, and Illumina adapters were added by using a NEBNext Sample Reagent Set (New England Biolabs). Ligation products were purified by Ampure XP (Beckmann Coulter) and DNA fragments (>200 bp) were PCR-amplified using Illumina adapter-specific primers and Platinum Pfx DNA polymerase (Invitrogen). The amplified library fragments were size selected on 3% agarose gel at around 300 bp. After library profile analysis by Agilent 2100 Bioanalyzer (Agilent Technologies, USA) and qPCR quantification (MxPro, Agilent Technologies, USA), the library was sequenced using 101 base-length read chemistry in a paired-end flow cell V3 on the Illumina Hiseq2000 sequencer (RTA version 1.13.48) (Illumina, USA) in order to obtain overlapping reads and generate meta-reads of 180 bp.

Nextera mate-paired library preparation and sequencing. Three mate pair libraries were prepared for each sample following the Nextera protocol (Nextera Mate Pair sample preparation kit, Illumina). Briefly, genomic DNA was simultaneously enzymatically fragmented and tagged with a biotinylated adaptor. Fragments were

size selected (3-5 Kb, 5-8 Kb and 8-11Kb) through regular gel electrophoresis, and circularized overnight with a ligase. Linear, non-circularized fragments were digested, and circularized DNA was fragmented to 300-1000-bp size range using Covaris E210. Biotinylated DNA was immobilized on streptavidin beads, end-repaired, then 3'-adenylated, and Illumina adapters were added. DNA fragments were PCR-amplified using Illumina adapter-specific primers and then purified. Finally, libraries were quantified by qPCR and libraries profiles were evaluated using an Agilent 2100 bioanalyzer (Agilent Technologies, USA). For enrichment culture Sob, 3-5kb, 5-8kb and 8-11Kb libraries were sequenced using 101 base length read chemistry (v1) in a paired-end flow cell on the Illumina HISEQ2500 sequencer (rapid mode, RTA version 1.17.21.3) (Illumina, USA). For *R. cohabitans*, the 8-11kb library was sequenced using 151 base-length read chemistry (v1) on a paired-end flow cell on the Illumina Miseq platform (RTA version 1.18.54) (Illumina, USA).

Assembly of the R. cohabitans genome. Reads from the paired-end library were down-sampled before being combined with sequences from the largest (8-11 kbp) mate-paired library and assembled with the ALLPATHS engine (Ribeiro et al. 2012).

Reconstruction of the genome for uncultured Spirochaetes bacterium bdmA 4. Although the enrichment culture Sob was dominated by sulfate-reducing Deltaproteobacteria N47 (Bergmann et al. 2011a, Selesi et al. 2010), with about 30% of the raw reads (from either the paired-end or mate-paired libraries) mapping to its genome, the metagenome was endowed with significant phylogenetic diversity and was estimated to harbor about 30-50 distinct genomes. A combination of assembly-free (binning) and targeted assembly techniques were used in order to direct assembly efforts towards lower complexity read partitions. This was achieved by using sequence clustering methods extracting coverage and/or compositional signals from the reads to partition the sequences in k-mer space in an overlap and alignment independent way (Gkanogiannis et al. 2016). The resulting partitions were then assembled independently, leading to the reconstruction of several dozens of megabase sized genomic fragments, including the nearly complete genome for uncultured Spirochaetes bacterium bdmA 4

(estimated 97% complete based on the distribution of 141 lineage specific marker genes compiled by the checkM software) (Parks et al. 2015).

The draft genomes of *R. cohabitans*, uncultured Spirochaetes bacterium bdmA 4, and uncultured Spirochaetes bacterium SA-8 were uploaded into the MicroScope genome annotation platform and automatically annotated (Vallenet et al. 2013). The annotations were manually curated and edited using the Magnifying Genome (MaGe) environment (Vallenet et al. 2006), and metabolic pathways were predicted using the integrated pathway tools of MaGe that are based on the KEGG and MicroCyc databases. Presence of glycoside hydrolases and extracellular peptidases was evaluated using dbCAN ($E<1e^{-10}$ and cover fraction >0.4) (Yin et al. 2012) and MEROPS ($E<1e^{-10}$) (Rawlings et al. 2016), respectively.

2.3. Phylogenetic analysis

2.3.1 16S rRNA gene analysis of *Pelotomaculum*

We picked the near-complete *Pelotomaculum* candidate BPL 16S rRNA gene, 16S RefSeq sequences for the closely related genera *Pelotomaculum* and *Desulfotomaculum,* every *Desulfotomaculum* sequence that was deposited in SILVA SSU r123 as well as an outgroup sequence *Thermincola potens* JR, which we used later to root the tree. We aligned those sequences to the SILVA reference alignment using SINA v1.2.12 and trimmed the resulting multiple sequence alignment to SILVA positions 1007 to 43293. Finally, a maximum-likelihood tree was calculated with RAxML v.8.2.8 using the combined rapid bootstrapping (1000 replicates) and maximum likelihood search algorithm with GTRCAT approximation model and with random seed 29582.

2.3.2 16S rRNA gene analysis of Spirochaetes

The phylogeny of the Spirochaetes was inferred using 16S rRNA gene sequences retrieved from the NCBI Genome Database. Sequences were aligned using the MUSCLE algorithm included in MEGA7 and trimmed to uniform length (Kumar et al. 2016). A maximum likelihood phylogenetic tree was computed by MEGA7 using a general time reversible substitution model and uniform rates among sites. The tree was bootstrapped with 500 replicates.

2.3.3 Hydrogenase classification and analysis

Potential genes encoding hydrogenase catalytic subunits were identified in the genomes of *R. cohabitans* and sulfate-reducing Deltaproteobacteria N47 (Bergmann et al. 2011a, Selesi et al. 2010) by screening translated sequences through the web database HydDB (Søndergaard et al. 2016). Sequences were validated as hydrogenases if they encoded cysteine-containing motifs characteristic of hydrogenases (Greening et al. 2016) and branched with hydrogenase reference sequences on phylogenetic trees. To infer evolutionary relationships, the source and reference sequences were aligned using the MUSCLE algorithm (Edgar 2004) and visualized on neighbor-joining phylogenetic trees (Saitou and Nei 1987) constructed with MEGA7 (Kumar et al. 2016) and bootstrapped with 500 replicates. For genetic organization maps, protein/domain function was predicted using the Conserved Domain Database (CDD) (Marchler-Bauer et al. 2011) and iron-sulfur clusters were predicted by identifying conserved cysteine residues as previously described (Greening et al. 2016).

2.4. Proteomic analysis

2.4.1 Shotgun proteomic analysis of the enrichment culture BPL

For proteomics, two independent experiments were performed in a similar way as follows. Extraction of proteins from bacterial cultures was performed as previously described (Abu Laban et al. 2010, Selesi et al. 2010). Comparative proteomic analysis is impossible here, because the culture cannot grow with any of the possible down-stream metabolites like toluene, benzoate, or phenol. Furthermore, it is an enrichment culture, and easily degradable substrates like butyrate and acetate will change the compositions of the microbial community. Thus we performed a qualitative proteomics experiment with benzene as substrate. Cells were harvested from a total of 1200 ml culture by centrifugation (30 min at 3,739 × g and 4°C). The cell pellet was washed three times with 1× phosphate buffered saline (PBS buffer), and resuspended in a mixture of 400 µl lysis buffer, including 9 M urea, 2 M thiourea, 4% 3-[(3-cholamidopropyl)-dimethylammonio]-1-propanesulfonate (CHAPS), and 1% dithiothreitol (DTT), and 66.8 µl of a 7× stock solution containing a complete EDTA-free mini-protease inhibitor cocktail tablet

(Roche Diagnostics GmbH, Penzberg, Germany). After 30 min of incubation at room temperature, the cell-buffer mixture was subjected to sonication in an ice-water bath for two minutes (amplitude: 0.3, cycle: 60%; UP50H, Hielscher GmbH, Germany). The homogenized solution was centrifuged for 10 min at 20,000 × g and 4°C. The supernatant was treated for 30 min at room temperature with 4 µl nuclease mix (GE Healthcare) and centrifuged for 30 min at 15,000 × g and 4°C. Estimation of protein concentrations in the supernatant was performed with the two-dimensional Quant kit according to the protocol of the manufacturer (GE Healthcare). However, quantification of protein was affected by interference with ferrous sulfide, prohibiting a proper estimation of protein concentrations.

For sample preparation, a modified filter-aided sample preparation (FASP) approach was performed (Wisniewski et al. 2009). After tryptic digestion, samples were stored at -20°C until further use.

LC-MS/MS analysis was performed as described previously on a LTQ-Orbitrap XL (Thermo Fisher) (von Toerne et al. 2013). Briefly, the pre-fractionated samples were automatically injected and loaded onto the trap column (Acclaim PepMap100, C18, 5 µm, 100 Å pore size, 300 µm ID × 5 mm µ-Precolumn - No 160454; Thermo Scientific). After 5 min, the peptides were eluted and passed to the analytical column (Acclaim PepMap100, C18, 3 µm, 100 Å pore size, 75 µm ID × 15 cm, nanoViper-No 164568; Thermo Scientific) by reversed phase chromatography which was operated on a nano-HPLC (Ultimate 3000, Dionex). A nonlinear 170 min gradient was used for elution with a mobile phase of 35% acetonitrile in 0.1% formic acid in water (A) and 0.1% formic acid in 98% acetonitrile (B) at a flow rate of 300 nL/min. The gradient settings were: 5-140 min: 14.5-90% A, 140-145 min: 90% A-95% B, 145-150 min: 95% B followed by equilibration for 15 min to starting conditions. The 10 most abundant peptide ions were selected from the MS pre-scan for fragmentation in the linear ion trap if they exceeded an intensity of at least 200 counts and were at least doubly charged. A high-resolution (60,000 full-width half maximum) MS spectrum was acquired in the Orbitrap with a mass range from 200 to 1500 Da during fragment analysis.

MS-MS spectra were searched against the BPL metagenome database (20979 entries) via the MASCOT search engine (version 2.5.1; Matrix Science). A mass tolerance of 10 ppm for peptide precursors and 0.6 Da for MS-MS peptide fragments was applied allowing no more than one missed cleavage. Fixed modifications were set to carbamidomethylation of cysteine and variable modifications to oxidation of methionine and deamidation of asparagine and glutamine.

The Scaffold software (version 4.4.1.1., Proteome Software Inc.) was used to validate peptide identifications and visualize results (Keller et al. 2002). Peptide threshold was set to a false discovery rate (FDR) of 1 percent. A decoy protein FDR of 2.2% was observed. Protein identifications were accepted if two or more unique peptides were identified.

2.4.2 Mass spectrometry-based proteome analyses of N47

For proteomics, the enrichment culture N47 and the culture of high enriched Deltaproteobacteria N47 were grown with naphthalene (four parallel cultures each). In addition, four cultures of *R. cohabitans* strain HM were grown with 10 mM glucose and 0.1% yeast extract. The cultures were harvested in the exponential growth phase and immediately frozen at -20 °C. The frozen cell pellets were warmed to room temperature and taken up in 1 mL phosphate buffered saline (PBS). The samples were lysed by ultrasonification in a Bioruptor® (Diagenode) for 5 min to break the cells, release the proteome and shear the genomic DNA. The turbid solution was cleared by centrifugation (12,000 × g, 4 °C, 5 min). The supernatant was transferred to a fresh 1.5 mL Eppendorf tube. The protein concentration was determined by using a modified Bradford assay (RotiNanoquant; Roth) following the manufacturer's instructions.

Reduction/alkylation and tryptic digestion. An aliquot corresponding to 25 µg total protein content was removed from each sample. Sodium dodecyl sulfate (SDS) and dithiothreitol were added to a final concentration of 2% and 5 mM respectively. The protein solution was incubated at 90 °C for 5 min. After the samples had cooled down to room temperature, 20 mM iodoacetamide was added and the

samples were incubated for 30 min at ambient temperature. A chloroform/methanol precipitation was performed in order to remove the reducing and alkylating agents and to remove the SDS (Wessel and Flugge 1984). The obtained protein pellet was then dissolved in 25 µL of 8M urea and 100 mM ammonium bicarbonate and extensively vortexed. The solutions were cleared by centrifugation and the supernatants transferred to 96 well plates (Eppendorf). To start the protein digestion we added 833 ng Lys-C (1:30; Wako Laboratory Chemicals) and incubated the samples for 3 h at 37 °C. Next the samples were diluted to 25 mM ammonium bicarbonate, supplemented with 1.0 M urea, and 1.25 µg sequencing grade Trypsin (1/20; Promega), and incubated overnight at 37 °C with shaking. On the next morning, the samples were acidified by adding formic acid (final 0.5% v/v).

Sample clean-up for LC-MS. Acidified tryptic digests were desalted on custom-made C18 StageTips as described (Rappsilber et al. 2007). Approximately 15 µg of peptides (based on the initial protein concentration) were loaded to each to two disc StageTip. After elution from the StageTips, samples were dried using a vacuum concentrator (Eppendorf) and the peptides were taken up in 10 µL 0.1 % formic acid solution.

LC-MS/MS. Experiments were performed on an Orbitrap Elite instrument (Thermo) (Michalski et al. 2012) that was coupled to an EASY-nLC 1000 liquid chromatography (LC) system (Thermo). The LC was operated in the one-column mode. The analytical column was a fused silica capillary (75 µm × 30 cm) with an integrated PicoFrit emitter (New Objective) packed in-house with Reprosil-Pur 120 C18-AQ 1.9 µm resin (Dr. Maisch). The analytical column was encased by a column oven (Sonation) and attached to a nanospray flex ion source (Thermo). The column oven temperature was adjusted to 45 °C during data acquisition and in all other modi at 30 °C. The LC was equipped with two mobile phases: solvent A (0.1% formic acid, FA, in water) and solvent B (0.1% FA in acetonitrile, ACN). All solvents were of UHPLC (ultra-high performance liquid chromatography) grade (Sigma). Peptides were directly loaded onto the analytical column with a maximum flow rate that would not exceed the set pressure limit of 980 bar (usually around 0.5 – 0.8 µL/min). Peptides were subsequently separated on the analytical column

by running a 300-min gradient of solvent A and solvent B (start with 7% B; gradient 7% to 35% B for 280 min; gradient 35% to 100% B for 10 min and 100% B for 10 min) at a flow rate of 300 nl/min. The mass spectrometer was operated using Xcalibur software (version 2.2 SP1.48). The mass spectrometer was set in the positive ion mode. Precursor ion scanning was performed in the Orbitrap analyzer (FTMS; Fourier Transform Mass Spectrometry) in the scan range of *m/z* 300-1800 and at a resolution of 60,000 with the internal lock mass option turned on (lock mass was 445.120025 *m/z*, polysiloxane) (Olsen et al. 2005). Product ion spectra were recorded in a data dependent fashion in the ion trap (ITMS; Ion Trap Mass Spectrometry) in a variable scan range and at a rapid scan rate. The ionization potential (spray voltage) was set to 1.8 kV. Peptides were analyzed using a repeating cycle consisting of a full precursor ion scan (1.0×10^6 ions or 30 ms) followed by 15 product ion scans (1.0×10^4 ions or 50 ms) where peptides are isolated based on their intensity in the full survey scan (threshold of 500 counts) for tandem mass spectrum (MS2) generation that permits peptide sequencing and identification. CID (collision-induced dissociation) collision energy was set to 35% for the generation of MS2 spectra. During MS2 data acquisition dynamic ion exclusion was set to 60 seconds with a maximum list of excluded ions consisting of 500 members and a repeat count of one. Ion injection time prediction, preview mode for the FTMS, monoisotopic precursor selection and charge state screening were enabled. Only charge states higher than 1 were considered for fragmentation.

Peptide and Protein Identification using MaxQuant. RAW spectra were submitted to an Andromeda (Cox et al. 2011) search in MaxQuant (version 1.5.0.25) using the default settings (Cox and Mann 2008). Label-free quantification and match-between-runs was activated (Cox et al. 2014). MS/MS spectra data were searched against the in-house generated protein sequences of Deltaproteobacteria N47 (5297 entries) (Bergmann et al. 2011a, Selesi et al. 2010) and *Rectinema cohabilitans* HM (2580 entries). All searches included a contaminants database (as implemented in MaxQuant, 267 sequences). The contaminants database contains known MS contaminants and was included to estimate the level of contamination. Andromeda searches allowed oxidation of methionine residues (16

Da), acetylation of protein N-terminus (42 Da), Carbamylation (K) and Deamidation (NQ) as dynamic modification and the static modification of cysteine (57 Da, alkylation with iodoacetamide). Enzyme specificity was set to “Trypsin/P”. The instrument type in Andromeda searches was set to Orbitrap and the precursor mass tolerance was set to ±20 ppm (first search) and ±4.5 ppm (main search). The MS/MS match tolerance was set to ±0.5 Da. The peptide spectrum match FDR and the protein FDR were set to 0.01 (based on target-decoy approach). Minimum peptide length was seven amino acids. For protein quantification, unique and razor peptides were allowed. Modified peptides were allowed for quantification. The minimum score for modified peptides was 40.

Data Analysis: Initial data analysis was performed by using the PERSEUS computational platform (version 1.5.5.3) (Tyanova et al. 2016). The mass spectrometry proteomics data have been deposited to the ProteomeXchange Consortium via the PRIDE (Vizcaino et al. 2016) partner repository (https://www.ebi.ac.uk/pride/archive/) with the dataset identifier PXD005624.

2.5. Spatial distribution profiles of microbial activities in GAC biofilms

Three parallel down-flow granular activated carbon (GAC) filters (GAC 1 – 3, 30 cm diameter, 180 cm length each) placed after an ozonation unit were used in this study. They are parts of a pilot plant (Muelheim, Germany) treating raw water from Ruhr River for drinking water production using a similar procedure as reported previously (Hammes et al. 2008). The water for the pilot plant originates from the river Ruhr. Before it enters the pilot plant it is filtered by slow sand filtration followed by ozonation. After ozonation the water is filtered by the multilayer filter which removes particulate impurities. Afterwards the water enters the GAC filters 1 and 2 filled with NORIT® GAC 830 as well as GAC filter 3 filled with NORIT® ROW 0.8 Supra. In the GAC filters mainly adsorption occurs. However, over time biofilms develop on the GAC turning it biologically active leading to the bio-degradation of organic compounds. When effluent DOC concentrations remained relatively stable, DOC was predominately removed by biological oxidation and GAC became biologically active carbon. At this stage, samples were taken to investigate the spatial distribution of microbial activities (Figure 6).

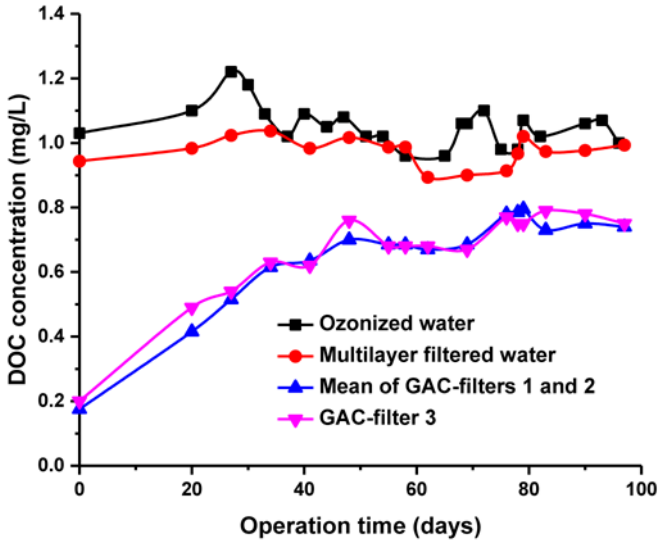

Figure 6. Evolution of influent and effluent DOC concentrations of the granular activated carbon filters as a function of time.

The GAC samples were taken from various depths of GAC filters (0 cm, 20 cm, 40 cm, 80 cm and 140 cm). For RIL experiments, the GAC particles from different depths were divided into triplicate portions (3 g each), and then transferred to three separate 250 mL serum bottles filled with 50 mL influent water (after ozonation) under a laminar flow box. Large air headspace was reserved to ensure oxic conditions in the closed bottles. For each microcosm, $NaH^{13}CO_3$ and $NaH^{12}CO_3$ at a ratio of 10:90 were injected separately through the stopper to produce a mixture of 10 mM bicarbonate in the medium. All bottles were incubated at 17 ^{o}C in the dark to mimic the temperature conditions of GAC filters. The pH values were regularly checked and remained stable at around 7 during the whole experiments.

2.6. Analytical methods

Toluene concentrations were determined using headspace analyses by GC/MS (GC, Trace-DSQ; MS, Thermo Finnigan, San Jose, CA) in selective ion monitoring mode with a fused-silica capillary column DB-5 as previously described (Abu Laban et al. 2009). Total concentrations of toluene in the cultures were calculated from the concentrations in the liquid phase and in the headspace using the dimensionless air water partitioning constant K_{aw} at 25 °C of 0.235 (Staudinger and Roberts 1996).

As we added naphthalene and 2-methynapthalene in 2,2,4,4,6,8,8-heptamethylnonane as carried phase prohibiting a reliable direct quantification of substrate concentrations (Kleemann and Meckenstock 2011), sulfate consumption was monitored using the barium-gelatin method to indirectly quantify naphthalene and 2-methynapthalene degradation (Tabatabai 2009). Iron(II) production was measured with the ferrozine assay (Stookey 2002). Cell growth was monitored by microscopically counting cell numbers.

Hydrogen was measured with a Shimadzu GC-8A Gas Chromatography according to Schuler and Conrad (1990). Briefly, aliquots of headspace air (250 µL) were firstly sampled from the headspace of the cultures after shaking by using a gas-tight syringe (VICI Precision Sampling). Then high concentrations of hydrogen (>100 ppmv) were measured with a thermal conductivity detector whereas low concentrations of hydrogen (<100 ppmv) with a reduction gas detector (RGD2 detector, Trace Analytical, Stanford, CA, USA). The measurements were calibrated with standard H_2 gases (Messer Schweiz) (2 and 50 ppmv for samples lower than 100 ppmv, 1,000 ppmv for samples higher than 100 ppmv).

2.7. Analysis of carbon stable isotope ratios

2.7.1 Sample preparation for carbon isotope ratio measurements

For sample preparation, we adopted a procedure which is used to analyze carbon isotope ratios in natural water samples by taking liquid samples and liberate CO_2 using phosphoric acid as reported previously (Assayag et al. 2006). (1) For GC-IRMS measurements, 0.5 mL liquid samples were directly taken from the culture bottles and immediately injected into 15 mL serum bottles sealed with butyl rubber stoppers. The vial had been pre-filled with 4.5 mL phosphoric acid (1M) and flushed with nitrogen or helium gas. (2) For IRIS measurements, 50 µL of 85% phosphoric acid were introduced into an uncapped 12 mL Labco Exetainer vial (Labco Limited, United Kingdom). Then, the vial was closed with screw-capped pierceable butyl rubber septa and flushed with CO_2-free synthetic air via an ASX-7100 autosampler (Teledyne CETAC Technologies, Omaha, USA) for two minutes. Afterwards, an aliquot (0.5 mL) from the culture bottle was taken and

injected into the vial through the septum. Then, we left the sample to equilibrate at stable room temperature overnight to liberate all CO_2 into the headspace.

2.7.2 Expression of carbon isotope ratios

All carbon isotope ratios ($^{13}C/^{12}C$, referred to as *R*) are reported in conventional delta notation ($\delta^{13}C$) as per mil (‰) values, relative to the Vienna Pee Dee Belemnite (VPDB) standard (Equation 1).

$$\delta^{13}C = \frac{R_{sample}}{R_{VPDB}} - 1 \quad (1)$$

where 0.0111802 is the ratio of $^{13}C/^{12}C$ in VPDB standard. To facilitate the comparison of results which are obtained from samples highly enriched in ^{13}C compared to natural samples, all carbon isotope ratios in this study were converted into ^{13}C atom fractions ($x(^{13}C)$) (%) from $\delta^{13}C$ values according to previous study (Coplen 2011).

2.7.3 Isotope Ratio Mass Spectrometry

CO_2 samples (100 µL) were taken from the headspace of 15 mL serum bottles with a gas-tight syringe and manually injected into a GC-IRMS system consisting of a TRACE GC Ultra gas chromatograph with split/splitless injector (GC) (both Thermo Fisher Scientific Corporation, Milan, Italy) coupled to a Finnigan MAT 253 isotope ratio mass spectrometer (IRMS) connected via a Finnigan GC combustion III interface (Thermo Fisher Scientific Corporation, Bremen, Germany). The temperature of the injector was held at 150 °C for 360 seconds. Helium 5.0 (AirLiquide, Oberhausen, Germany) was used as carrier gas with a constant flow rate of 1.6 mL min^{-1}. The split flow was fixed at 160 mL min^{-1}. CO_2 was separated from other gases using a 30 m Rtx-Qbond column with an inner diameter of 0.32 mm and a film thickness of 10 µm (Restek GmbH, Bad Homburg, Germany). Certified pure CO_2 gas ($\delta^{13}C$ = -35.28 ‰) (AirLiquide, Oberhausen, Germany) was used as working reference gas. All samples were measured in triplicate. When compared to isotope ratio mid-infrared spectroscopy (IRIS), a secondary standard

of $^{13}CO_2$ gas ($x(^{13}C)$ = 10%, Sigma-Aldrich, Taufkirchen, Germany) was analyzed to correct data using a two-point calibration approach.

2.7.4 Isotope Ratio Mid-Infrared Spectroscopy

Samples were analyzed using a Thermo Fisher Delta Ray CO_2 Isotope Ratio Infrared Spectrometer with Universal Reference Interface (URI) Connect (Di Martino et al. 2016, Fischer and Lopez 2016, Rizzo et al. 2015, van Geldern et al. 2014). IRIS is capable of measuring both carbon and oxygen isotope compositions of CO_2 in air. The instrument's analyzer uses a tunable diode laser absorption (TDLA) technique operated at a mid-infrared wavelength of 4.3 µm. During analysis, the laser scans over the absorption lines for the various CO_2 isotopologues of the sample (i.e. $^{12}C^{16}O^{16}O$, $^{13}C^{16}O^{16}O$, and $^{12}C^{16}O^{18}O$) and fits the average signal spectrum to a reference to simultaneously quantify CO_2 isotope ratios. CO_2-free synthetic air (Air Liquide, Düsseldorf, Germany) was used as the carrier gas. CO_2 in synthetic air at 414.2 ppm (Air Liquide, Düsseldorf, Germany) was used for CO_2 concentration calibration. Before measurements, two pure CO_2 reference gases were used for calibration of carbon isotope ratios: one with $\delta^{13}C$ values of -9.7‰ ($x(^{13}C)$ = 1.10%, Thermo Fisher, Bremen, Germany) and the other with $x(^{13}C)$ = 10% (Sigma-Aldrich, Taufkirchen, Germany). For sample measurements, pure CO_2 gas with $x(^{13}C)$ = 10% was used as working reference gas and samples were bracketed with working reference gas. The CO_2 concentration for the working reference gas and the sample gas coming into the analyzer was set to 380 ppm to achieve optimal precision. The $\delta^{13}C$ values were reported as average of five minutes' measurements. The long measurement time under constant gas flows implies that IRIS needs a relatively larger gas sample size compared to IRMS.

2.8. Calculations of CO_2 production using carbon isotope ratios

The conversions of $x(^{13}C)$ changes to CO_2 production were based on isotope mass balance equations as follows.

(1). CO_2 production under anoxic conditions was calculated following two mass balance equations:

$$CO_{2_{total}} = CO_{2_{background}} + CO_{2_{produced}} \quad (2)$$

$$CO_{2_{total}} \times x(^{13}C)_{total} = CO_{2_{background}} \times x(^{13}C)_{background} + CO_{2_{produced}} \times x(^{13}C)_{produced} \quad (3)$$

where $CO_{2_{total}}$ is the final amount of total inorganic carbon in the system (mmole), $CO_{2_{background}}$ is the initial total inorganic carbon in the system (mmole), $CO_{2_{produced}}$ is the total released CO_2 from microbial mineralization of aromatic compounds (mmole), $x(^{13}C)_{total}$ is the final carbon isotope ratio of total inorganic carbon in the system, $x(^{13}C)_{background}$ is the initial carbon isotope ratio of total inorganic carbon in the system, $x(^{13}C)_{produced}$ is the carbon isotope ratio of CO_2 released from microbial production, assumed to be 1.1%. $CO_{2_{background}}$ can be calculated from the initial total DIC content in the liquid ($DIC_{measured}$) and the volume of 20% CO_2 gas in the headspace (confirmed by measurements, $0.2 \cdot n_{gas,headspace}$) :

$$CO_{2_{background}} = DIC_{measured} + 0.2 \cdot n_{gas,headspace} \quad (4)$$

Thus, the total CO_2 production can be obtained via Equation 5 which is based on the combination of Equations 2 - 4:

$$CO_{2_{produced}} = \frac{(DIC_{measured} + 0.2 \cdot n_{gas,headspace}) \times (x(^{13}C)_{background} - x(^{13}C)_{total})}{x(^{13}C)_{total} - x(^{13}C)_{produced}} \quad (5)$$

For data interpretation, we evaluated isotope ratios of CO_2 from the liquid phase without further correction, since equilibrium carbon isotope fractionation between the carbonate species acts on all samples in the same way and cancels out in the comparison between standard and samples. Therefore, the carbon isotope ratio of DIC can be taken as representative of the whole closed system:

$$x(^{13}C)_{total} = x(^{13}C)_{total\ DIC} \quad (6)$$

$$x(^{13}C)_{background} = x(^{13}C)_{background\ DIC} \quad (7)$$

(2). CO_2 production under oxic conditions was calculated based on the same mass balance equations as under anoxic conditions (Equations 2 and 3). As negligible amounts of CO_2 exist in the headspace, $CO_{2_{background}}$ can be calculated using different equation:

$$CO_{2_{background}} = CO_{2_{\text{bicarbonate solution}}} + CO_{2_{natural}} \quad (8)$$

Where $CO_{2_{\text{bicarbonate solution}}}$ is the amount of inorganic carbon in the added bicarbonate solution (mmole) and $CO_{2_{natural}}$ is the amount of inorganic carbon in the natural water (mmole). Thus, the total CO_2 production can be obtained via Equation 5 which is based on the combination of Equations 2, 3 and 8:

$$CO_{2_{produced}} = \frac{\left(CO_{2_{natural}} + CO_{2_{\text{bicarbonate solution}}}\right) \times \left(x(^{13}C)_{background} - x(^{13}C)_{total}\right)}{x(^{13}C)_{total} - x(^{13}C)_{produced}} \quad (9)$$

$CO_{2_{natural}}$ can be obtained via the following equation:

$$CO_{2_{background}} \times x(^{13}C)_{background} = CO_{2_{\text{bicarbonate solution}}} \times x(^{13}C)_{\text{bicarbonate solution}} + CO_{2_{natural}} \times x(^{13}C)_{natural} \quad (10)$$

$x(^{13}C)_{\text{bicarbonate solution}}$ is the carbon isotope ratio of the added bicarbonate solution and $x(^{13}C)_{natural}$ is the carbon isotope ratio of the natural water (assuming that the carbon isotope ratio of the natural water is 1.1%).

3. Results

3.1. Reconstructing metabolic pathways of a member of the genus *Pelotomaculum* suggesting its potential to oxidize benzene to carbon dioxide with direct reduction of sulfate

Benzene is a widely distributed pollutant in groundwater posing a hazardous risk to drinking water resources (Manoli and Samara 1999). Several recent microcosm studies and lab cultures have shown that benzene and other aromatic compounds can be mineralized to CO_2 under nitrate-reducing, iron-reducing, sulfate-reducing, and methanogenic conditions (Kunapuli et al. 2007, Luo et al. 2014, Musat and Widdel 2008, Ulrich and Edwards 2003, van der Zaan et al. 2012). The enrichment culture BPL used in this study is able to degrade benzene with sulfate as electron acceptor (Abu Laban et al. 2009). Previous community analysis based on 16S rRNA gene sequencing and FISH revealed that the dominant bacterial member (~95%) belongs to the phylum Firmicutes genus *Pelotomaculum* (Abu Laban et al. 2009). Members of the genus *Pelotomaculum* are mostly obligate syntrophs that need methanogens as syntrophic partners to oxidize propionate, alcohols, or aromatic compounds (Imachi et al. 2002, Stams and Plugge 2009). However, it is hypothesized here that the anaerobic benzene degradation in the enrichment culture BPL is performed as a single cell process by a novel member of the genus *Pelotomaculum* which is able to reduce sulfate as electron acceptor.

3.1.1 Phylogenetic binning and proteome

Metagenomic sequencing of enrichment culture BPL yielded an assembly of 16.9 million base pairs into 5,842 contigs with a N50 of 12.3 thousand base pairs. Gene prediction with the IMG/M pipeline produced 20,979 open reading frames with 12,736 (60.03%) being assigned to a putative functional name.

The metagenome contigs were manually divided into four genome bins: (1) *Pelotomaculum* operational taxonomic unit (OTU) (described as *Pelotomaculum* candidate BPL) with a relative abundance of 54.27%; (2) *Gracilibacter* OTU with 32.40%; (3) *Desulfomonile* OTU with 7.41%; and (4) *Ignavibacterium* OTU with 5.92%. The discrepancy for population abundance estimates for *Pelotomaculum*

candidate BPL between 454 read coverage here and PCR-based 16S rRNA gene frequency reported previously (Abu Laban et al. 2009) can be explained by experimental bias and varying 16S rRNA gene operon copy numbers. For instance, rrnDB v.4.4.4 (Nov 2015) (Stoddard et al. 2015) reports two operons for *Pelotomaculum*, only one for *Desulfomonile* and *Ignavibacterium*, and an unknown number for *Gracilibacter*. The program CheckM v1.0.3 (Parks et al. 2015) was used to determine the completeness and contamination of the four genome bins. Based on the lineage-specific single-copy marker gene analysis by CheckM, the constructed genomes for *Pelotomaculum* and *Gracilibacter* OTUs are 99% and 97% complete, respectively (Figure 7). The genomes for *Desulfomonile* and *Ignavibacterium* OTUs could not be recovered in full length (Figure 7).

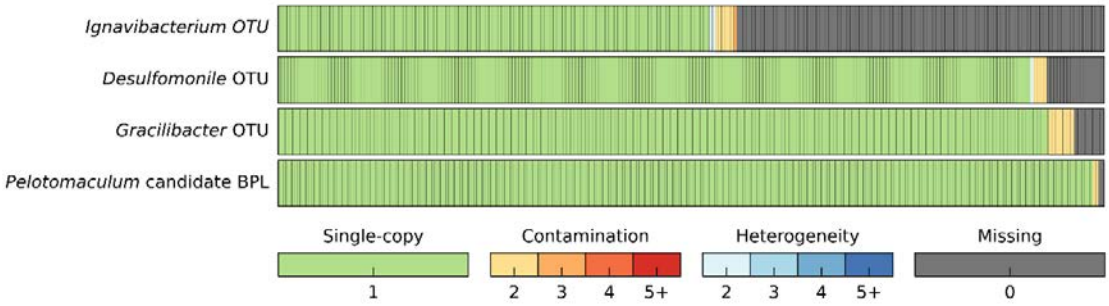

Figure 7. Identification of marker genes within recovered bins with CheckM. Each bar represents a marker gene. Bars in green represent markers identified exactly once, while bars in grey represent missing markers. Markers identified multiple times in the genome are represented by shades of blue or red depending on the AAI between pairs of multi-copy genes and the total number of copies present (2-5+). Pairs of multi-copy genes with an AAI ≥90% are indicated with shades of blue, while genes with less amino acid similarity are shown in red. A gene present 3 or more times may have pairs with an AAI ≥90% and pairs with an AAI < 90%.

The shotgun proteomic analysis of the enrichment culture BPL community from two independent experiments produced a total of 545 proteins encoded by the genes located on the contigs of the metagenome. Almost 97% of the proteins were assigned to both the *Pelotomaculum* candidate BPL (354 proteins, 64%, Table A1) and *Gracilibacter* OTU bin (166 proteins, 30%). We did not analyze the *Desulfomonile* and *Ignavibacterium* OTUs because of their minor abundances in

the metagenome and their low coverage in the proteome (only 3% of the total proteins).

In the genome of *Gracilibacter* OTU (IMG ID: clostridium Ga0073690), no genes for sulfate reduction could be detected. If *Gracilibacter* activated benzene, *Gracilibacter* should have the capability to perform the corresponding downstream degradation. However, among the proteins classified to the *Gracilibacter* OTU, only a few matched enzymes that could be related to benzoate degradation. Possibly the *Gracilibacter* OTU grew by fermentation of metabolites produced by *Pelotomaculum* candidate BPL. For example, an indication could be the identification of pyruvate ferredoxin oxidoreductase in the proteome.

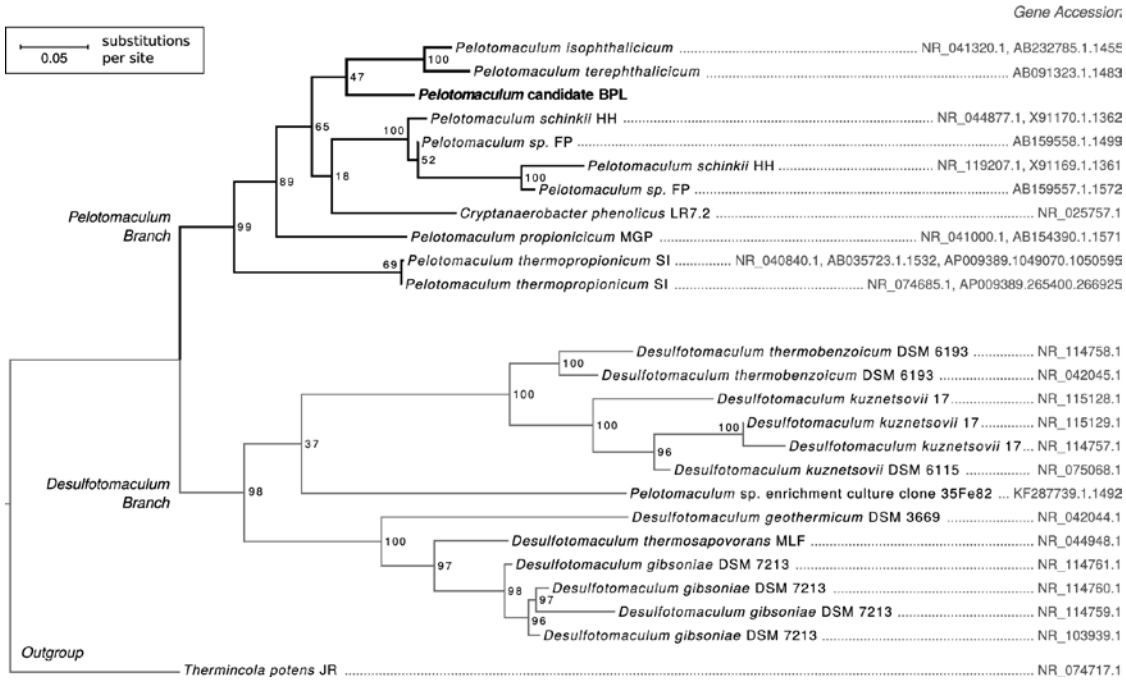

Figure 8. Maximum likelihood tree of near-complete 16S rRNA genes with bootstrap support values (%) showing the phylogenetic affiliation of *Pelotomaculum* candidate BPL. Strain names are followed by the corresponding RefSeq or SILVA sequence identifiers. Thick branch lines indicate a closer phylogenetic neighborhood of *Pelotomaculum* candidate BPL. The sequence of the 16S rRNA gene of *Pelotomaculum* candidate BPL can be found in Database A1.

3.1.2 A novel member of the genus *Pelotomaculum*

The reconstructed *Pelotomaculum* candidate BPL genome (IMG ID: pelotomaculum Ga0073689) consisted of 99 high-quality contigs with a total length of 2.97 Mbp and an average GC content of 53.71%. They were assembled from 454 reads (mean > 500 bp) according to standard procedures in isolate genome sequencing, using a 72-fold average positional coverage. Their length ranges from 1 kb to 234 kb with a mean of 30 kb. *Pelotomaculum thermopropionicum* SI is the only strain in the genus *Pelotomaculum* for which a full genome is available in the public resources. The genome has a total length of 3.03 Mbp with an average G+C content of 53.0%. It is reported to be a fermenting syntrophic organism whose metabolism depends on coupling with other microbes. Thus, we performed genomic comparisons between the *Pelotomaculum* candidate BPL and the *Pelotomaculum thermopropionicum* SI genomes (NCBI Reference Sequence: NC_009454.1). Comparative analyses of the average nucleotide identity (ANI) based on the IMG/M platform indicated that the two genomes represent different *Pelotomaculum* species, with an ANI value of 75.98%, far below an ANI threshold range for species delineation (95–96%) (Kim et al. 2014). This was in agreement with their low 16S rRNA gene sequence identity (< 95%). The corresponding identity scatter plot showed that the contigs from *Pelotomaculum* candidate BPL covered the entire genome of *Pelotomaculum thermopropionicum* SI (Figure A1). However, the nucleotide sequence similarity was limited leaving many gaps (Figure A1), which emphasized the differences between the reconstructed *Pelotomaculum* candidate BPL genome and the RefSeq isolate genome sequence. The gene distributions of the genomes were compared for Clusters of Orthologous Groups (COG). We found significant differences in the COG categories distributions at the level of $p < 0.05$ by the Chi-squared test, with several differences in the reference genome of *Pelotomaculum thermopropionicum* SI (Figure A2), indicating different metabolic capacities. Employing a phylogenetic analysis of the near-complete 16S rRNA gene (position 113-1661, Database A1), we found that among known members of the *Peptococcaceae* family, the BPL candidate is clearly separate from *Pelotomaculum thermopropionicum* SI (Figure 1). Furthermore, it has the closest

phylogenetic relationship (with 95% 16S rRNA gene sequence similarities) to *Pelotomaculum isophthalicicum* and *Pelotomaculum terephthalicicum* that both can utilize benzoate and other low-molecular weight aromatic compounds when grown in co-culture with hydrogenotrophic methanogens (Qiu et al. 2006) (Figure 8).

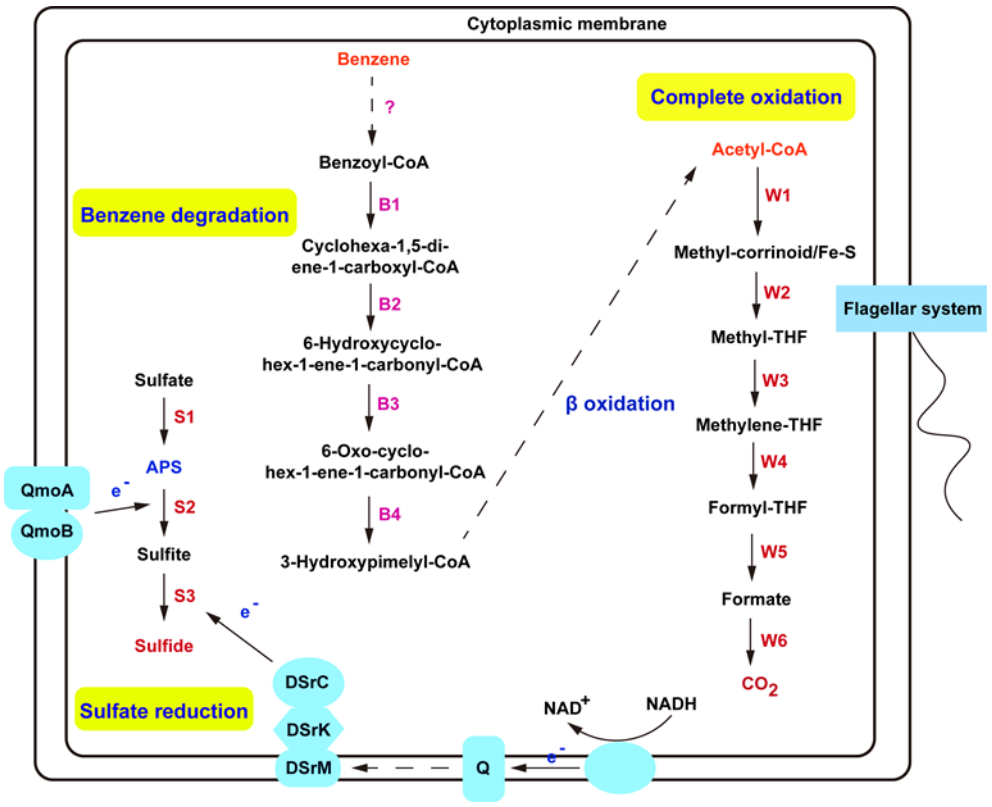

Figure 9. Metabolic pathway reconstruction for *Pelotomaculum* candidate BPL. Benzene degradation and sulfate reduction pathways are evidenced by proteome analysis. Numbers correspond to the following enzymes: B1, class II benzoyl-CoA reductase (Bam type); B2, cyclohex-1,5-diencarbonyl-CoA hydratase; B3, 6-hydroxycyclohex-1-ene-1-carbonyl-CoA dehydrogenases; B4, 6-oxo-cyclohex-1-ene-carbonyl-CoA hydrolase; W1, carbon monoxide dehydrogenase/acetyl-CoA synthetase; W2, 5-methyltetrahydrofolate methyltransferase; W3, methylenetetrahydrofolate reductase; W4, methylene-tetrahydrofolate dehydrogenase; W5, formate-tetrahydrofolate synthetase; W6, formate dehydrogenase; S1, ATP sulfurylase, S2, adhenosine-5'-phosphosulfate reductase; S3, dissimilatory sulfite reductase. Abbreviations are: APS, adenosine-5'-phosphosulfate; QmoAB, quinone-interacting membrane-bound oxidoreductase; DsrABC, dissimilatory sulfite reductase cytoplasmic subunits; DsrMK, transmembrane dissimilatory sulfite reductase complex; e^-, electron.

3.1.3 Initial activation of benzene

In order to find evidence for methylation as the initial activation reaction, we tried to identify genes related to anaerobic degradation of toluene in the genome. Benzylsuccinate synthase (Bss) is a key enzyme in the anaerobic toluene degradation pathway. However, we could neither identified *bss* alpha-subunit (*bssA*)-like genes in the genome nor genes for beta-oxidation of benzylsuccinate to benzoyl-CoA. Thus, we exclude a degradation of benzene via methylation to toluene. Anaerobic phenol degradation to benzoyl-CoA was known to proceed with the participation of phenylphosphate synthase, phenylphosphate carboxylase, 4-hydroxybenzoate-CoA ligase and 4-hydroxybenzoyl-CoA reductase (Abu Laban et al. 2010). Only a few hits could be identified for genes showing homology to individual subunits of these enzymes. However, when looking at the genetic context, genes encoding for the other subunits of these proteins which would be needed to build catalytically active enzymes are lacking. The absence of relevant key genes for anaerobic phenol degradation excludes activation of benzene via hydroxylation in this culture. The earlier reported inability of culture BPL to grow on toluene or phenol confirmed this genomic analysis (Abu Laban et al. 2009).

Previous metabolite analyses (e.g. benzoate as an intermediate) and substrate tests indicated a direct carboxylation of benzene as the initial activation mechanism for *Pelotomaculum* candidate BPL (Abu Laban et al. 2009). Thus, we searched for genes encoding for the proposed anaerobic benzene carboxylase (AbcA and AbcD) responsible for direct carboxylation to benzoate in the iron-reducing culture BF (Abu Laban et al. 2010). In the genome of *Pelotomaculum* candidate BPL, we identified one gene copy (Ga0073689_2617920776) assigned as 4-hydroxy-3-polyprenylbenzoate decarboxylase which shared 33% amino acid sequence identity to the anaerobic benzene carboxylase gene *abcA*. However, no *abcD* homologue could been detected in the proximity of gene Ga0073689_2617920776 and no gene product of gene Ga0073689_2617920776 could be identified in the proteome. We thus conclude that *Pelotomaculum* candidate BPL does not utilize an anaerobic benzene carboxylase similar to culture BF.

Furthermore in culture BF, a gene for a putative benzoate-CoA ligase was located next to the carboxylase genes. This ligase is intended to convert the carboxylation product benzoate to benzoyl-CoA which can be further degraded through the benzoyl-CoA degradation pathway. If benzene carboxylation occurred, we would expect genes encoding benzoate-CoA ligase which further activates benzoate to benzoyl-CoA in the genome. In *Geobacter metallireducens* GS-15, there are two different enzymes for benzoyl-CoA production: the ATP-dependent benzoate-CoA ligase (BamY) and succinyl-CoA: benzoate CoA transferase (Bct) (Oberender et al. 2012). Three hits (Ga0073689_2617922070, 2617921892, and 2617920988) were obtained in our genome showing only 27-29% amino acid sequence identities to the *bamY* gene of *Geobacter metallireducens* GS-15. Additionally, we could not identify genes homologous to *bct* in *Geobacter metallireducens* GS-15 or the putative benzoate-CoA ligase *bzlA* in the iron-reducing enrichment culture BF (Abu Laban et al. 2010).

3.1.4 Central benzoyl-CoA degradation pathway

According to present knowledge, anaerobic degradation of benzene has to proceed via the central intermediate, benzoyl-CoA, regardless of the initial activation mechanisms. Two distinct classes of benzoyl-CoA reductases (BCRs) are presently known for the reduction of benzoyl-CoA to cyclohexa-1,5-diene-1-carboxyl-CoA (dienoyl-CoA). The ATP-dependent Class I BCR (BcrABCD) is predominantly found in facultative anaerobes; the ATP-independent and tungsten cofactor-containing class II BCR (BamBCDEFGHI) occurs in obligate anaerobic bacteria (Fuchs et al. 2011, Kung et al. 2009, Loffler et al. 2011). As expected for an obligate anaerobic sulfate reducer degrading aromatic compounds, a protein similar to the active site subunit of the class II BCR in *Geobacter metallireducens* GS-15 (BamB, Ga0073689_2617921884) was detected in the proteome (Figure 9 and Table A1). The gene is located adjacent to a *bamC* paralogue (Ga0073689_2617921883) with 66% amino acid sequence identity to the *bamC* gene in *Geobacter metallireducens*. Candidate genes for *bamDEFGHI* putatively encoding benzoyl-CoA reductase were identified in at least one copy in the genome of *Pelotomaculum* candidate BPL. They shared amino acid sequence identities ranging from 33% to 71% to the respective proteins described in

Geobacter metallireducens GS-15 (Loffler et al. 2011, Wischgoll et al. 2005), indicating that *Pelotomaculum* candidate BPL degraded benzoate-CoA via the class II benzoyl-CoA reductase (Bam type).

Products of a gene cluster (Ga0073689_2617919856-8) were detected in the proteome putatively encoding 6-oxo-cyclohex-1-ene-carbonyl-CoA hydrolase (Oah), cyclohex-1,5-diencarbonyl-CoA hydratase (Dch), and 6-hydroxycyclohex-1-ene-1-carbonyl-CoA dehydrogenases (Had), respectively. These genes and gene products suggest further transformation of dienoyl-CoA to 3-hydroxypimelyl-CoA (Figure 9 and Table A1). The hydratase (Dch) could catalyze water addition to a carbon-carbon double bond, followed by dehydrogenation (Had), and hydrolytic ring cleavage (Oah) (Holmes et al. 2012, Wischgoll et al. 2005). Proteins for further β-oxidation of 3-hydroxypimelyl-CoA to acetyl-CoA and CO_2 via glutaryl-CoA were also identified in the proteome, i.e. glutaryl-CoA dehydrogenase (Ga0073689_2617919859), enoyl-CoA hydratase (Ga0073689_2617921893), and 3-hydroxyacyl-CoA dehydrogenase (Ga0073689_2617921894) (Table A1).

3.1.5 Complete oxidation via the Wood-Ljungdahl pathway

For complete oxidation of acetyl-CoA to CO_2, many sulfate reducers run the Wood-Ljungdahl pathway in reverse, also termed as oxidative carbon monoxide dehydrogenase/acetyl-CoA pathway. These are e.g. *Desulfatibacillum alkenivorans* AK-01, *Desulfobacula toluolica* Tol2, *Desulfobacterium autotrophicum* HRM2, or *Desulfotomaculum acetoxidans* DSM 771 (Callaghan et al. 2012, Spormann and Thauer 1988, Strittmatter et al. 2009, Wohlbrand et al. 2013). Likewise, all necessary enzymes involved in the Wood-Ljungdahl pathway were detected in the proteome and encoded in the *Pelotomaculum* candidate BPL genome (Figure 9 and Table A1). Namely, they contained the key enzyme carbon monoxide dehydrogenase/acetyl coenzyme A (CoA) synthetase CODH/ACS (Ga0073689_2617920888 and 2617921376-80), and the enzymes for the methyl branch of the pathway including 5-methyltetrahydrofolate methyltransferase AcsE (Ga0073689_2617921126), methylenetetrahydrofolate reductase MetF (Ga0073689_2617921113), methylene-tetrahydrofolate dehydrogenase FolD (Ga0073689_2617920380), formate-tetrahydrofolate synthetase Fhs

(Ga0073689_2617921323), and formate dehydrogenase FhdA (Ga0073689_2617922225).

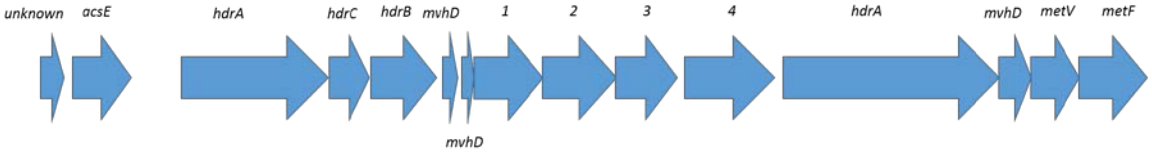

Figure 10. Genomic context of the *metF* gene in the genome of *Pelotomaculum* candidate BPL. Unknown, hypothetical protein; *acsE*, methyltetrahydrofolate-corrinoid iron-sulfur protein Co-methyltransferase; *hdrACB*, heterodisulfide reductase; *mvhD*, methyl-viologen-reducing hydrogenase, delta subunit; 1, 4Fe-4S dicluster domain-containing protein; 2, 4Fe-4S dicluster domain-containing protein; 3, NAD(P)H-flavin reductase; 4, Fe-S oxidoreductase; *metV*, Methylene-tetrahydrofolate reductase C terminal; metF, 5,10-methylenetetrahydrofolate reductase (ferredoxin).

An interesting feature is the detection of genes encoding heterodisulfide reductase (Hdr) related proteins which co-localize with methylenetetrahydrofolate reductase MetF (Ga0073689_2617921113) (Figure 10). The methylenetetrahydrofolate reductase gene *metF* is tightly associated with a gene (Ga0073689_2617921112) designated as the N-terminus of MetF (*metV*) and they are located next to *mvhD* encoding the delta subunit of methyl-viologen-reducing hydrogenase and *hdrA* encoding heterodisulfide reductase iron-sulfur subunit A (Figure 10). The function of the delta subunit MvhD and HdrA is described as transferring reducing equivalents to methylenetetrahydrofolate reductase MetF in an electron-bifurcation process (Buckel and Thauer 2013, Mock et al. 2014, Wohlbrand et al. 2013). Similar gene clusters of *metVF* genes together with the *hdrA-mvhD* genes are also present in other acetate-oxidizing sulfate reducers, i.e. *Desulfatibacillum alkenivorans* AK-01, *Desulfobacula toluolica* Tol2, *Desulfobacterium autotrophicum* HRM2 (Wohlbrand et al. 2013). We conclude that *Pelotomaculum* candidate BPL has a similar way of energy conservation from acetate oxidation and sulfate reduction as described previously for sulfate-reducing bacteria.

Among possible genes of the tricarboxylic acid (TCA) cycle, we have found malate dehydrogenase (NAD) (Ga0073689_2617921286) from the oxidative branch and isocitrate dehydrogenase (NADP) (Ga0073689_2617922024) from the reductive

branch indicating that this part of the genome might be incomplete. Absence of the key enzyme α-ketoglutarate dehydrogenase at least indicates that *Pelotomaculum* candidate BPL cannot operate a TCA cycle for oxidation of acetyl-CoA to CO_2 which agrees with the presence of a complete Wood-Ljungdahl pathway for oxidation of acetate.

3.1.6 Sulfate reduction in the genus *Pelotomaculum*

So far, members of the genus *Pelotomaculum* are supposed to be unable to grow by sulfate reduction (Imachi et al. 2006). However, the closely related genus *Desulfotomaculum* is well-known for sulfate reduction. The key enzymes of dissimilatory sulfate reduction ATP sulfurylase (Sat) (Ga0073689_2617919560), adenosine -5'-phosphosulfate reductase (Apr) (Ga0073689_2617919558-9), and dissimilatory sulfite reductase (Dsr) (Ga0073689_2617920264-5), have been found in the proteome of our *Pelotomaculum* candidate BPL (Figure 9 and Table A1). ATP sulfurylase catalyzes the initial activation of sulfate to adenosine-5'-phosphosulfate (APS) releasing pyrophosphatase. Pyrophosphate can be used to create a proton motive force by an annotated, putative proton-translocating membrane pyrophosphatase (Ga0073689_2617919937). Genome analysis revealed the genes *aprA* and *aprB* encoding the sulfite-forming APS reductase are located adjacent to the *sat* gene. In close proximity to the *sat* and *apr* genes are *qmoAB* genes (Ga0073689_2617919556-7) probably encoding for an adenylylsulfate reductase-associated electron transfer protein which is homologous to heterodisulfide reductases (Ramos et al. 2015). The QmoAB redox complex is proposed to be the electron donor of APS reductase in Gram-positive sulfate-reducing bacteria (Junier et al. 2010). Interestingly, gene Ga0073689_2617919555 was automatically annotated by the IMG platform as the membrane subunit of the QmoABC complex (*qmoC*), which has been observed only in Gram-negative sulfate-reducing bacteria so far (Pereira et al. 2011). Our further search found that the product of the gene lacked transmembrane helices and should therefore encode a different function (Junier et al. 2010). Further reduction of sulfite to sulfide could be catalyzed by dissimilatory sulfite reductase encoded by *dsrAB* genes (Ga0073689_2617920264-5). The electrons for DsrAB reductase are probably transferred from the quinone pool by the DsrMK complex

and DsrC (Junier et al. 2010). According to the Gene Ortholog Neighborhoods tool in the IMG platform, *Pelotomaculum* candidate BPL exhibited the same gene organization for the *dsr* operon as other Gram-positive sulfate-reducing bacteria, e.g. *Desulfotomaculum reducens* MI-1 or *Desulfotomaculum acetoxidans* DSM 771 (Junier et al. 2010). Similar to *Desulfotomaculum reducens* MI-1, the identified *dsrM* (Ga0073689_2617920256) encoding a membrane protein functioning as a conduit to transfer electrons from quinones in *Desulfotomaculum reducens* MI-1 was also annotated as the nitrate reductase gamma subunit in the IMG platform. The electrons for the quinone pool might come from NADH oxidation coupled with proton translocation catalyzed by the energy-conserving NADH-quinone oxidoreductase (Complex I, Ga0073689_2617921751-61). Another essential protein, dissimilatory sulfite reductase subunit C (DsrC, Ga0073689_2617920254) was also identified in the proteome. The proteogenomic data presented here clearly indicate that *Pelotomaculum* candidate BPL has a complete sulfate reduction pathway which is active during anaerobic benzene degradation.

3.1.7 Hydrogenases and formate dehydrogenases

No genes encoding [FeFe] and [NiFe] hydrogenases could be identified in the genome. Their absence suggests that *Pelotomaculum* candidate BPL neither has the capability for H_2 oxidation nor for fermentation with H_2 production. This was unexpected as members of the genus *Pelotomaculum* are typical fermenting organisms and usually possess hydrogenases. Three genes putatively encoding formate dehydrogenases (Ga0073689_2617920664, 2617920666, and 2617922225) were identified in the genome but neither of them could be identified in the proteome. This suggests that formate transfer rather than hydrogen transfer may be important if *Pelotomaculum* candidate BPL would possibly grow in syntrophic fermentation when sulfate is not available.

3.2. Fermentative Spirochaetes drive nutrient cycling by a subsurface microbial loop in hydrocarbon-contaminated habitats

Our studies have shown that Spirochaetes are prominent members of the naphthalene-degrading, sulfate-reducing enrichment culture N47 derived from sediments of a contaminated aquifer (Meckenstock et al. 2000, Selesi et al. 2010). Based on 16S rRNA gene sequence analysis, ~93% of the culture comprises a sulfate-reducing deltaproteobacterium that catalyzes naphthalene degradation and the remainder comprises Spirochaetes (Bergmann et al. 2011a, Selesi et al. 2010). We separated the enrichment culture into a highly enriched Deltaproteobacteria N47 culture (without Spirochaetes) (Bergmann et al. 2011a, Selesi et al. 2010) and a pure isolate of the spirochaete *Rectinema cohabitans* strain HM (Koelschbach et al. 2017). In this work, the aim was to elucidate the functional role of the Spirochaetes in this enrichment culture. Results from physiological, genomic, and proteomic analyses indicated that *R. cohabitans* grows by fermentation of organic compounds derived from dead biomass (necromass), recycling electrons as H_2 and short chain fatty acids or alcohols to the sulfate-reducing Deltaproteobacteria N47. The co-culture of the two organisms thus provides an example of a simple microbial loop. Further comparative and community genome analyses indicated that other Spirochaetes, both uncultured and isolated, are hydrogen-producing fermentative microbes fulfilling similar roles as *R. cohabitans* in supporting biodegradation.

3.2.1 The genome and proteome of *R. cohabilitans* suggest it is an obligate fermenter

A draft genome of *R. cohabitans* HM was sequenced and assembled to develop hypotheses about its ecophysiological role in the naphthalene-degrading culture N47. The 2.82 Mb genome comprises 41 contigs and, based on CheckM analysis (Parks et al. 2015), is estimated to be 98% complete with no measurable strain-level heterogeneity. The organism encodes two 16S-23S-5S ribosomal RNA (rRNA) operons, 46 transfer RNA (tRNA) genes for all 20 amino acids, and 2583 protein-coding sequences. As in other nonspiral Spirochaetes, genes associated

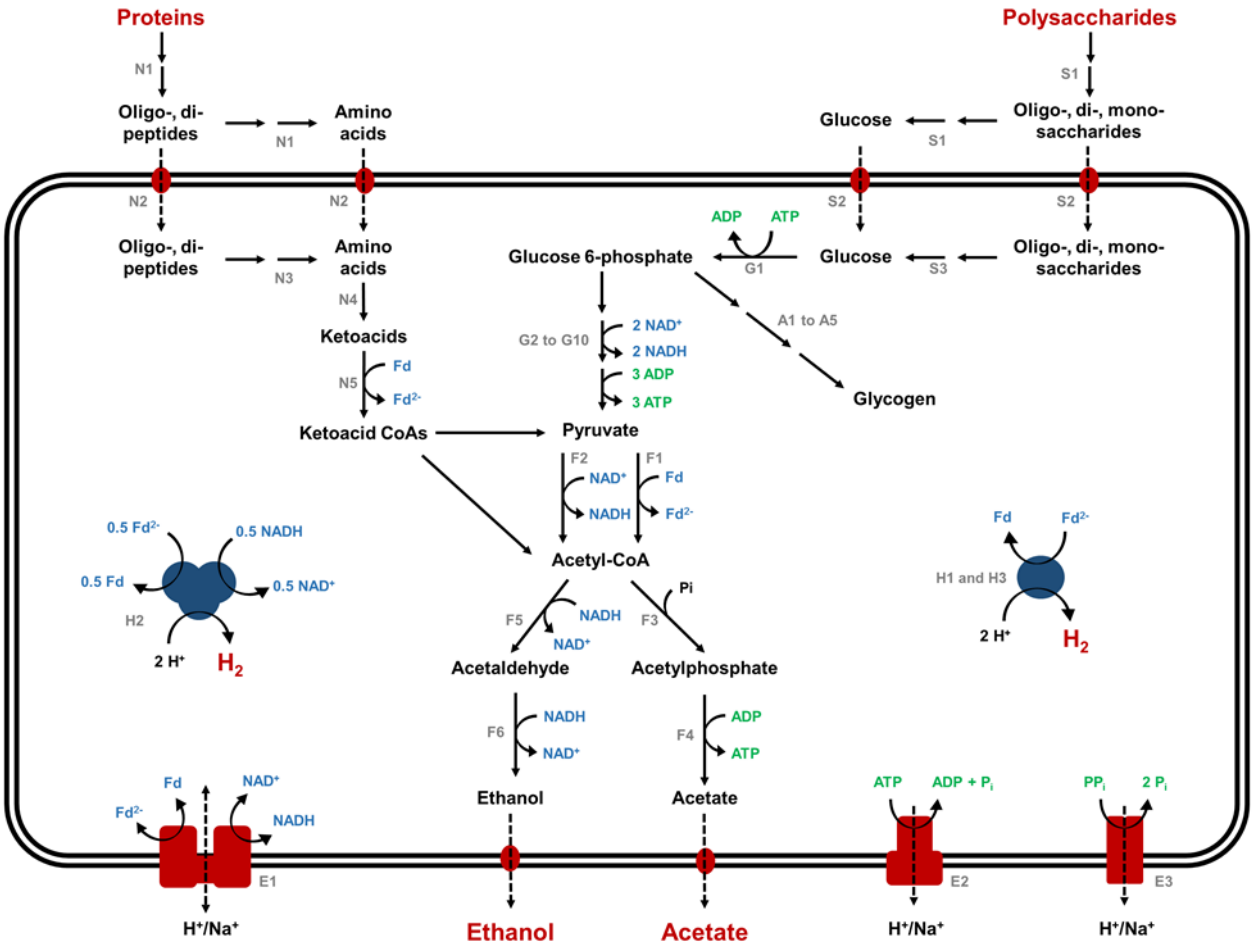

Figure 11. Metabolic pathway reconstruction for Spirochaetes in hydrocarbon- and organohalide-contaminated environments. Genes for the illustrated pathways were detected in the genomes of *R. cohabitans*, uncultured Spirochaetes bacterium bdmA 4, and uncultured Spirochaetes bacterium SA-8. Predicted proteins indicated by numbers in the figure can be found in Table A2.

with motility and chemotaxis are absent (Caro-Quintero et al. 2012). Analysis of the metabolic capacity from the genome suggests *R. cohabitans* adopts a fermentative lifestyle, with a large fraction of enzymes associated with carbohydrate, protein, and molecular hydrogen (H_2) metabolism (Figure 11). In contrast, key genetic determinants of aerobic and anaerobic respiration, the tricarboxylic acid cycle, and acetogenic carbon fixation are absent from the genome. This is consistent with previous work showing that various Spirochaetes isolated from the genera *Sphaerochaeta*, *Spirochaeta*, *Borrelia*, and *Treponema* also adopt an obligately fermentative lifestyle (Caro-Quintero et al. 2012).

The genome suggests that *R. cohabitans* degrades proteins, peptides, and carbohydrates. For example, genes encoding several extracellular peptidases (Merops family M23B, S8A, S26A, and S33) may mediate decomposition of bacterial proteins and cell wall constituents (Figure 11 and Table A2). These enzymes may be secreted by the predicted Type II secretory system encoded in the genome (Table A2). The genome also contains a diverse suite of genes encoding transporters for branched amino-acids, dipeptides, and oligopeptides, suggesting that *R. cohabitans* has the capacity to import hydrolysis products into the cell (Figure 11). Also identified were numerous genes encoding intracellular peptidases, aminotransferases, and four ketoacid-ferredoxin oxidoreductases (Figure 11 and Table A2). The genome also encodes 92 predicted carbohydrate-active enzymes, including hydrolases, extracellular binding proteins and ABC transporters involved in carbohydrate acquisition and breakdown (Figure 11), consistent with its ability to utilize saccharides as carbon sources (Koelschbach et al. 2017).

For central metabolism, the genome encodes a complete Embden-Meyerhof-Parnas glycolysis pathway for oxidizing glucose to pyruvate concomitant with ATP and NADH production (Figure 11 and Table A2). The determinants of the classical pentose phosphate pathway involved in NADPH and pentose synthesis were also found (Table A2). The resulting pyruvate from glycolysis can be converted to acetyl-CoA through ferredoxin-dependent (pyruvate-ferredoxin oxidoreductase) or NAD-dependent (pyruvate dehydrogenase complex) enzymes. Like many other fermenting bacteria, *R. cohabitans* is predicted to convert acetyl-CoA to the

fermentation product acetate with concomitant ATP production by phosphate acetyltransferase and acetate kinase (James et al. 2016). The presence of genes for aldehyde and alcohol dehydrogenases suggests that acetyl-CoA can also be reduced to ethanol in two steps using. Proteomic analysis of *R. cohabitans* grown on glucose revealed that genes related to mixed-acid fermentation were expressed at high peptide abundances (Table A3).

Furthermore, a set of genes are also present in the genome encoding a membrane-bound RnfABCDGE-type redox complex (Figure 11 and Table A2). This complex is frequently found in the genomes of anaerobic organisms, including other obligately fermentative bacteria (Dodsworth et al. 2013, Sorokin et al. 2014), and was recently shown to link the oxidation of reduced ferredoxin and reduction of NAD^+ to electrogenic pumping of protons or sodium ions across the cell membrane (Biegel et al. 2011, Tremblay et al. 2012). This complex is likely to have dual roles in maintaining the redox balance and generating membrane potential to fuel ATP synthesis and active transport. A V-type ATPase and a membrane-associated pyrophosphatase are also likely to support the membrane potential maintenance *via* ATP and pyrophosphate hydrolysis. Proteomic analysis revealed that genes related to the V-type ATPase and pyrophosphatase were expressed at high peptide abundances (Table A3).

3.2.2 Interspecies hydrogen transfer supports a naphthalene-degrading enrichment culture

Hydrogen gas, a diffusible end product of bacterial fermentation and a primary electron source for sulfate-reducing deltaproteobacteria, might be transferred between the members of the N47 enrichment culture (Schwartz et al. 2013). Supporting this hypothesis, we identified putative hydrogenase genes in the genomes of both *R. cohabitans* and Deltaproteobacteria N47 (Bergmann et al. 2011a, Selesi et al. 2010). To gain insight into their potential ecophysiological roles, we classified them using their primary sequence-based phylogeny and genetic organization according to our recently developed hydrogenase classification scheme (Greening et al. 2016, Søndergaard et al. 2016). Seven putative [FeFe]-hydrogenase genes were identified in the genome of the

spirochaete. Three are monomeric [FeFe] Group A1 or B hydrogenases (Figures 12A and 12C) which couple oxidation of reduced ferredoxin to evolution of H_2 during carbohydrate and protein fermentation in diverse bacteria (Wolf et al. 2016). Two others encode the trimeric electron-bifurcating [FeFe] Group A3 hydrogenases (Figures 12A and 12C), which reversibly couple the oxidation of ferredoxin and NADH to the evolution of H_2, thereby providing a novel mechanism to balance redox state and ATP demand. The genome also encodes [FeFe] Group C1 and C3 hydrogenases, both candidate subgroups implicated in H_2 sensing (Søndergaard et al. 2016).

Re-analysis of the genome for Deltaproteobacteria N47 (Bergmann et al. 2011a, Kummel et al. 2015) revealed the presence of two Group 1a and Group 1b [NiFe]-hydrogenases (Figure 12B) that couple H_2 oxidation to cytochrome c_3 reduction in the respiratory chains of sulfate-reducing deltaproteobacteria. Whereas the former sequence is incomplete due to sequence coverage gaps, a complete operon encoding the 1b enzyme and its cytochrome c_3 partner is detectable (Figure 12D) (Greening et al. 2016).

To confirm that *R. cohabitans* is a fermentative H_2 producer, we performed pure culture growth experiments with glucose as carbon substrates. Gas chromatography demonstrated that H_2 rapidly accumulated in the headspace during cultivation with glucose resulting in H_2 concentrations up to 400,000 ppmv after two weeks (Figure 13A). Proteomic analysis of cells grown with glucose confirmed the expression of all hydrogenase-related genes with high peptide abundances (Table A3). Also consistent with genome-based predictions, we observed a gradual decrease in H_2 concertation when highly enriched Deltaproteobacteria N47 was cultivated under naphthalene-degrading, sulfate-reducing conditions and a headspace supplemented with a limited amount of H_2 gas (~ 8285 ppmv) (Figure 13A). Consumption of H_2 by Deltaproteobacteria N47 was inhibited when sodium molybdate ($NaMoO_4$) was added at Day 31 (Figure 13A), a known potent inhibitor of sulfate reduction (Lovley and Klug 1983). This suggests that, in common with classical sulfate-reducing isolates (Schwartz et al. 2013), Deltaproteobacteria N47 directly couples H_2 oxidation to sulfate reduction in an anaerobic respiratory process.

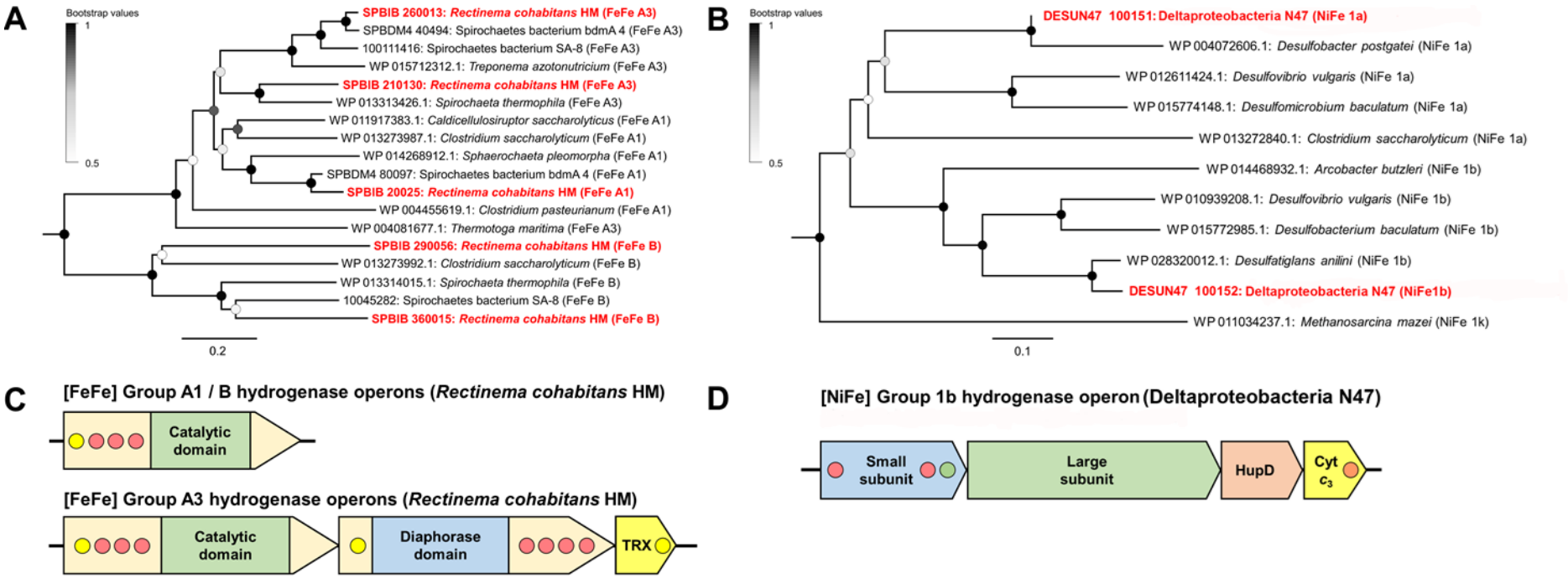

Figure 12. Determinants of H_2 metabolism in Spirochaetes in hydrocarbon- and organohalide-contaminated environments. (A) Phylogenetic tree of the [FeFe]-hydrogenase catalytic subunit sequences detected in *R. cohabitans*, uncultured Spirochaetes bacterium bdmA 4, and uncultured Spirochaetes bacterium SA-8; (B) Phylogenetic tree of the [NiFe]-hydrogenase catalytic subunit sequences detected in Deltaproteobacteria N47; (C) Genetic organization of hydrogenases from *R. cohabitans*; (D) Genetic organization of the hydrogenase operon detected in Deltaproteobacteria N47. The illustrated tree for Figure 12A is condensed, with the full tree in Figures A3. Genetic organization diagrams are shown to-scale and genes/domains are color-coded as follows: green = catalytic site; blue = secondary subunit; yellow = electron acceptor or donor; light orange = maturation factor. Redox-active centers are shown in circles, where: yellow = [2Fe2S] cluster, green=[3Fe4S] cluster, and red = [4Fe4S] cluster.

Finally, in order to reveal a potential mutualistic relationship between the two strains, we monitored H_2 concentrations in the enrichment culture N47, comprising *R. cohabitans* and Deltaproteobacteria N47, under naphthalene-degrading, sulfate-reducing conditions. Under these conditions, the concentration of H_2 remained constant (~ 2 ppmv) for one month (Figure 13A). However, a sharp increase in H_2 concentration was observed when sulfate reduction by Deltaproteobacteria N47 was inhibited due to the addition of sodium molybdate. This suggests that there is a tight coupling between spirochaete-mediated fermentative H_2 evolution and deltaproteobacterium-mediated respiratory H_2 consumption under naphthalene-degrading, sulfate-reducing conditions.

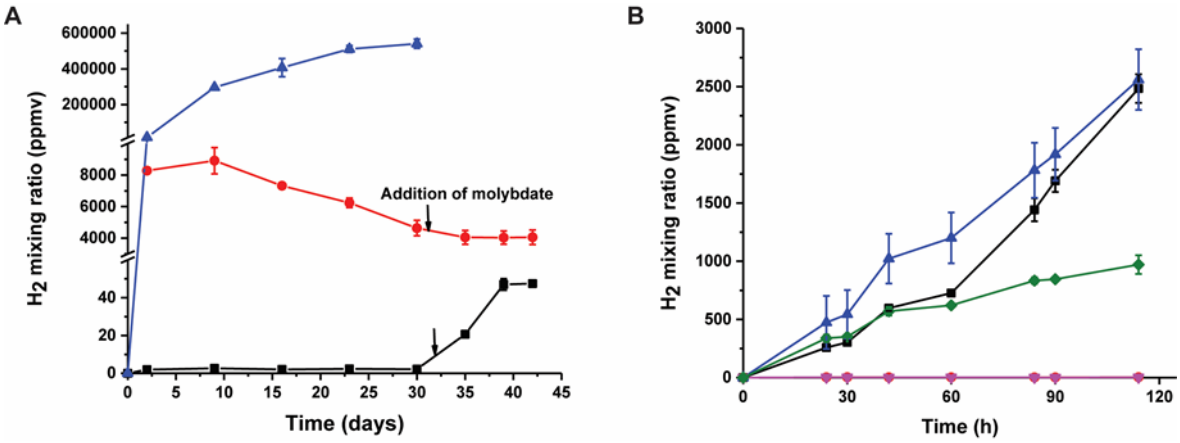

Figure 13. H_2 oxidation and evolution under different growth conditions. (A) Interspecies hydrogen exchange between *R. cohabitans* and Deltaproteobacteria N47. Blue triangles: *R. cohabitans* + glucose; red circles: Deltaproteobacteria N47 + naphthalene + H_2; black squares: co-culture of the two strains + naphthalene. (B) Hydrogen evolution with dead biomass and metabolites as carbon sources for *R. cohabitans*. Blue up-triangles: *R. cohabitans* + killed Deltaproteobacteria N47 cells; black squares: *R. cohabitans* + filtered Deltaproteobacteria N47 supernatant; green diamonds: carry-over control of *R. cohabitans*; red circles: control of filtered Deltaproteobacteria N47 supernatant; pink down-triangles: control of killed Deltaproteobacteria N47 cells. Values are means of two or three individual incubations measured twice each. Error bars indicate SD of biological replicates.

3.2.3 *R. cohabitans* feeds on organic carbon derived from necromass

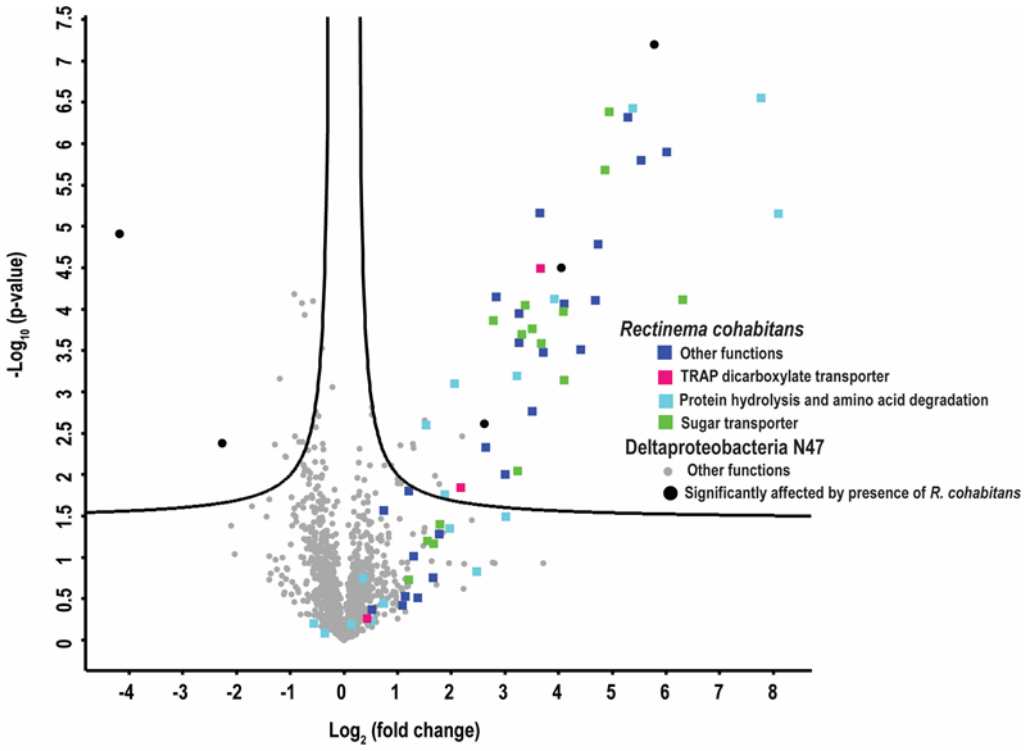

Figure 14. Quantitative proteomic analysis of highly enriched Deltaproteobacteria N47 and enrichment culture N47 grown in the presence of naphthalene. The volcano plot was generated using the PERSEUS software. The calculated Log2 (fold change) (x-axis) was then plotted against the corresponding p-values (y-axis). Proteins to the left and above the significance line are significantly depletes in the co-culture and proteins to the right and above the significance line are significantly enriched in the co-culture. The filled squares indicate proteins from *R. cohabitans*; the filled circles represent proteins from Deltaproteobacteria N47.

While the above results demonstrate that H_2 is an important electron link between *R. cohabitans* and Deltaproteobacteria N47, the question remained about the origin of reducing equivalents (i.e. carbon sources) used for H_2 production by *R. cohabitans*. Considering that *R. cohabitans* cannot utilize naphthalene, its carbon source must be supplied by Deltaproteobacteria N47 given no other exogenous sources were added. Thus, we analyzed the proteomes of *R. cohabitans* and Deltaproteobacteria N47 grown as highly enriched Deltaproteobacteria N47 and enrichment culture N47 respectively. Comparing the proteomes of the two cultures

under naphthalene-degrading conditions revealed that only five proteins of Deltaproteobacteria N47 were differentially expressed, none of which could be assigned a distinct ecophysiological role (Figure 14). However, 53 proteins belonging to *R. cohabitans* were identified under the co-culture conditions (Table A4). Most of them are related to transporters for oligopeptides, dipeptides, amino acids, sugars, and dicarboxylic acids (Figure 14 and Table A4), suggesting that these compounds are actively taken up from the medium by *R. cohabitans*. Other enriched enzymes include protease M41, glutamate dehydrogenase (amino acid catabolism), pyruvate-ferredoxin oxidoreductase (ferredoxin reduction), and components of the Sec translocon (secretion of hydrolases, insertion of transporters) (Table A4).

We subsequently confirmed that *R. cohabitans* can use organic carbon sources derived from Deltaproteobacteria N47 to support fermentative H_2 production by cultivating *R. cohabitans* with autoclaved biomass of Deltaproteobacteria N47. After three days, the H_2 production by *R. cohabitans* was twofold higher in fresh media incubations supplemented either with heat-killed cells or filtered supernatant from Deltaproteobacteria N47 (Figure 13B). This provides further evidence that *R. cohabitans* can use necromass and potentially exudates from Deltaproteobacteria N47 to support its obligately fermentative lifestyle. This finding is also in line with growth experiments revealing that *R. cohabitans* obligately requires the presence of 0.1% yeast extract to grow in pure culture but not in co-culture with Deltaproteobacteria N47 (Koelschbach et al. 2017). Pimelate and other dicarboxylic acids are important downstream metabolites of anaerobic naphthalene degradation and have been detected in the supernatant of the enrichment culture N47 (Meckenstock et al. 2016). It is also possible that dicarboxylic acids released during naphthalene degradation are taken up by some of the identified transporters and further catabolized. But the genomic search in *R. cohabitans* did not support this hypothesis, as we could not find genes for the β-oxidation of dicarboxylic acids (Harrison and Harwood 2005), in agreement with the proteome analysis. Together, these observations suggest that *R. cohabitans* primarily feeds on proteins, sugars, and possibly other compounds derived from detrital Deltaproteobacteria N47 biomass.

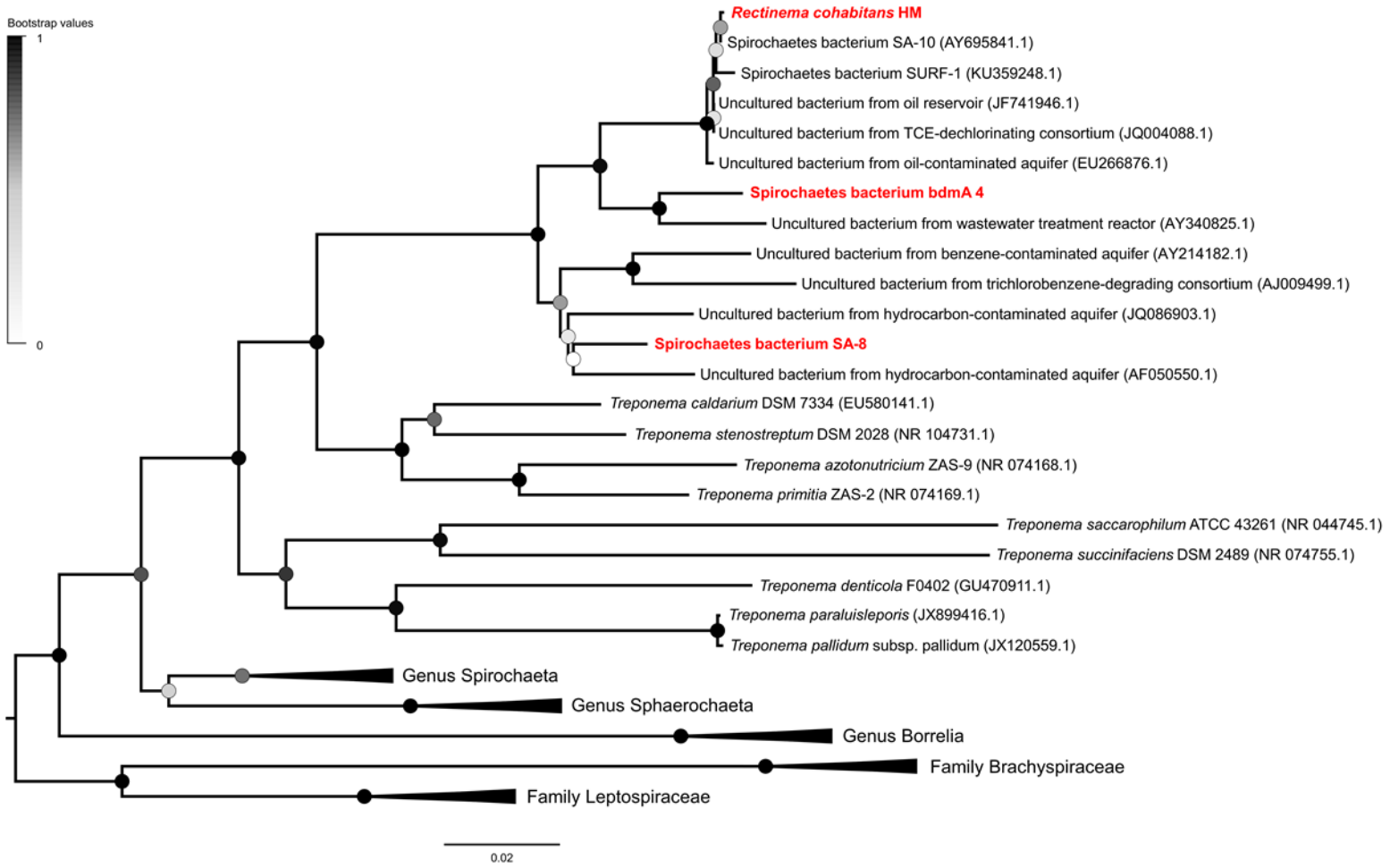

Figure 15. Condensed maximum likelihood tree of partial 16S rRNA gene sequences of Spirochaetes showing the phylogenetic affiliation of *R. cohabitans*, uncultured Spirochaetes bacterium bdmA 4, and uncultured Spirochaetes bacterium SA-8. Phylogenetic trees were constructed by the maximum-likelihood method and are bootstrapped with 500 replicates. The expanded tree is shown in Figure A4.

3.2.4 Spirochaetes may generally drive microbial loops in hydrocarbon- and organohalide-contaminated environments

To further illuminate the ecological niche of Spirochaetes in polluted habitats, we compared the genome of *R. cohabitans* with the draft genomes of two uncultured environmental Spirochaetes reconstructed from metagenomics sequences: uncultured Spirochaetes bacterium SA-8, originating from a terephthalate-degrading, methane-producing bioreactor (Nobu et al. 2015), and uncultured Spirochaetes bacterium bdmA 4, derived from a naphthalene-degrading, sulfate-reducing culture enriched from a creosote spill (Kummel et al. 2015). Genome-based metabolic reconstructions suggest that, akin to *R. cohabitans*, both organisms are nonspiral Spirochaetes and obligate fermenters (Figure 11 and Table A2). In addition, both organisms encode [FeFe] Groups A and B hydrogenases that are phylogenetically related to those of *R. cohabitans* (Figures 12A and A3), suggesting that they also fermentatively produce H_2, sustaining associated hydrogenotrophic methanogens and sulfate reducers. Revisiting the published genomes of the nonspiral Spirochaetes *S. pleomorpha* and *S. globosa* from trichloroethene-degrading cultures also indicates a potential for H_2 production via saccharolytic mixed-acid fermentation (Figures 12A and A3) (Caro-Quintero et al. 2012).

The 16S rRNA gene sequences of *R. cohabitans*, uncultured Spirochaetes bacterium bdmA 4, and uncultured Spirochaetes bacterium SA-8 are 95% identical to each other, and form a common clade distinct from *Treponema* species in the 16S rRNA based phylogenetic tree (Figures 15 and A4). In the same clade, we could also identify numerous 16S rRNA gene sequences associated with contaminated aquifers or bioreactors containing hydrocarbons or organohalides and oil reservoirs (a small selection is shown in Figure 15). This indicates that *Rectinema* species are ubiquitous in hydrocarbon- and organohalide-polluted anoxic sites. *S. globosa* and *S. pleomorpha* strains are distantly related to the three members of the genus *Rectinema* (Koelschbach et al. 2017), suggesting that nonspiral morphology evolved multiple times and that a similar metabolism is present in distinct groups of environmental Spirochaetes (Figure A4). Altogether, comparative genomic analyses suggest that these environmental nonspiral

Spirochaetes fulfill ecophysiological functions similar to *R. cohabitans* in their communities: recycling necromass and providing H_2 to respiring bacteria (e.g. sulfate reducers) or hydrogenotrophic methanogens in these communities.

3.3. Monitoring microbial mineralization using reverse stable isotope labelling analysis by mid-infrared laser spectroscopy

In the classical stable isotope labelling experiments, fully or partially ^{13}C-labelled compounds are added to the cultivation medium which is buffered with bicarbonate at natural $^{13}C/^{12}C$ isotopic abundance (i.e., with a ^{13}C fraction $x(^{13}C) \approx 1.11\%$). The change of the $^{13}C/^{12}C$ isotope ratio of CO_2 in the headspace is then followed over time and used to calculate the quantity of evolved $^{13}CO_2$. In our reverse stable isotope labelling approach, we simply set out to reverse this set up by adding ^{13}C-labelled bicarbonate with $x(^{13}C)$ values ranging from 2-50%, depending on the expected production of CO_2. Then, a regular substrate or mixture for microbial degradation is supplied which has a normal stable isotope ratio at natural abundance ($x(^{13}C) \approx 1.11\%$). Consequently, CO_2 with a stable isotope ratio at natural abundance is released during mineralization. As the stable isotope ratio of the released CO_2 differs significantly from the isotope ratio of the labelled background dissolved inorganic carbon (DIC), one can measure the changes in the $^{13}C/^{12}C$ isotope ratio of the total DIC (i.e. the sum of inorganic carbon species in the medium) over time which can be used to provide evidence for CO_2 production and to calculate its absolute amount.

Here, to demonstrate the feasibility and usefulness of the RIL method, we studied anaerobic degradation of aromatic hydrocarbons, which belong to the most recalcitrant priority pollutants in contaminated aquifers. The broader environmental relevance of this method was further shown by aerobic mineralization of DOC adsorbed to granular activated carbon (GAC) during drinking water production.

3.3.1 Verification of the method

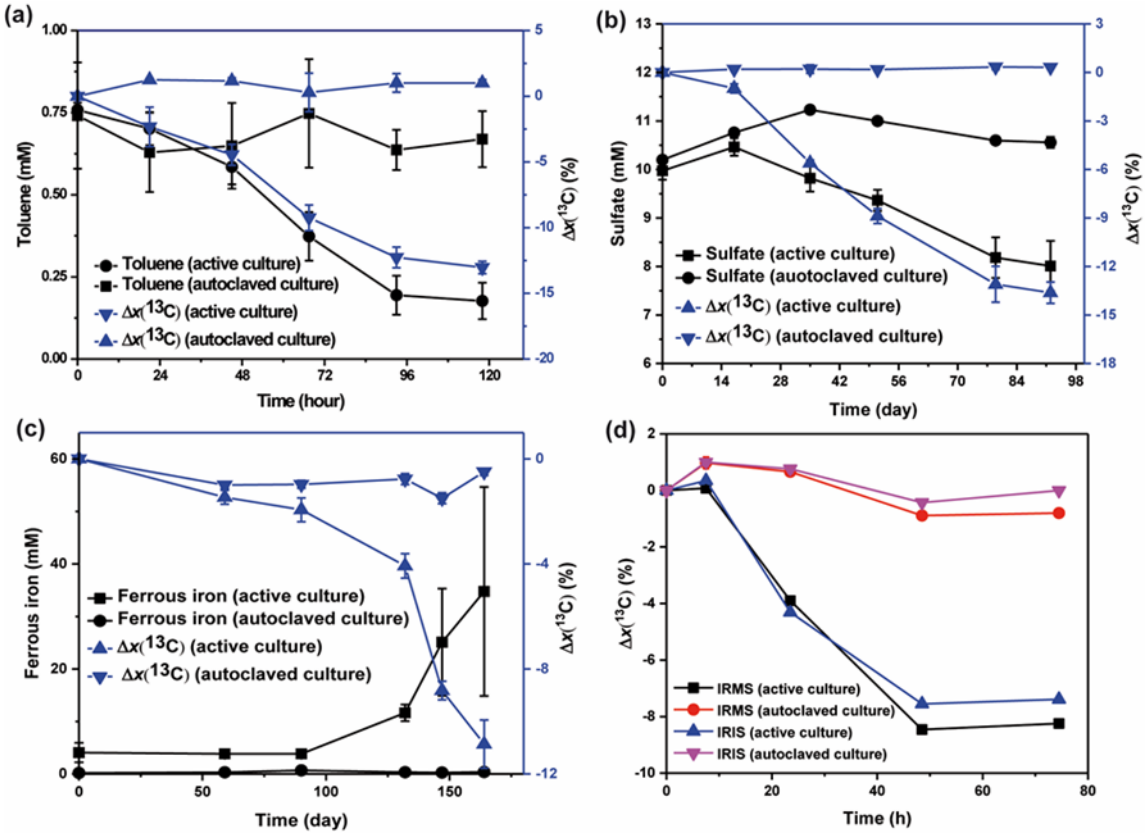

Figure 16. Anaerobic degradation profiles of (a) toluene by *G. metallireducens*, (b) 2-methylnaphthalene by the enrichment culture N47, (c) naphthalene by an uncharacterized iron-reducing enrichment culture SN, and (d) toluene by *T. aromatica*. The added bicarbonate buffer (30 mM) consisted of non-labelled and ^{13}C-labelled sodium bicarbonate at a ratio of 50:50 for *G. metallireducens* (a) and the enrichment culture N47 (b), 80:20 for the enrichment culture SN (c), and 90:10 for *T. aromatica* (d). Sulfate or iron reduction as surrogate measurements indicated methylnaphthalene or naphthalene degradation. Carbon isotope ratio changes were expressed as a percentage compared to the initial $x(^{13}C)$ value: $\Delta x(^{13}C) = (x(^{13}C)_t - x(^{13}C)_{initial})/x(^{13}C)_{initial} \times 100$. The $x(^{13}C)$ values of DIC samples for (a)-(c) were only measured by IRMS. Both IRMS and IRIS were performed for (d). Data are means of two or three parallel incubations measured three times each. Error bars represent standard deviation of the biological replicates.

The proof of principle for the reverse stable isotope labelling (RIL) method was first verified with two reference cultures: (1) anaerobic toluene degradation by *G. metallireducens* and (2) anaerobic 2-methylnaphthalene degradation by the enrichment culture N47 (Figure 16). The medium was supplemented with unlabelled and ^{13}C-labelled sodium bicarbonate at a ratio of 50:50 and carbon

stable isotope ratios of DIC samples were measured with IRMS. During anaerobic toluene degradation by *G. metallireducens*, the initial ^{13}C fractions of DIC samples ($x(^{13}C)_{initial}$ = 33.16%) decreased by $\Delta x(^{13}C)$ = 13.03 %, which corresponded to the consumption of total toluene from 0.75 to 0.18 mM (Figure 16a). No significant changes could be observed for toluene concentrations or ^{13}C fractions in control bottles. During anaerobic degradation of 2-methylnaphthalene by the enrichment culture N47, the initial ^{13}C fractions of DIC samples ($x(^{13}C)_{initial}$ = 34.01%) decreased by 13.62% concomitant with a measured reduction of sulfate from 9.97 to 8.01 mM (equal to consumption of 0.29 mM of 2-methylnaphthalene) (Figure 16b). No significant changes could be observed for sulfate concentrations or ^{13}C fractions in control bottles. These two experiments provided proof-of-principle that measuring stable carbon isotope ratios of DIC by the RIL method can be used for demonstrating microbial degradation.

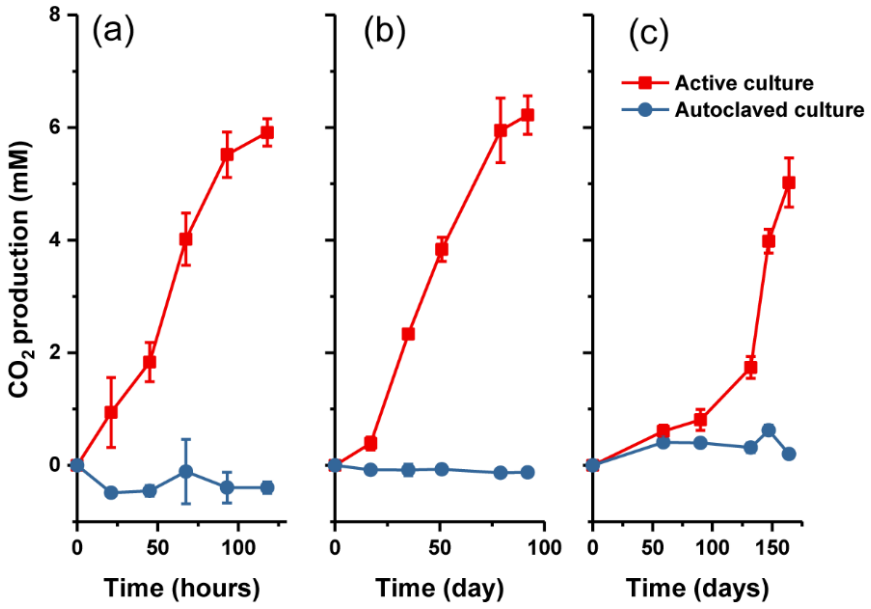

Figure 17. The calculated CO_2 production for anaerobic degradation of (a) toluene by *G. metallireducens* (Figure 16a), (b) 2-methylnaphthalene by the enrichment culture N47 (Figure 16b), (c) naphthalene by an uncharacterized iron-reducing enrichment culture SN (Figure 16c). Data points depict means of two or three parallel incubations measured three times each. Error bars represent standard deviation of the biological replicates.

We then used the RIL method to test if an uncharacterized enrichment culture can mineralize naphthalene under iron-reducing conditions (Figure 16c). In contrast to previous experiments, unlabelled and ^{13}C-labelled sodium bicarbonate were added

at a ratio of 80:20, making the initial $x(^{13}C)$ values lower than in the proof-of-principle study. Carbon stable isotope ratios of DIC samples were measured with IRMS. Naphthalene was the sole organic carbon source added. In control bottles inoculated with autoclaved cultures, the ^{13}C fractions of DIC samples remained stable at ~15.46%. In the bottles inoculated with active cultures, a considerable lag phase of about 90 days took place before a decrease in $x(^{13}C)$ values and an increase of ferrous iron could be observed. Then, the initial ^{13}C fraction of DIC samples ($x(^{13}C)_{initial}$ = 15.26%) dropped by 10.86% coupled to a concomitant ferrous iron production of 31 mM. This data provided clear evidence that naphthalene mineralization to CO_2 occurred coupled with iron reduction. But due to the non-linearity of IRMS measurement at high isotope ratios (see below), the calculation of CO_2 production and the electron balance were not accurate (Figure 17 and Table 2).

Table 2. Stoichiometric calculations of the measured and the theoretical ratios between the reduction of electron acceptors or donors and CO_2 production at the last sampling point for Figures 16a-c.

	Figure 16a	Figure 16b	Figure 16c
	Toluene oxidation: CO_2 production	Sulfate reduction: CO_2 production	Iron reduction: CO_2 production
Theoretical ratios	0.17	0.61	4.80
Calculated ratios	0.59	0.31	7.43

3.3.2 Evaluation of highly enriched $x(^{13}C)$ values measured by IRMS

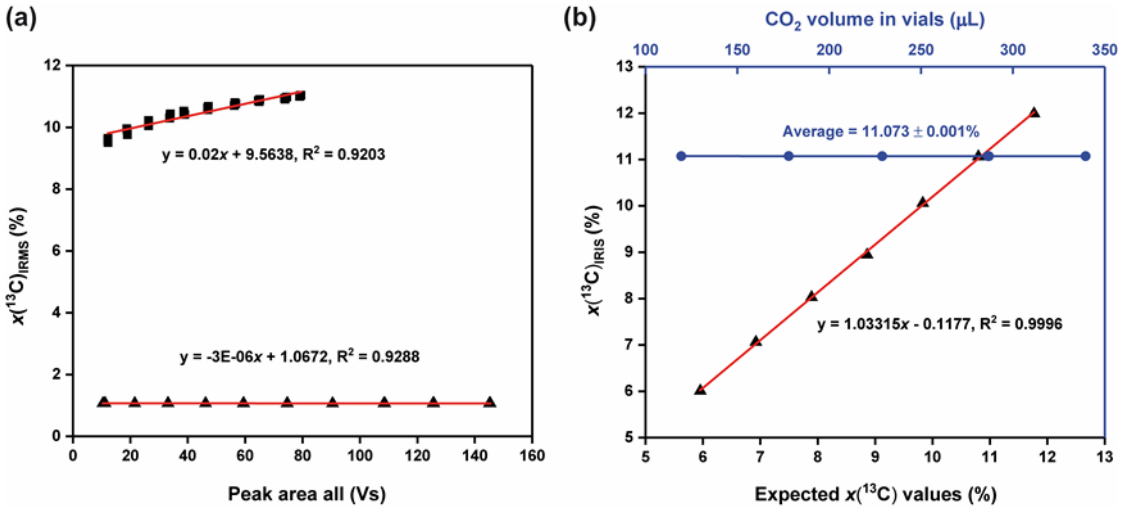

Figure 18. Performance comparison of IRIS and IRMS. (a) Effect of CO_2 concentrations (proportional to Peak Area All, i.e. sum of peak areas of *m/z* 44, 45, and 46 of CO_2) on the IRMS-measured ^{13}C atom fractions for ^{13}C-enriched gas ($x(^{13}C)$ = 11.073%; black squares) and natural abundance gas ($x(^{13}C)$ = 1.0671%; black triangles), n = 3. (b) Effect of CO_2 concentrations on the IRIS-measured ^{13}C atom fractions ($x(^{13}C)$ = 10.3%; blue circles) and the linear regression line showing IRIS-measured enriched ^{13}C samples plotted against theoretical $x(^{13}C)$ values (n = 5; black triangles). No error bars are shown as they lie within the dimensions of the symbol.

For analysis of carbon stable isotope ratios by IRMS, CO_2 samples are firstly ionized to different ions mass-to-charge ratios (*m/z*) at 44, 45, and 46. The resulting streams of ions are subsequently separated in a magnetic field. Then, the Faraday cup collectors are used to specifically collect signals of each ion beam. In the case of natural abundance samples, the ^{13}C atom fractions are at $x(^{13}C)$ = ~1.11%, making signals (voltage outputs) of *m/z* 45 and 46 much weaker compared to *m/z* 44 (Figure A5a). In order to get comparative intensities for the highest quality results, each Faraday cup is designed to connect its own amplification ohmic resistor, at a ratio of 3:300:1000 for *m/z* 44, 45, and 46, respectively (Figure A5a). In contrast, when measuring samples highly enriched in ^{13}C (*e.g.* $x(^{13}C)$ = 15-35%) by using the same standard setting, the amplified signals will not be in the same range, but with *m/z* 45 dominating the peak (Figure A5b), even though the absolute ratio of $^{13}C/^{12}C$ is smaller than 1. Consequently, the IRMS response could be imprecise. Aware of this, we preformed two linearity

tests on an IRMS using two different reference gases to investigate if reported $x(^{13}C)$ values could significantly alter with changes in CO_2 concentrations. Results showed a good linearity when we measured the natural abundance reference gas ($x(^{13}C)$ = 1.067%) (Figure 18a). For highly enriched samples ($x(^{13}C)$ = 10.3%), however, the measured $x(^{13}C)$ values increased with elevated gas partial pressures showing a larger positive slope of 0.02 (significantly linearly dependent on the CO_2 concentration) (Figure 18a). This indicated that the results shown in Figures 16a-c could be inaccurate, as we could not apply working reference gases at the same concentration. This was further confirmed by the stoichiometric calculations which showed great differences between the measured and the theoretical ratios between the reduction of electron acceptors or donors and CO_2 production (Figure 17 and Table 2). Nevertheless, we could obtain a semi-quantitative assessment of the degradation activities as shown from the results.

One possible solution to alleviate this problem is to switch the feedback resistor of the preamplifier to adjust *m/z* 44 signal to an appropriate range (Goodman and Brenna 1992). Unfortunately, this cannot be achieved due to the limitations of the IRMS we used. Reinsch and Ambus adjusted resistor settings of the mass spectrometer to obtain higher measurement precision, but still they found that $x(^{13}C)$ values measured by IRMS for ^{13}C-enriched samples ($x(^{13}C)$ = 50%) were also significantly dependent on CO_2 concentrations (Reinsch and Ambus 2013). They subsequently used the empirical relationship to correct data but the measured $x(^{13}C)$ values never showed the expected values. Using IRMS is therefore not straightforward for determination of $x(^{13}C)$ values in the highly-enriched samples, which motivated us to search for a better alternative.

3.3.3 Using IRIS for analyzing highly enriched ^{13}C samples

In contrast to IRMS, IRIS is capable of measuring enrichments up to $x(^{13}C)$ = 25%. Some other early-designed $^{13}CO_2/^{12}CO_2$ infrared gas analyzer using TDLA techniques have been shown to measure values of $x(^{13}C)$ as high as 5% or 10%, as long as the $^{13}CO_2$ concentration is within the $^{13}CO_2$ range of the calibration gas (Dannoura et al. 2011, Plain et al. 2009). Therefore, infrared gas analyzers can be a good alternative for measuring highly enriched samples in $^{13}CO_2$-labelling

experiments. The TDLA technique employed by the Delta Ray IRIS follows the Beer-Lambert law (Bowling et al. 2003). While a laser beam scans through absorption lines of $^{13}CO_2$ and $^{12}CO_2$ of samples, the decrease of intensity of the laser can be directly linked to the concentration of the respective molecular species and hence carbon isotope ratios. For quantifications, absorptions within the scan range can be fitted by an algorithm adapted to certain environmental conditions within the laser cell (100 mbar pressure). For natural abundance samples, the peak areas for $^{13}CO_2$ are relatively small compared to that for $^{12}CO_2$ (Figure A6a) (van Geldern et al. 2014). For ^{13}C-enriched samples (e.g. $x(^{13}C)$ = 10.0 %), the peak areas for $^{13}CO_2$ increase strongly (Figure A6b). However, as long as the $^{13}CO_2$ band does not reach the saturation level, it can be used to determine carbon isotope ratios. In all our tests, we did not observe any saturation during measurements. Besides, IRIS can automatically determine CO_2 concentrations and adjust the CO_2 concentrations of samples to an optimal and constant concentration (380 ppm) going into the optical cell, which could address the issue of isotope ratio drifts caused by CO_2 concentrations (van Geldern et al. 2014).

To further confirm that IRIS can measure highly enriched ^{13}C samples, we measured bicarbonate mixtures with different $x(^{13}C)$ values. The measured $x(^{13}C)$ versus expected $x(^{13}C)$ values showed an excellent linear correspondence (correlation coefficient R^2 = 0.9996) over a wide range from $x(^{13}C)$ = 6% to $x(^{13}C)$ = 12%, giving a trendline of $y = 1.0315x - 0.1177$ (Figure 18b), demonstrating its capability to measure high ^{13}C enrichments. The standard deviations of $x(^{13}C)$ values varied with sample enrichments but were all below 0.006%. The precision is more than adequate for biological studies, where sample variation is considerably large than this analytical error (for details see next section). We subsequently sampled different aliquots (0.2 to 0.6 mL) from a 10% ^{13}C-labelled bicarbonate solution and added these into the vials to produce samples with different CO_2 concentrations. Results illustrated that even though the CO_2 concentrations of samples changed significantly the resultant variation was very low (11.073% ± 0.001%) and remained within the analytical precision (Figure 18b),

therefore demonstrating the efficiency of the automatic concentration adjustment by the analyzer.

For a direct comparison of using the RIL method to provide evidence for biodegradation via IRMS or IRIS, non-labelled and ^{13}C-labelled sodium bicarbonate were added at a ratio of 90:10 to an anaerobic toluene degradation experiment with *T. aromatica*. IRIS and IRMS measurements produced a similar decreasing trend of $x(^{13}C)$ values, both indicating toluene mineralization (Figure 16d). Despite identical drops of $x(^{13}C)$ values, IRIS data showed a systematical offset from IRMS data at $x(^{13}C)$ = 0.145 % on average. We are currently investigating the reasons for this unexpected difference. However, the variations could be related to the failure to produce the same concentration of injected CO_2 samples as working reference gases for IRMS.

3.3.4 Sensitivity of CO_2 quantification under anoxic conditions

The enrichment culture was cultivated in the presence of 10% ^{13}C-labelled sodium bicarbonate as an example to investigate if the RIL method can be used to sensitively quantify CO_2 production based on IRIS measurement. Naphthalene was added as the sole organic carbon source while sulfate was supplied as the electron acceptor. In bottles inoculated with active cultures, we observed a reduction of 6.98 mM sulfate, concomitant with a production of 11.87 mM CO_2 (Figure 18). The ratio for sulfate consumption to CO_2 production (5.9:10) is very close to the theoretical stoichiometry (a ratio of 6:10) (Meckenstock et al. 2016). The high precision of measuring the $x(^{13}C)$ values with IRIS together with the closed electron balance indicates that the RIL method is reliable to quantify the extent of microbial mineralization.

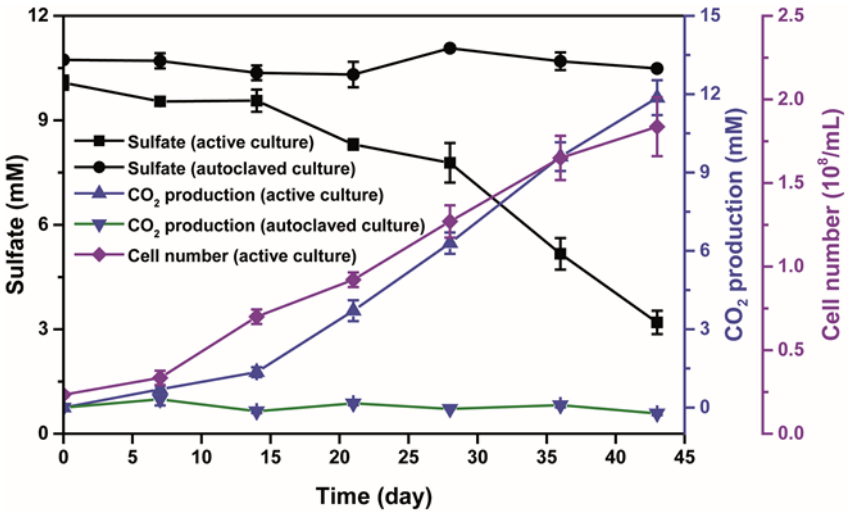

Figure 19. Anaerobic degradation of naphthalene by the enrichment culture N47. The added bicarbonate buffer (30 mM) consisted of non-labelled and ^{13}C-labelled sodium bicarbonate at a ratio of 90:10. The $x(^{13}C)$ values of DIC samples were measured by IRIS. Data are means of two or three parallel incubations. Error bars represent standard deviation of the biological replicates.

In control bottles with autoclaved cultures, a maximum variability of $x(^{13}C)$ = 0.05% was determined during the whole incubation time, which depicts the experimental error due to the sampling process and analytical uncertainty. To conclude that there is distinct evidence of biodegradation in bottles with active cultures, depletion in ^{13}C-enrichment of CO_2 ($x(^{13}C)_{background} - x(^{13}C)_{total}$) should be at least two times larger than the experimental error, meaning a production of 0.38 mM CO_2 would be sufficient to provide evidence of biodegradation. This corresponds to 38 µM of naphthalene or 1.6% of the 2.34 mM of added naphthalene and clearly demonstrates the sensitivity of the method. This small extent of biodegradation would be impossible to assess using other methods, except for methods using direct stable or radio isotope labelled substrates. However, further theoretical consideration of the precision of the analysis predicts that the sensitivity of the method could be improved by a factor of 5 to 10 concerning the developed CO_2. For example, optimization of measurements by IRIS showed that contamination of ambient air in the autosampler system could greatly contribute to analytical uncertainties. In fact, adding a pre-flushing step to the autosampler system with CO_2-free synthetic air reduced the standard deviations of measured $x(^{13}C)$ from

0.028% down to 0.008% (n=12, samples were taken one by one from the same culture bottle).

3.3.5 Determining aerobic mineralization rate of GAC biomass

Biologically activated carbon filters, usually placed after the step of ozonation, are widely used in the drinking water production system for removal of undesired biodegradable DOC (Simpson 2008, Velten et al. 2011). During the steady-state of GAC filters when biomass concentration of the biofilm and effluent DOC concentration remain constant, the removal process is predominately performed by the indigenous microbial communities attached on the surface of activated carbon (i.e., GAC biofilms). One particular interest in this stage is to characterize the spatial distribution of microbial activities along the GAC filters, which can guide the operation and design of GAC filters. Most current studies focus on investigations of active biomass densities to indirectly describe it, e.g. adenosine tri-phosphate (ATP) analyses (Gibert et al. 2013, Velten et al. 2007, Wen et al. 2015). Here we show that our RIL method can be used as an alternative approach but to directly assess the aerobic mineralization potential of DOC by biomass attached on the GAC filters and resolve their spatial distribution profiles.

We simply cultivated BAC particles in lab microcosms filled with influent water (after ozonation) and 10% ^{13}C-labelled sodium bicarbonate. DIC samples were taken regularly and shifts in isotopic composition of DIC samples were measured by IRIS for calculation of CO_2 production. In 22 days, no observable CO_2 production could be found for incubations of only ozonized river water or multilayer filtered water (Figure 20). Insignificant amounts of CO_2 production were observed n incubations of fresh GAC, which was most likely caused by carbonate adsorbed to the surface, in agreement with the decrease of pH values. For active microcosms with incubations of GAC particles + influent water, however, we could observe significant CO_2 production. During the first two days, the degradation rate decreased and stayed almost linear afterwards (Figure 20). Thus, these data indicated that the RIL method can be used to monitor microbial DOC mineralization rates performed by the biofilm matrix attached to the solid surface of GAC.

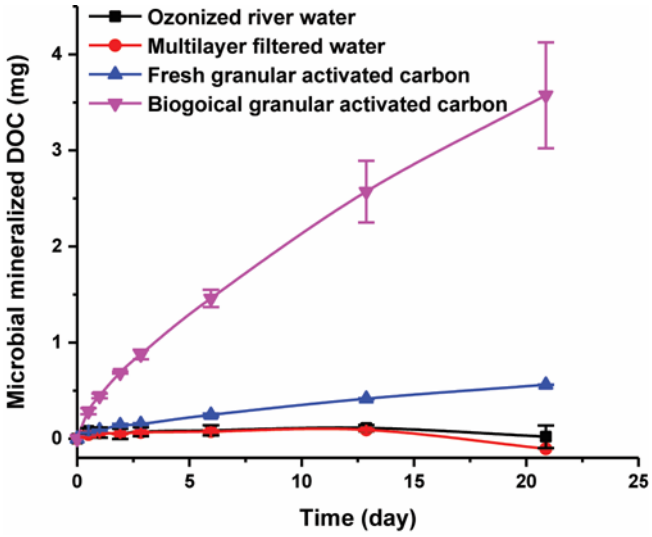

Figure 20. Aerobic mineralization of DOC adsorbed on the GAC filters by biomass attached on GAC surfaces. The added bicarbonate buffer (10 mM) consisted of non-labelled and ^{13}C-labelled sodium bicarbonate at a ratio of 90:10. The *x*(^{13}C) values of DIC samples were measured by IRIS. Data are means of three parallel incubations. Error bars represent standard deviation of the biological replicates.

As no clear DOC mineralization can be found in control microcosms so that the measured mineralization for active microcosms all came from biofilms attached on the granular activated carbon. The regression polynomials (2nd degree) for the first 24 hours of incubation were used to calculate the mineralization rates (i.e. regression slope) in each microcosm can be calculated. As shown in Figure 21, for GAC filters 1 and 2, the highest mineralization rate was observed at the second sampling point (20 cm depth from the top) and decreased by factors of 1.2 and 1.3 to the bottom of filters, respectively. From a spatial distribution point of view, the results are in line with previous studies where densities of biomass attached on the filters decreased along with the increase of the depth from the top to the bottom (Gibert et al. 2013, Velten et al. 2011). But for GAC filter 3 we observed the opposite trend. This can be due to the distinct types of GAC used for these three filters, which suggested the importance of choosing the right type of granular activated carbon.

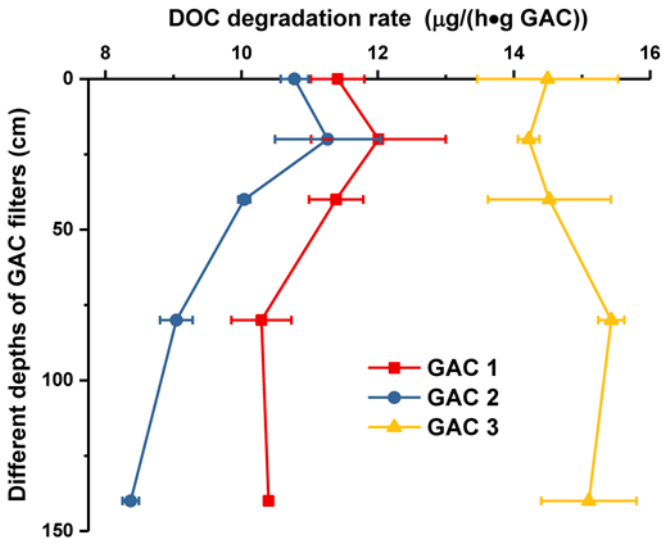

Figure 21. Aerobic mineralization potential of DOC by biomass attached on GAC surfaces at different depths of the GAC filters. The added bicarbonate buffer (10 mM) consisted of non-labelled and ^{13}C-labelled sodium bicarbonate at a ratio of 90:10. The $x(^{13}C)$ values of DIC samples were measured by IRIS. Data are means of three parallel incubations. Error bars represent standard deviation of the biological replicates.

4. Discussion

A major question in biodegradation of benzene and naphthalene under anoxic conditions is (1) to answer who are the key players and how they complete the degradation process. Combined genomic and proteomic techniques were used to analyze an enrichment culture anaerobically utilizing benzene under sulfate-reducing conditions. The results provide evidence that benzene degradation is coupled to sulfate reduction in a single cell process, which is unusual for bacteria affiliated to *Pelotomaculum* genus (Chapter 4.1.).

Another important question is (2) to understand who else is there and what its function is in the community or ecosystem. A naphthalene-degrading, sulfate-reducing enrichment culture was taken as an example, and results from physiological, genomic, and proteomic analyses are presented indicating that environmental Spirochaetes recycle detrital biomass and convert it into end products or electrons that support growth of associated degraders. This finding emphasizes the importance of microbes that are not involved in the key processes (Chapter 4.2.).

A crucial step in studying microbial degradation of benzene and naphthalene is using microcosm experiments to prove the degradability and to obtain degradation rates. Of special interest is (3) to assess if the compounds are fully mineralized to CO_2 or if they are just transformed to metabolites which might be even more toxic in some cases. A novel reverse stable isotope labelling analysis is developed as a sensitive means to monitor biodegradation, focusing on hydrocarbon substrates (Chapter 4.3.).

4.1. A member of the genus *Pelotomaculum* oxidizes benzene to carbon dioxide with direct reduction of sulfate

Three types of initial activation reactions for anaerobic benzene degradation have been proposed: methylation to toluene, hydroxylation to phenol, and direct carboxylation to benzoate. Methylation of benzene to toluene was mostly based on the recovery of labeled toluene when labeled benzene was added to cultures (Aburto-Medina and Ball 2014, Meckenstock and Mouttaki 2011). However, the key product of anaerobic toluene activation, benzylsuccinate, has never been detected in benzene-degrading cultures, and so far no other evidence has been reported to support ring methylation as the initial activation reaction. There is also indication for hydroxylation of benzene to phenol as initial activation reaction by *Geobacter metallireducens* which metabolized benzene with Fe(III) citrate as the electron acceptor (Caldwell and Suflita 2000, Zhang et al. 2012, Zhang et al. 2013). Several groups suggested a direct carboxylation of benzene to benzoate as the first step for anaerobic benzene metabolism (Abu Laban et al. 2010, Holmes et al. 2011, Luo et al. 2016). In the Fe(III)-reducing enrichment culture BF, combined genomic and proteomic studies revealed genes encoding for two subunits of a putative anaerobic benzene carboxylase (AbcD and AbcA) (Abu Laban et al. 2010).

Based on proteogenomic analysis of the enrichment culture BPL, we propose that *Pelotomaculum* candidate BPL might not employ any of the three above-mentioned initial activation reactions proposed for benzene degradation. *Pelotomaculum* candidate BPL is not the only case of lacking genomic evidence for any of the activation reactions proposed so far. In a benzene-degrading methanogenic culture, benzene degradation was affiliated to a *Deltaproteobacterium* bacterium ORM2 (Devine 2013, Luo et al. 2016). There, the authors could not identify genes involved in toluene or phenol activation, either. Additionally, they failed to identify genes encoding for UbiD-like carboxylases and benzoate-CoA ligases. They therefore proposed an alternative carbonylation pathway for transformation of benzene to benzoyl-CoA via either a Wood-Ljungdhal-type reaction or a Gatterman-Koch-type mechanism (Devine 2013). Similarly, in a sulfate-reducing, benzene-degrading consortium enriched by Phelps

et al. (2001), benzoate was detected in culture supernatants but it could not support cell growth. Thus, the authors proposed that benzene was directly transformed to benzoyl-CoA (Phelps et al. 2001). In another study performed by Taubert *et al.* (2012), a similar benzene-degrading, sulfate-reducing enrichment culture was analyzed using protein-based stable isotope probing. Although this might be due to the poor detection limit of the method, they could not find proteins of known or proposed pathways for benzene activation.

Taking together, the genomic information on anaerobic benzene degradation from literature and the data presented here indicate a common observation for benzene activation. The iron- and nitrate-reducing bacteria known so far seem to activate benzene via carboxylation (Abu Laban et al. 2010, Luo et al. 2014). Fermenting- and sulfate-reducing bacteria including candidate *Pelotomaculum* BPL studied here might have developed so far unknown, oxygen-independent strategies for anaerobic benzene activation.

Members of the genus *Pelotomaculum* are mostly obligate syntrophs that need methanogens as syntrophic partners to oxidize propionate, alcohols, or aromatic compounds (Imachi et al. 2002, Stams and Plugge 2009). Recent studies propose that syntrophic metabolism during biodegradation of benzene and other hydrocarbons might occur in the presence of electron acceptors, such as sulfate or nitrate (Gieg et al. 2014). For example, stable isotope probing (SIP) with the Fe(III)-reducing enrichment culture BF revealed that members of the *Peptococcaceae* were the primary benzene degraders and shared electrons with members of the family *Desulfobulbaceae* (Kunapuli et al. 2007). Similar results were obtained for two denitrifying cultures based on either batch or chemostat studies (Luo et al. 2014, van der Zaan et al. 2012).

P. thermopropionicum is the only member whose genome has been sequenced in the genus *Pelotomaculum*. Similar to other known representatives in the genus, it lacks the capability to reduce sulfate, even though the related genes for sulfate reduction have been identified in the genome (Plugge et al. 2011). Previously, a draft genome for an uncultured *Pelotomaculum* spp. was retrieved in a terephthalate-degrading culture (Lykidis et al. 2011). Combined with the

subsequent proteomic studies, *Pelotomaculum* spp. was confirmed to degrade terephthalate via syntrophic interactions with methanogens (Wu et al. 2013). The given examples provide more and more evidence that members of the genus *Pelotomaculum* carry out syntrophic metabolism with anaerobic respiring microorganisms.

In another study, *Pelotomaculum* members were also proposed to degrade benzene in a similar sulfate-reducing enrichment culture (Herrmann et al. 2010). The authors hypothesized that benzene degradation by *Pelotomaculum* occurred by fermentation coupled to sulfate reduction performed by another organism in the enrichment culture (Herrmann et al. 2010, Rakoczy et al. 2011, Taubert et al. 2012). Interspecies hydrogen transfer was suggested to play an important role for benzene mineralization (Rakoczy et al. 2011).

However, by using the integrated genomic and proteomic data, we conclude in our study that the anaerobic benzene degradation in the enrichment culture BPL is performed as a single cell process by a novel member of the genus *Pelotomaculum* which is able to reduce sulfate as electron acceptor. This indicates that detection of *Pelotomaculum* species in benzene-contaminated areas therefore does not literally indicate the occurrence of benzene fermentation but can also be linked to direct sulfate-dependent benzene mineralization.

4.2. A hydrogen-driven subsurface microbial loop

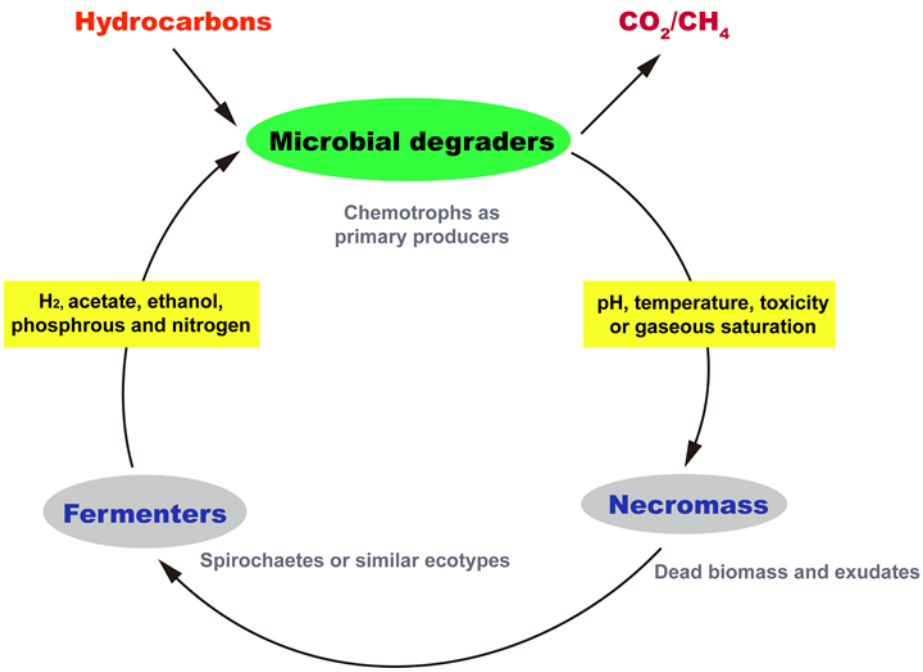

Figure 22. A simplified scheme of subsurface microbial loop in hydrocarbon-containing and organohalide-contaminated sites. Fermentative bacteria like environmental Spirochaetes fulfill the biomass recycling without a food chain, stimulating the microbial degradation process performed by key players (e.g. sulfate reducers) in this system.

Molecular analyses of microbial communities showed that environmental Spirochaetes are common and abundant in contaminated sites and in enrichment cultures degrading hydrocarbons and organohalides. Our study of several enrichment cultures now provides a functional trait to these frequently detected organisms. Their primary role is to degrade necromass *via* fermentation, resulting in production of hydrogen, short-chain fatty acids, and alcohols. These products are then utilized by sulfate-reducing bacteria and likely hydrogenotrophic methanogens, thereby recycling the necromass. Hydrocarbon-containing and organohalide-contaminated sites are extreme habitats where high concentrations of organic solvents challenge the integrity of cell membranes, inducing cell leakage or lysis (Rodriguez Martinez et al. 2008, Sherry et al. 2014). Thus, there might be high biomass turnover in such ecosystems (Griebler and Lueders 2009) and mechanisms to utilize electrons released as necromass might be important for ecosystem function. Such processes are likely to occur both in natural

hydrocarbon-containing environments and in ecosystems that have been contaminated with hydrocarbons and organohalides due to anthropogenic influences.

We thus propose that environmental Spirochaetes and similar ecotypes fill an important ecological niche by forming a subsurface microbial loop that recycles dead biomass and exudate (Figure 22). Through this loop, the electrons derived from necromass are continuously recycled by chemolithotrophs and chemoorganotrophs. This process alone will only support limited biomass production due to the high energy loss between trophic levels. Hydrocarbons and organohalides are therefore important as exogenous energy, electron, and carbon inputs in such systems. This differs from the traditional microbial loops described in marine and freshwater ecosystems, which are driven by photo-litho-auto-trophy rather than chemo-organo-hetero-trophy (Fenchel 2008). As electron donors are present in excess in hydrocarbon-contaminated aquifers, hydrocarbon degradation might be stimulated by the nutrients released from the microbial loop, as long as electron acceptors such as sulfate do not become rate-limiting. Thus, environmental Spirochaetes and other necromass-degrading microorganisms might contribute to enhancing biodegradation rates at contaminated plume fringes in groundwater or in oil reservoirs where the electron donors (e.g. hydrocarbons) and acceptors (e.g. sulfate or nitrate) meet in opposing gradients and where the highest degradation activity and biomass is found (Meckenstock et al. 2015). The subsurface microbial loop may also be important for recycling of nutrients such as phosphorus and nitrogen, similar to the well-described microbial loops of aquatic ecosystems (Fenchel 2008, Kerner et al. 2003).

The presented example of a simple microbial loop puts the importance of necromass and H_2-cycling in the subsurface into a new perspective. Moreover, the data reported here align with recent metagenomic studies on hydrogen-driven chemo-litho-auto-trophic deep subsurface processes and gaseous CO_2-saturated deeply sourced groundwater (Bagnoud et al. 2016, Probst et al. 2017). Altogether, this suggests the microbial loop as a generic theoretical concept for subsurface.

4.3. Reverse stable isotope labelling analysis as a novel tool to monitor biodegradation

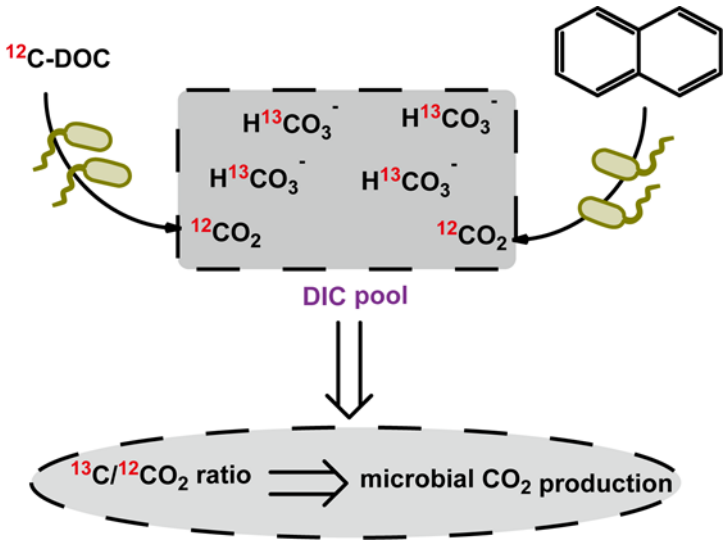

Figure 23. Reverse stable isotope labelling analysis as a novel tool to (1) analyze if microorganisms in environmental samples or enrichment cultures can degrade specific organic compounds to CO_2, like hydrocarbon degradation experiments and (2) sensitively detect biodegradation of complex organic substrates such as DOC.

The novel RIL method can assess the biodegradation of organic compounds in a suit of different applications. A typical question for research or practice would be to analyze if microorganisms in environmental samples or enrichment cultures can degrade specific organic compounds to CO_2, similar to the hydrocarbon degradation experiments presented here (Figure 23). Compared to other methods such as following substrate disappearance, the RIL can proof the mineralization to CO_2. It does also not come along with problems of substrate adsorption to matrix or stoppers, evaporation or other unspecific losses. However, the method runs into limitations if other easily degradable organic carbon is present in the sample (sediment or water) leading to additional release of non-labelled CO_2. This is a common problem in microcosm experiments also appearing if e.g. the disappearance of electron acceptors such as molecular oxygen (respiration test) or production of sulfide or ferrous iron are employed to follow biodegradation activity. In many cases, this problem is solved by appropriate controls without substrate if the organic carbon background is not too high.

However, this also turns into a big potential of RIL: the very sensitive detection of biodegradation of complex organic substrates such as DOC, as demonstrated in our experiments with granular activated carbon (Figure 23). Measuring DOC degradation is notoriously difficult and needs severe experimental efforts. Due to its high sensitivity, RIL can detect even tiny degradation activities that are difficult to assess, otherwise. Only using labelled organic compounds could compete with this sensitivity, but organics such as DOC cannot be labelled. RIL has the advantage that it can analyze degradation of natural organic matter in such environmental samples even under pristine conditions by only adding of a little ^{13}C-labelled DIC. Another big advantage is that degradation of compounds can be analyzed that are adsorbed to solid matrices, which is very difficult or almost impossible to measure with other methods at this precision and sensitivity. In the case of e.g. wood or plastics degradation, this could also include the degradation of the solid itself.

As demonstrated here, RIL performs under different biodegradation scenarios. Extremely slow biodegradation experiments with very difficult, anaerobic degradation of polycyclic aromatic hydrocarbons can be analyzed as well as faster, aerobic degradation of DOC. The precise analysis of carbon stable isotope ratios by IRMS or IRIS allows for the detection of very small CO_2 production. This makes RIL much more sensitive compared to directly measuring DIC concentrations or respiration tests (e.g. ISO 9408 and OECD 301B).

If the production of DIC/CO_2 during microbial degradation is large, e.g. by fast-growing aerobic microorganisms and higher amounts of organic substrates, conventional GC-MS can be used for analyzing degradation of stable isotope-labelled compounds (Liou et al. 2008). For tiny or slow biodegradation, however, GC-MS cannot compete with tools for analyzing stable isotope ratios of CO_2 such as IRMS and IRIS. IRMS does not produce accurate results if the carbon isotope ratios are too high and out of the linearity range. Thus, the Delta Ray™ IRIS provides the easiest and cheapest as well as the most precise analysis for $^{13}C/^{12}C$ ratios much higher than natural abundance.

A limitation for RIL is the need of closed systems. For example, aerobic incubations with continuous oxygen supply or open microcosms cannot be assessed by this method. In most cases, however, one can perform the same experiment in closed, stoppered vials when providing sufficient headspace (Bahr et al. 2015). As the major advantage of RIL is assessing small amounts of biodegradation, aerobic degradation of big amounts of substrates will anyway not be a typical field of application.

It is important that CO_2 fixation by photosynthetic organisms, other autotrophs, or heterotrophic CO_2 fixation does not affect RIL experiments. The release of CO_2 during biodegradation changes the stable isotope ratio of the DIC because of the additional amount of $^{12}CO_2$. CO_2 fixation, however, does not change the isotope ratio of the DIC because both isotopomers are consumed with the same rate. Stable isotope fractionation effects by discrimination of $^{13}CO_2$ during fixation are orders of magnitude smaller than the changes in the isotope ratios observed here and do not have to be accounted for. This even applies to systems such as methanogenesis where CO_2 is both released and consumed. While the release of CO_2 during substrate degradation by fermenting organisms changes the stable isotope ratio of the DIC indicating biodegradation the consumption by methanogen does not significantly.

5. Conclusions and Outlook

5.1. General conclusions

In this thesis, new insights into anaerobic benzene and naphthalene degradation were obtained through a series of experiments, with the aid of omics techniques, physiological experiments, and stable isotopes.

(1) Proteogenomic analyses of *Pelotomaculum* candidate BPL shed new light on anaerobic benzene degradation by sulfate-reducing microorganisms and in particular by the genus *Pelotomaculum*. The member of the genus *Pelotomaculum* identified here, candidate strain BPL, did not only degrade benzene in the absence of molecular oxygen but also performed sulfate reduction, making it the first representative of the genus *Pelotomaculum* which has the capacity to grow by dissimilatory sulfate reduction. Comparison with other benzene-degrading cultures indicates that such co-cultures might be wide spread. Detection of *Pelotomaculum* species in cultures or natural samples therefore does not literally indicate fermentation, especially in the case of the anaerobic hydrocarbon degradation.

(2) The current view upon anaerobic degradation processes is mostly focused on key player perspective. However, plenty of molecular studies, and recently metagenomics studies indicate some microbial species exist in high abundances in the community but they are apparently not involved in the key degradation process. By the example of environmental Spirochaetes who recycle detrital biomass in a simple subsurface microbial loop, an explanation was provided for these microbes. They are most likely involved in necromass recycling providing electrons and nutrients to associated degraders. Thus, they are similarly important as the key organisms. Such loops are likely to be especially important in hydrocarbon-containing sites and other extreme habitats where physicochemical conditions challenge bacterial integrity as well as in oligotrophic subsurface habitats like the deep terrestrial subsurface.

(3) Assessing the mineralization of many substrates like PAHs and crude oil mixtures can be very difficult because of issues such as low water solubility and

complexity. While CO_2 production can be readily measured by starting with radiolabeled substrates (^{14}C), special facilities are typically required. In contrast, stable isotopes are safer and easier to handle but aside from a few ^{13}C-labeled substrates (especially hydrocarbons) are not commercially available. Compared to them, the advantage of the RIL method lies in the very precise analysis of the $^{13}C/^{12}C$ ratio which allows for the detection of very small CO_2 production and in the relatively cheap addition of $^{13}CO_2$ instead of ^{13}C-labelled organic compounds. This could also be measured with classical IRMS but the application of the new Delta Ray promises a much easier and cheaper analysis. Mass balance can be used to denote equations to calculate microbial CO_2 production. The method can be used in a wide range of applications, such as monitoring crude oil degradation under anoxic conditions and discovering organic carbon turnover under aerobic conditions.

5.2. Future perspective

Cultivation-independent genomics has greatly improved our understanding of microbial physiology and ecology. Especially, relying on the fast development of bioinformatics methods, enormous amounts of draft genomes with high qualities have been produced these days. More strikingly, there are even a lot of candidate phyla found with no cultivated representatives (Hug et al. 2016). With these genomic data, one can easily reconstruct metabolic pathways as shown in this thesis for *Pelotomaculum* candidate BPL and *R. cohabitans*. But it should be noted that they can only provide potential metabolic functions. Further solid biochemistry should be warranted to provide unambiguous evidence, as shown for experiments of *R. cohabitans* in this thesis.

Besides, a lot of predicted genes in the genome cannot be annotated properly because we just do not know their functions. For example, one goal of the thesis at the beginning is to understand the initial activation mechanism for benzene degradation. However, in this thesis I failed to provide in-depth information about it. The most important reason is due to the limited availability of closely related known proteins. This makes a definitive annotation of the sequences currently unfeasible. Therefore, it is suggested that the further study on the enrichment

culture BPL or other benzene-degrading cultures is to isolate a pure culture for benzene degradation. The cultivation efforts can be not only guided with the genomic data but also beneficial from novel isolation methods (Sizova et al. 2012, Solden et al. 2016). However, most likely the isolation process is extremely difficult and it is even impossible as microbes can only live via interactions with their partners. In this case, we have to play with mixed cultures combining gold standard methods for pure cultures and novel techniques, e.g. comparative omics (transcriptomics and proteomics), stable isotope probing, and high-resolution microscopy.

6. References

Abu Laban, N., Selesi, D., Jobelius, C. and Meckenstock, R.U. (2009) Anaerobic benzene degradation by Gram-positive sulfate-reducing bacteria. FEMS Microbiol Ecol 68(3), 300-311.

Abu Laban, N., Selesi, D., Rattei, T., Tischler, P. and Meckenstock, R.U. (2010) Identification of enzymes involved in anaerobic benzene degradation by a strictly anaerobic iron-reducing enrichment culture. Environ Microbiol 12(10), 2783-2796.

Aburto-Medina, A. and Ball, A.S. (2014) Microorganisms involved in anaerobic benzene degradation. Annals of Microbiology 65(3), 1201-1213.

Assayag, N., Rive, K., Ader, M., Jezequel, D. and Agrinier, P. (2006) Improved method for isotopic and quantitative analysis of dissolved inorganic carbon in natural water samples. Rapid Commun Mass Spectrom 20(15), 2243-2251.

Bagnoud, A., Chourey, K., Hettich, R.L., de Bruijn, I., Andersson, A.F., Leupin, O.X., Schwyn, B. and Bernier-Latmani, R. (2016) Reconstructing a hydrogen-driven microbial metabolic network in Opalinus Clay rock. Nat Commun 7, 12770.

Bahr, A., Fischer, A., Vogt, C. and Bombach, P. (2015) Evidence of polycyclic aromatic hydrocarbon biodegradation in a contaminated aquifer by combined application of in situ and laboratory microcosms using ^{13}C-labelled target compounds. Water Res 69(0), 100-109.

Berdugo-Clavijo, C., Dong, X., Soh, J., Sensen, C.W. and Gieg, L.M. (2012) Methanogenic biodegradation of two-ringed polycyclic aromatic hydrocarbons. FEMS Microbiol Ecol 81(1), 124-133.

Bergmann, F., Selesi, D., Weinmaier, T., Tischler, P., Rattei, T. and Meckenstock, R.U. (2011a) Genomic insights into the metabolic potential of the polycyclic aromatic hydrocarbon degrading sulfate-reducing Deltaproteobacterium N47. Environ Microbiol 13(5), 1125-1137.

Bergmann, F.D., Abu Laban, N.M., Meyer, A.H., Elsner, M. and Meckenstock, R.U. (2011b) Dual (C, H) isotope fractionation in anaerobic low molecular weight (poly)aromatic hydrocarbon (PAH) degradation: potential for field studies and mechanistic implications. Environ Sci Technol 45(16), 6947-6953.

Berry, T.D., Filley, T.R., Clavijo, A.P., Bischoff Gray, M. and Turco, R. (2017) Degradation and Microbial Uptake of C60 Fullerols in Contrasting Agricultural Soils. Environ Sci Technol 51(3), 1387-1394.

Biegel, E., Schmidt, S., Gonzalez, J.M. and Muller, V. (2011) Biochemistry, evolution and physiological function of the Rnf complex, a novel ion-motive electron transport complex in prokaryotes. Cell Mol Life Sci 68(4), 613-634.

Bolliger, C., Hohener, P., Hunkeler, D., Haberli, K. and Zeyer, J. (1999) Intrinsic bioremediation of a petroleum hydrocarbon-contaminated aquifer and assessment of mineralization based on stable carbon isotopes. Biodegradation 10(3), 201-217.

Bowling, D.R., Sargent, S.D., Tanner, B.D. and Ehleringer, J.R. (2003) Tunable diode laser absorption spectroscopy for stable isotope studies of ecosystem–atmosphere CO_2 exchange. Agr Forest Meteorol 118(1-2), 1-19.

Buckel, W. and Thauer, R.K. (2013) Energy conservation via electron bifurcating ferredoxin reduction and proton/Na(+) translocating ferredoxin oxidation. Biochim Biophys Acta 1827(2), 94-113.

Caldwell, M.E. and Suflita, J.M. (2000) Detection of phenol and benzoate as intermediates of anaerobic benzene biodegradation under different terminal electron-accepting conditions. Environ Sci Technol 34(7), 1216-1220.

Callaghan, A.V., Morris, B.E., Pereira, I.A., McInerney, M.J., Austin, R.N., Groves, J.T., Kukor, J.J., Suflita, J.M., Young, L.Y., Zylstra, G.J. and Wawrik, B. (2012) The genome sequence of *Desulfatibacillum alkenivorans* AK-01: a blueprint for anaerobic alkane oxidation. Environ Microbiol 14(1), 101-113.

Caro-Quintero, A., Ritalahti, K.M., Cusick, K.D., Loffler, F.E. and Konstantinidis, K.T. (2012) The chimeric genome of *Sphaerochaeta*: nonspiral spirochetes that break with the prevalent dogma in spirochete biology. mBio 3(3).

Coplen, T.B. (2011) Guidelines and recommended terms for expression of stable-isotope-ratio and gas-ratio measurement results. Rapid Commun Mass Spectrom 25(17), 2538-2560.

Cox, J., Hein, M.Y., Luber, C.A., Paron, I., Nagaraj, N. and Mann, M. (2014) Accurate proteome-wide label-free quantification by delayed normalization and maximal peptide ratio extraction, termed MaxLFQ. Mol Cell Proteomics 13(9), 2513-2526.

Cox, J. and Mann, M. (2008) MaxQuant enables high peptide identification rates, individualized p.p.b.-range mass accuracies and proteome-wide protein quantification. Nature Biotechnol 26(12), 1367-1372.

Cox, J., Neuhauser, N., Michalski, A., Scheltema, R.A., Olsen, J.V. and Mann, M. (2011) Andromeda: a peptide search engine integrated into the MaxQuant environment. J Proteome Res 10(4), 1794-1805.

Crosson, E.R., Ricci, K.N., Richman, B.A., Chilese, F.C., Owano, T.G., Provencal, R.A., Todd, M.W., Glasser, J., Kachanov, A.A., Paldus, B.A., Spence, T.G. and Zare, R.N. (2002) Stable isotope ratios using cavity ring-down spectroscopy: determination of $^{13}C/^{12}C$ for carbon dioxide in human breath. Anal Chem 74(9), 2003-2007.

Dannoura, M., Maillard, P., Fresneau, C., Plain, C., Berveiller, D., Gerant, D., Chipeaux, C., Bosc, A., Ngao, J., Damesin, C., Loustau, D. and Epron, D. (2011) In situ assessment of the velocity of carbon transfer by tracing ^{13}C in trunk CO_2 efflux after pulse labelling: variations among tree species and seasons. New Phytol 190(1), 181-192.

Dean, J.A. (1987) Handbook of organic chemistry, McGraw-Hill Book Company New York.

Devine, C.E. (2013) Identification of key organisms, genes and pathways in benzene-degrading methanogenic cultures, University of Toronto.

Di Martino, R.M.R., Capasso, G. and Camarda, M. (2016) Spatial domain analysis of carbon dioxide from soils on Vulcano Island: Implications for CO_2 output evaluation. Chem Geol 444, 59-70.

Dodsworth, J.A., Blainey, P.C., Murugapiran, S.K., Swingley, W.D., Ross, C.A., Tringe, S.G., Chain, P.S., Scholz, M.B., Lo, C.C., Raymond, J., Quake, S.R. and Hedlund, B.P. (2013) Single-cell and metagenomic analyses indicate a fermentative and saccharolytic lifestyle for members of the OP9 lineage. Nat Commun 4, 1854.

Dolfing, J. (2014) Syntrophy in microbial fuel cells. ISME J 8(1), 4-5.

Droge, J., Gregor, I. and McHardy, A.C. (2015) Taxator-tk: precise taxonomic assignment of metagenomes by fast approximation of evolutionary neighborhoods. Bioinformatics 31(6), 817-824.

Duhamel, M. and Edwards, E.A. (2006) Microbial composition of chlorinated ethene-degrading cultures dominated by *Dehalococcoides*. FEMS Microbiol Ecol 58(3), 538-549.

Edgar, R.C. (2004) MUSCLE: multiple sequence alignment with high accuracy and high throughput. Nucleic Acids Res 32(5), 1792-1797.

Elsner, M. (2010) Stable isotope fractionation to investigate natural transformation mechanisms of organic contaminants: principles, prospects and limitations. J Environ Monit 12(11), 2005-2031.

Ezaki, T. (2015) Bergey's Manual of Systematics of Archaea and Bacteria, John Wiley & Sons, Ltd.

Fenchel, T. (2008) The microbial loop – 25 years later. J Exp Mar Biol Ecol 366(1-2), 99-103.

Fischer, A., Herklotz, I., Herrmann, S., Thullner, M., Weelink, S.A., Stams, A.J., Schlomann, M., Richnow, H.H. and Vogt, C. (2008) Combined carbon and hydrogen isotope fractionation investigations for elucidating benzene biodegradation pathways. Environ Sci Technol 42(12), 4356-4363.

Fischer, A., Manefield, M. and Bombach, P. (2016) Application of stable isotope tools for evaluating natural and stimulated biodegradation of organic pollutants in field studies. Curr Opin Biotechnol 41, 99-107.

Fischer, T.P. and Lopez, T.M. (2016) First airborne samples of a volcanic plume for $\delta^{13}C$ of CO_2 determinations. Geophys Res Lett 43(7), 3272-3279.

Flores, E., Viallon, J., Moussay, P., Griffith, D.W. and Wielgosz, R.I. (2017) Calibration Strategies for FT-IR and Other Isotope Ratio Infrared Spectrometer Instruments for Accurate delta ^{13}C and delta ^{18}O Measurements of CO_2 in Air. Anal Chem 89(6), 3648-3655.

Fuchs, G., Boll, M. and Heider, J. (2011) Microbial degradation of aromatic compounds - from one strategy to four. Nat Rev Microbiol 9(11), 803-816.

Gibert, O., Lefevre, B., Fernandez, M., Bernat, X., Paraira, M., Calderer, M. and Martinez-Llado, X. (2013) Characterising biofilm development on granular activated carbon used for drinking water production. Water Res 47(3), 1101-1110.

Gieg, L.M., Fowler, S.J. and Berdugo-Clavijo, C. (2014) Syntrophic biodegradation of hydrocarbon contaminants. Curr Opin Biotechnol 27, 21-29.

Gkanogiannis, A., Gazut, S., Salanoubat, M., Kanj, S. and Bruls, T. (2016) A scalable assembly-free variable selection algorithm for biomarker discovery from metagenomes. BMC Bioinformatics 17(1), 311.

Goodman, K.J. and Brenna, J.T. (1992) High sensitivity tracer detection using high-precision gas chromatography-combustion isotope ratio mass spectrometry and highly enriched uniformly carbon-13 labeled precursors. Anal Chem 64(10), 1088-1095.

Greening, C., Biswas, A., Carere, C.R., Jackson, C.J., Taylor, M.C., Stott, M.B., Cook, G.M. and Morales, S.E. (2016) Genomic and metagenomic surveys of hydrogenase distribution indicate H_2 is a widely utilised energy source for microbial growth and survival. ISME J 10(3), 761-777.

Gregor, I., Droge, J., Schirmer, M., Quince, C. and McHardy, A.C. (2016) PhyloPythiaS+: a self-training method for the rapid reconstruction of low-ranking taxonomic bins from metagenomes. PeerJ 4, e1603.

Griebler, C. and Lueders, T. (2009) Microbial biodiversity in groundwater ecosystems. Freshwater Biology 54(4), 649-677.

Griebler, C., Safinowski, M., Vieth, A., Richnow, H.H. and Meckenstock, R.U. (2004) Combined application of stable carbon isotope analysis and specific metabolites determination for assessing in situ degradation of aromatic hydrocarbons in a tar oil-contaminated aquifer. Environ Sci Technol 38(2), 617-631.

Hammes, F., Berney, M., Wang, Y., Vital, M., Koster, O. and Egli, T. (2008) Flow-cytometric total bacterial cell counts as a descriptive microbiological parameter for drinking water treatment processes. Water Res 42(1-2), 269-277.

Harrison, F.H. and Harwood, C.S. (2005) The *pimFABCDE* operon from *Rhodopseudomonas palustris* mediates dicarboxylic acid degradation and participates in anaerobic benzoate degradation. Microbiology 151(Pt 3), 727-736.

Hernsdorf, A.W., Amano, Y., Miyakawa, K., Ise, K., Suzuki, Y., Anantharaman, K., Probst, A., Burstein, D., Thomas, B.C. and Banfield, J.F. (2017) Potential for microbial H_2 and metal transformations associated with novel bacteria and archaea in deep terrestrial subsurface sediments. ISME J, DOI: 10.1038/ismej.2017.1039.

Herrmann, S., Kleinsteuber, S., Chatzinotas, A., Kuppardt, S., Lueders, T., Richnow, H.H. and Vogt, C. (2010) Functional characterization of an anaerobic benzene-degrading enrichment culture by DNA stable isotope probing. Environ Microbiol 12(2), 401-411.

Holmes, D.E., Risso, C., Smith, J.A. and Lovley, D.R. (2011) Anaerobic oxidation of benzene by the hyperthermophilic archaeon *Ferroglobus placidus*. Appl Environ Microbiol 77(17), 5926-5933.

Holmes, D.E., Risso, C., Smith, J.A. and Lovley, D.R. (2012) Genome-scale analysis of anaerobic benzoate and phenol metabolism in the hyperthermophilic archaeon *Ferroglobus placidus*. ISME J 6(1), 146-157.

Hu, P., Tom, L., Singh, A., Thomas, B.C., Baker, B.J., Piceno, Y.M., Andersen, G.L. and Banfield, J.F. (2016) Genome-resolved metagenomic analysis reveals roles for candidate phyla and other microbial community members in biogeochemical transformations in oil reservoirs. mBio 7(1), e01669-01615.

Hug, L.A., Baker, B.J., Anantharaman, K., Brown, C.T., Probst, A.J., Castelle, C.J., Butterfield, C.N., Hernsdorf, A.W., Amano, Y., Ise, K., Suzuki, Y., Dudek, N., Relman, D.A., Finstad, K.M., Amundson, R., Thomas, B.C. and Banfield, J.F. (2016) A new view of the tree of life. Nat Microbiol 1, 16048.

Hunkeler, D. (2008) A guide for assessing biodegradation and source identification of organic ground water contaminants using compound specific isotope analysis (CSIA), Office of Research and Development, National Risk Management Research Laboratory, US Environmental Protection Agency.

Imachi, H., Sekiguchi, Y., Kamagata, Y., Hanada, S., Ohashi, A. and Harada, H. (2002) *Pelotomaculum thermopropionicum* gen. nov., sp. nov., an anaerobic, thermophilic, syntrophic propionate-oxidizing bacterium. Int J Syst Evol Microbiol 52(Pt 5), 1729-1735.

Imachi, H., Sekiguchi, Y., Kamagata, Y., Loy, A., Qiu, Y.L., Hugenholtz, P., Kimura, N., Wagner, M., Ohashi, A. and Harada, H. (2006) Non-sulfate-reducing, syntrophic bacteria affiliated with desulfotomaculum cluster I are widely distributed in methanogenic environments. Appl Environ Microbiol 72(3), 2080-2091.

Jackson, B.E. and McInerney, M.J. (2002) Anaerobic microbial metabolism can proceed close to thermodynamic limits. Nature 415(6870), 454-456.

James, K.L., Rios-Hernandez, L.A., Wofford, N.Q., Mouttaki, H., Sieber, J.R., Sheik, C.S., Nguyen, H.H., Yang, Y., Xie, Y., Erde, J., Rohlin, L., Karr, E.A., Loo, J.A., Ogorzalek Loo, R.R., Hurst, G.B., Gunsalus, R.P., Szweda, L.I. and McInerney, M.J. (2016) Pyrophosphate-dependent ATP formation from acetyl Coenzyme A in *Syntrophus aciditrophicus*, a new twist on ATP formation. mBio 7(4).

Jiménez, N., Richnow, H.H., Vogt, C., Treude, T. and Krüger, M. (2016) Methanogenic hydrocarbon degradation: evidence from field and laboratory studies. J Mol Microb Biotech 26(1-3), 227-242.

Johnsen, A.R., Binning, P.J., Aamand, J., Badawi, N. and Rosenbom, A.E. (2013) The gompertz function can coherently describe microbial mineralization of growth-sustaining pesticides. Environ Sci Technol 47(15), 8508-8514.

Junier, P., Junier, T., Podell, S., Sims, D.R., Detter, J.C., Lykidis, A., Han, C.S., Wigginton, N.S., Gaasterland, T. and Bernier-Latmani, R. (2010) The genome of the Gram-positive metal- and sulfate-reducing bacterium *Desulfotomaculum reducens* strain MI-1. Environ Microbiol 12(10), 2738-2754.

Keller, A., Nesvizhskii, A.I., Kolker, E. and Aebersold, R. (2002) Empirical statistical model to estimate the accuracy of peptide identifications made by MS/MS and database search. Anal Chem 74(20), 5383-5392.

Keller, A.H., Schleinitz, K.M., Starke, R., Bertilsson, S., Vogt, C. and Kleinsteuber, S. (2015) Metagenome-based metabolic reconstruction reveals the ecophysiological function of *Epsilonproteobacteria* in a hydrocarbon-contaminated sulfidic aquifer. Front Microbiol 6(1396), 1396.

Kerner, M., Hohenberg, H., Ertl, S., Reckermann, M. and Spitzy, A. (2003) Self-organization of dissolved organic matter to micelle-like microparticles in river water. Nature 422(6928), 150-154.

Kim, M., Oh, H.S., Park, S.C. and Chun, J. (2014) Towards a taxonomic coherence between average nucleotide identity and 16S rRNA gene sequence similarity for species demarcation of prokaryotes. Int J Syst Evol Microbiol 64(Pt 2), 346-351.

Kleemann, R. and Meckenstock, R.U. (2011) Anaerobic naphthalene degradation by Gram-positive, iron-reducing bacteria. FEMS Microbiol Ecol 78(3), 488-496.

Koelschbach, J.S., Mouttaki, H., Pickl, C., Heipieper, H.J., Rachel, R., Lawson, P.A. and Meckenstock, R.U. (2017) *Rectinema cohabitans* gen. nov., sp. nov., a rod-shaped spirochete isolated from an anaerobic naphthalene-degrading enrichment culture. Int J Syst Evol Microbiol DOI: 10.1099/ijsem.0.001799.

Kumar, S., Stecher, G. and Tamura, K. (2016) MEGA7: Molecular Evolutionary Genetics Analysis Version 7.0 for Bigger Datasets. Mol Biol Evol 33(7), 1870-1874.

Kummel, S., Herbst, F.A., Bahr, A., Duarte, M., Pieper, D.H., Jehmlich, N., Seifert, J., von Bergen, M., Bombach, P., Richnow, H.H. and Vogt, C. (2015) Anaerobic naphthalene degradation by sulfate-reducing *Desulfobacteraceae* from various anoxic aquifers. FEMS Microbiol Ecol 91(3).

Kunapuli, U., Lueders, T. and Meckenstock, R.U. (2007) The use of stable isotope probing to identify key iron-reducing microorganisms involved in anaerobic benzene degradation. ISME J 1(7), 643-653.

Kung, J.W., Loffler, C., Dorner, K., Heintz, D., Gallien, S., Van Dorsselaer, A., Friedrich, T. and Boll, M. (2009) Identification and characterization of the tungsten-containing class of benzoyl-coenzyme A reductases. Proc Natl Acad Sci U S A 106(42), 17687-17692.

Laso-Pérez, R., Wegener, G., Knittel, K., Widdel, F., Harding, K.J., Krukenberg, V., Meier, D.V., Richter, M., Tegetmeyer, H.E., Riedel, D., Richnow, H.-H., Adrian, L., Reemtsma, T., Lechtenfeld, O.J. and Musat, F. (2016) Thermophilic archaea activate butane via alkyl-coenzyme M formation. Nature 539(7629), 396-401.

Lee, W.P., Stromberg, M.P., Ward, A., Stewart, C., Garrison, E.P. and Marth, G.T. (2014) MOSAIK: a hash-based algorithm for accurate next-generation sequencing short-read mapping. PLoS ONE 9(3), e90581.

Liou, J.S., Derito, C.M. and Madsen, E.L. (2008) Field-based and laboratory stable isotope probing surveys of the identities of both aerobic and anaerobic benzene-metabolizing microorganisms in freshwater sediment. Environ Microbiol 10(8), 1964-1977.

Loffler, C., Kuntze, K., Vazquez, J.R., Rugor, A., Kung, J.W., Bottcher, A. and Boll, M. (2011) Occurrence, genes and expression of the W/Se-containing class II benzoyl-coenzyme A reductases in anaerobic bacteria. Environ Microbiol 13(3), 696-709.

Lovley, D.R. and Klug, M.J. (1983) Sulfate reducers can outcompete methanogens at freshwater sulfate concentrations. Appl Environ Microbiol 45(1), 187-192.

Lueders, T. (2017) The ecology of anaerobic degraders of BTEX hydrocarbons in aquifers. FEMS Microbiol Ecol 93(1), fiw220-fiw220.

Luo, F., Devine, C.E. and Edwards, E.A. (2016) Cultivating microbial dark matter in benzene-degrading methanogenic consortia. Environ Microbiol 18(9), 2923-2936.

Luo, F., Gitiafroz, R., Devine, C.E., Gong, Y., Hug, L.A., Raskin, L. and Edwards, E.A. (2014) Metatranscriptome of an anaerobic benzene-degrading, nitrate-reducing enrichment culture reveals involvement of carboxylation in benzene ring activation. Appl Environ Microbiol 80(14), 4095-4107.

Lykidis, A., Chen, C.L., Tringe, S.G., McHardy, A.C., Copeland, A., Kyrpides, N.C., Hugenholtz, P., Macarie, H., Olmos, A., Monroy, O. and Liu, W.T. (2011) Multiple syntrophic interactions in a terephthalate-degrading methanogenic consortium. ISME J 5(1), 122-130.

Madigan, M.T., Martinko, J.M., Dunlap, P.V. and Clark, D.P. (2008) Brock Biology of Microorganisms 12th edn.

Mancini, S.A., Devine, C.E., Elsner, M., Nandi, M.E., Ulrich, A.C., Edwards, E.A. and Lollar, B.S. (2008) Isotopic evidence suggests different initial reaction mechanisms for anaerobic benzene biodegradation. Environ Sci Technol 42(22), 8290-8296.

Manoli, E. and Samara, C. (1999) Polycyclic aromatic hydrocarbons in natural waters: sources, occurrence and analysis. Trends Analyt Chem 18(6), 417-428.

Marchler-Bauer, A., Lu, S., Anderson, J.B., Chitsaz, F., Derbyshire, M.K., DeWeese-Scott, C., Fong, J.H., Geer, L.Y., Geer, R.C., Gonzales, N.R., Gwadz, M., Hurwitz, D.I., Jackson, J.D., Ke, Z., Lanczycki, C.J., Lu, F., Marchler, G.H., Mullokandov, M., Omelchenko, M.V., Robertson, C.L., Song, J.S., Thanki, N., Yamashita, R.A., Zhang, D., Zhang, N., Zheng, C. and Bryant, S.H. (2011) CDD: a Conserved Domain Database for the functional annotation of proteins. Nucleic Acids Res 39(Database issue), D225-229.

Markowitz, V.M., Chen, I.M., Chu, K., Szeto, E., Palaniappan, K., Pillay, M., Ratner, A., Huang, J., Pagani, I., Tringe, S., Huntemann, M., Billis, K., Varghese, N., Tennessen, K., Mavromatis, K., Pati, A., Ivanova, N.N. and Kyrpides, N.C. (2014) IMG/M 4 version of the integrated metagenome comparative analysis system. Nucleic Acids Res 42(Database issue), D568-573.

Mavrovouniotis, M.L. (1990) Group contributions for estimating standard gibbs energies of formation of biochemical compounds in aqueous solution. Biotechnol Bioeng 36(10), 1070-1082.

McFarland, M.J. and Sims, R.C. (1991) Thermodynamic framework for evaluating PAH degradation in the subsurface. Ground Water 29(6), 885-896.

Meckenstock, R.U., Annweiler, E., Michaelis, W., Richnow, H.H. and Schink, B. (2000) Anaerobic naphthalene degradation by a sulfate-reducing enrichment culture. Appl Environ Microbiol 66(7), 2743-2747.

Meckenstock, R.U., Boll, M., Mouttaki, H., Koelschbach, J.S., Cunha Tarouco, P., Weyrauch, P., Dong, X. and Himmelberg, A.M. (2016) Anaerobic degradation of benzene and polycyclic aromatic hydrocarbons. J Mol Microbiol Biotechnol 26(1-3), 92-118.

Meckenstock, R.U., Elsner, M., Griebler, C., Lueders, T., Stumpp, C., Aamand, J., Agathos, S.N., Albrechtsen, H.J., Bastiaens, L., Bjerg, P.L., Boon, N., Dejonghe, W., Huang, W.E., Schmidt, S.I., Smolders, E., Sorensen, S.R., Springael, D. and van Breukelen, B.M. (2015) Biodegradation: Updating the concepts of control for microbial cleanup in contaminated aquifers. Environ Sci Technol 49(12), 7073-7081.

Meckenstock, R.U. and Mouttaki, H. (2011) Anaerobic degradation of non-substituted aromatic hydrocarbons. Curr Opin Biotechnol 22(3), 406-414.

Meckenstock, R.U. and Richnow, H.H. (2010) Handbook of Hydrocarbon and Lipid Microbiology. Timmis, K. (ed), pp. 3603-3611, Springer Berlin Heidelberg.

Meckenstock, R.U., von Netzer, F., Stumpp, C., Lueders, T., Himmelberg, A.M., Hertkorn, N., Schmitt-Kopplin, P., Harir, M., Hosein, R., Haque, S. and Schulze-Makuch, D. (2014) Water droplets in oil are microhabitats for microbial life. Science 345(6197), 673-676.

Michalski, A., Damoc, E., Lange, O., Denisov, E., Nolting, D., Muller, M., Viner, R., Schwartz, J., Remes, P., Belford, M., Dunyach, J.J., Cox, J., Horning, S., Mann, M. and Makarov, A. (2012) Ultra high resolution linear ion trap Orbitrap mass spectrometer (Orbitrap Elite) facilitates top down LC MS/MS and versatile peptide fragmentation modes. Mol Cell Proteomics 11(3), O111 013698.

Milne, I., Stephen, G., Bayer, M., Cock, P.J., Pritchard, L., Cardle, L., Shaw, P.D. and Marshall, D. (2013) Using Tablet for visual exploration of second-generation sequencing data. Brief Bioinform 14(2), 193-202.

Mittal, M. and Rockne, K.J. (2008) Indole production by *Pseudomonas stutzeri* strain NAP-3 during anaerobic naphthalene biodegradation in the presence of dimethyl formamide. J Environ Sci Health A Tox Hazard Subst Environ Eng 43(9), 1027-1034.

Mock, J., Wang, S., Huang, H., Kahnt, J. and Thauer, R.K. (2014) Evidence for a hexaheteromeric methylenetetrahydrofolate reductase in *Moorella thermoacetica*. J Bacteriol 196(18), 3303-3314.

Morasch, B., Hohener, P. and Hunkeler, D. (2007) Evidence for in situ degradation of mono-and polyaromatic hydrocarbons in alluvial sediments based on microcosm experiments with ^{13}C-labeled contaminants. Environ Pollut 148(3), 739-748.

Morasch, B., Hunkeler, D., Zopfi, J., Temime, B. and Hohener, P. (2011) Intrinsic biodegradation potential of aromatic hydrocarbons in an alluvial aquifer--potentials and limits of signature metabolite analysis and two stable isotope-based techniques. Water Res 45(15), 4459-4469.

Morris, B.E., Henneberger, R., Huber, H. and Moissl-Eichinger, C. (2013) Microbial syntrophy: interaction for the common good. FEMS Microbiol Rev 37(3), 384-406.

Musat, F., Galushko, A., Jacob, J., Widdel, F., Kube, M., Reinhardt, R., Wilkes, H., Schink, B. and Rabus, R. (2009) Anaerobic degradation of naphthalene and 2-methylnaphthalene by strains of marine sulfate-reducing bacteria. Environ Microbiol 11(1), 209-219.

Musat, F. and Widdel, F. (2008) Anaerobic degradation of benzene by a marine sulfate-reducing enrichment culture, and cell hybridization of the dominant phylotype. Environ Microbiol 10(1), 10-19.

Nijenhuis, I., Stelzer, N., Kästner, M. and Richnow, H.-H. (2007) Sensitive detection of anaerobic monochlorobenzene degradation using stable isotope tracers. Environ Sci Technol 41(11), 3836-3842.

Nobu, M.K., Narihiro, T., Rinke, C., Kamagata, Y., Tringe, S.G., Woyke, T. and Liu, W.T. (2015) Microbial dark matter ecogenomics reveals complex synergistic networks in a methanogenic bioreactor. ISME J 9(8), 1710-1722.

Oberender, J., Kung, J.W., Seifert, J., von Bergen, M. and Boll, M. (2012) Identification and characterization of a succinyl-coenzyme A (CoA):benzoate CoA transferase in Geobacter metallireducens. J Bacteriol 194(10), 2501-2508.

Olsen, J.V., de Godoy, L.M., Li, G., Macek, B., Mortensen, P., Pesch, R., Makarov, A., Lange, O., Horning, S. and Mann, M. (2005) Parts per million mass accuracy on an Orbitrap mass spectrometer via lock mass injection into a C-trap. Mol Cell Proteomics 4(12), 2010-2021.

Oosterkamp, M.J., Veuskens, T., Talarico Saia, F., Weelink, S.A., Goodwin, L.A., Daligault, H.E., Bruce, D.C., Detter, J.C., Tapia, R., Han, C.S., Land, M.L., Hauser, L.J., Langenhoff, A.A., Gerritse, J., van Berkel, W.J., Pieper, D.H., Junca, H., Smidt, H., Schraa, G., Davids, M., Schaap, P.J., Plugge, C.M. and Stams, A.J. (2013) Genome analysis and physiological comparison of *Alicycliphilus denitrificans* strains BC and K601(T.). PLoS ONE 8(6), e66971.

Parks, D.H., Imelfort, M., Skennerton, C.T., Hugenholtz, P. and Tyson, G.W. (2015) CheckM: assessing the quality of microbial genomes recovered from isolates, single cells, and metagenomes. Genome Res 25(7), 1043-1055.

Pereira, I.A., Ramos, A.R., Grein, F., Marques, M.C., da Silva, S.M. and Venceslau, S.S. (2011) A comparative genomic analysis of energy metabolism in sulfate reducing bacteria and archaea. Front Microbiol 2, 69.

Phelps, C.D., Zhang, X. and Young, L.Y. (2001) Use of stable isotopes to identify benzoate as a metabolite of benzene degradation in a sulphidogenic consortium. Environ Microbiol 3(9), 600-603.

Philipp, B. and Schink, B. (2012) Different strategies in anaerobic biodegradation of aromatic compounds: nitrate reducers versus strict anaerobes. Environ Microbiol Rep 4(5), 469-478.

Plain, C., Gerant, D., Maillard, P., Dannoura, M., Dong, Y., Zeller, B., Priault, P., Parent, F. and Epron, D. (2009) Tracing of recently assimilated carbon in respiration at high temporal resolution in the field with a tuneable diode laser absorption spectrometer after in situ $^{13}CO_2$ pulse labelling of 20-year-old beech trees. Tree Physiol 29(11), 1433-1445.

Plugge, C.M., Zhang, W., Scholten, J.C. and Stams, A.J. (2011) Metabolic flexibility of sulfate-reducing bacteria. Front Microbiol 2, 81.

Probst, A.J., Castelle, C.J., Singh, A., Brown, C.T., Anantharaman, K., Sharon, I., Hug, L.A., Burstein, D., Emerson, J.B., Thomas, B.C. and Banfield, J.F. (2017) Genomic resolution of a cold subsurface aquifer community provides metabolic insights for novel microbes adapted to high CO_2 concentrations. Environ Microbiol 19(2), 459-474.

Qiu, Y.L., Sekiguchi, Y., Hanada, S., Imachi, H., Tseng, I.C., Cheng, S.S., Ohashi, A., Harada, H. and Kamagata, Y. (2006) *Pelotomaculum terephthalicum* sp. nov. and *Pelotomaculum isophthalicum* sp. nov.: two anaerobic bacteria that degrade phthalate isomers in syntrophic association with hydrogenotrophic methanogens. Arch Microbiol 185(3), 172-182.

Ragsdale, S.W. (2016) Deep-sea secrets of butane metabolism. Nature 539(7629), 367-368.

Rakoczy, J., Schleinitz, K.M., Muller, N., Richnow, H.H. and Vogt, C. (2011) Effects of hydrogen and acetate on benzene mineralisation under sulphate-reducing conditions. FEMS Microbiol Ecol 77(2), 238-247.

Ramos, A.R., Grein, F., Oliveira, G.P., Venceslau, S.S., Keller, K.L., Wall, J.D. and Pereira, I.A. (2015) The FlxABCD-HdrABC proteins correspond to a novel NADH dehydrogenase/heterodisulfide reductase widespread in anaerobic bacteria and involved in ethanol metabolism in *Desulfovibrio vulgaris* Hildenborough. Environ Microbiol 17(7), 2288-2305.

Rappsilber, J., Mann, M. and Ishihama, Y. (2007) Protocol for micro-purification, enrichment, pre-fractionation and storage of peptides for proteomics using StageTips. Nat Protoc 2(8), 1896-1906.

Rawlings, N.D., Barrett, A.J. and Finn, R. (2016) Twenty years of the MEROPS database of proteolytic enzymes, their substrates and inhibitors. Nucleic Acids Res 44(D1), D343-350.

Reinsch, S. and Ambus, P. (2013) In situ $^{13}CO_2$ pulse-labeling in a temperate heathland--development of a mobile multi-plot field setup. Rapid Commun Mass Spectrom 27(13), 1417-1428.

Ribeiro, F.J., Przybylski, D., Yin, S., Sharpe, T., Gnerre, S., Abouelleil, A., Berlin, A.M., Montmayeur, A., Shea, T.P., Walker, B.J., Young, S.K., Russ, C., Nusbaum, C., MacCallum, I. and Jaffe, D.B. (2012) Finished bacterial genomes from shotgun sequence data. Genome Res 22(11), 2270-2277.

Ritalahti, K.M., Justicia-Leon, S.D., Cusick, K.D., Ramos-Hernandez, N., Rubin, M., Dornbush, J. and Loffler, F.E. (2012) *Sphaerochaeta globosa* gen. nov., sp. nov. and *Sphaerochaeta pleomorpha* sp. nov., free-living, spherical spirochaetes. Int J Syst Evol Microbiol 62(Pt 1), 210-216.

Rizzo, A.L., Liuzzo, M., Ancellin, M.A. and Jost, H.J. (2015) Real-time measurements of $\delta^{13}C$, CO_2 concentration, and CO_2/SO_2 in volcanic plume gases at Mount Etna, Italy, over 5 consecutive days. Chem Geol 411, 182-191.

Rodriguez Martinez, M.F., Kelessidou, N., Law, Z., Gardiner, J. and Stephens, G. (2008) Effect of solvents on obligately anaerobic bacteria. Anaerobe 14(1), 55-60.

Saitou, N. and Nei, M. (1987) The neighbor-joining method: a new method for reconstructing phylogenetic trees. Mol Biol Evol 4(4), 406-425.

Salinero, K.K., Keller, K., Feil, W.S., Feil, H., Trong, S., Di Bartolo, G. and Lapidus, A. (2009) Metabolic analysis of the soil microbe *Dechloromonas aromatica* str. RCB: indications of a surprisingly complex life-style and cryptic anaerobic pathways for aromatic degradation. BMC Genomics 10(1), 351.

Samanta, S.K., Singh, O.V. and Jain, R.K. (2002) Polycyclic aromatic hydrocarbons: environmental pollution and bioremediation. Trends Biotechnol 20(6), 243-248.

Schmidt, T.C. and Jochmann, M.A. (2012) Origin and fate of organic compounds in water: characterization by compound-specific stable isotope analysis. Annu Rev Anal Chem (Palo Alto Calif) 5(1), 133-155.

Schuler, S. (1990) Soils contain two different activities for oxidation of hydrogen. FEMS Microbiol Lett 73(1), 77-84.

Schwartz, E., Fritsch, J. and Friedrich, B. (2013) The Prokaryotes: Prokaryotic Physiology and Biochemistry. Rosenberg, E., DeLong, E.F., Lory, S., Stackebrandt, E. and Thompson, F. (eds), pp. 119-199, Springer Berlin Heidelberg, Berlin, Heidelberg.

Selesi, D., Jehmlich, N., von Bergen, M., Schmidt, F., Rattei, T., Tischler, P., Lueders, T. and Meckenstock, R.U. (2010) Combined genomic and proteomic approaches identify gene clusters involved in anaerobic 2-methylnaphthalene degradation in the sulfate-reducing enrichment culture N47. J Bacteriol 192(1), 295-306.

Sherry, A., Grant, R.J., Aitken, C.M., Jones, D.M., Head, I.M. and Gray, N.D. (2014) Volatile hydrocarbons inhibit methanogenic crude oil degradation. Front Microbiol 5(131), 131.

Sieber, J.R., McInerney, M.J. and Gunsalus, R.P. (2012) Genomic insights into syntrophy: the paradigm for anaerobic metabolic cooperation. Annu Rev Microbiol 66(1), 429-452.

Siegert, M., Cichocka, D., Herrmann, S., Grundger, F., Feisthauer, S., Richnow, H.H., Springael, D. and Kruger, M. (2011) Accelerated methanogenesis from aliphatic and aromatic hydrocarbons under iron- and sulfate-reducing conditions. FEMS Microbiol Lett 315(1), 6-16.

Simpson, D.R. (2008) Biofilm processes in biologically active carbon water purification. Water Res 42(12), 2839-2848.

Sizova, M.V., Hohmann, T., Hazen, A., Paster, B.J., Halem, S.R., Murphy, C.M., Panikov, N.S. and Epstein, S.S. (2012) New approaches for isolation of previously uncultivated oral bacteria. Appl Environ Microbiol 78(1), 194-203.

Solden, L., Lloyd, K. and Wrighton, K. (2016) The bright side of microbial dark matter: lessons learned from the uncultivated majority. Curr Opin Microbiol 31, 217-226.

Søndergaard, D., Pedersen, C.N.S. and Greening, C. (2016) HydDB: a web tool for hydrogenase classification and analysis. Sci Rep 6, 34212.

Sorokin, D.Y., Gumerov, V.M., Rakitin, A.L., Beletsky, A.V., Damste, J.S., Muyzer, G., Mardanov, A.V. and Ravin, N.V. (2014) Genome analysis of *Chitinivibrio alkaliphilus* gen. nov., sp. nov., a novel extremely haloalkaliphilic anaerobic chitinolytic bacterium from the candidate phylum Termite Group 3. Environ Microbiol 16(6), 1549-1565.

Spormann, A.M. and Thauer, R.K. (1988) Anaerobic acetate oxidation to CO_2 by *Desulfotomaculum acetoxidans*. Arch Microbiol 150(4), 374-380.

Stackebrandt, E. (2014) The Prokaryotes: Firmicutes and Tenericutes. Rosenberg, E., DeLong, E.F., Lory, S., Stackebrandt, E. and Thompson, F. (eds), pp. 285-290, Springer Berlin Heidelberg, Berlin, Heidelberg.

Stams, A.J. and Plugge, C.M. (2009) Electron transfer in syntrophic communities of anaerobic bacteria and archaea. Nat Rev Microbiol 7(8), 568-577.

Starke, R., Keller, A., Jehmlich, N., Vogt, C., Richnow, H.H., Kleinsteuber, S., von Bergen, M. and Seifert, J. (2016) Pulsed $^{13}C_2$-Acetate Protein-SIP unveils *Epsilonproteobacteria* as dominant acetate utilizers in a sulfate-reducing microbial community mineralizing benzene. Microb Ecol 71(4), 901-911.

Staudinger, J. and Roberts, P.V. (1996) A critical review of Henry's law constants for environmental applications. Crit. Rev. Environ. Sci. Technol. 26(3), 205-297.

Stoddard, S.F., Smith, B.J., Hein, R., Roller, B.R. and Schmidt, T.M. (2015) rrnDB: improved tools for interpreting rRNA gene abundance in bacteria and archaea and a new foundation for future development. Nucleic Acids Res 43(Database issue), D593-598.

Stookey, L.L. (2002) Ferrozine---a new spectrophotometric reagent for iron. Anal Chem 42(7), 779-781.

Straub, K.L., Benz, M. and Schink, B. (2001) Iron metabolism in anoxic environments at near neutral pH. FEMS Microbiol Ecol 34(3), 181-186.

Strittmatter, A.W., Liesegang, H., Rabus, R., Decker, I., Amann, J., Andres, S., Henne, A., Fricke, W.F., Martinez-Arias, R., Bartels, D., Goesmann, A., Krause, L., Puhler, A., Klenk, H.P., Richter, M., Schuler, M., Glockner, F.O., Meyerdierks, A., Gottschalk, G. and Amann, R. (2009) Genome sequence of *Desulfobacterium autotrophicum* HRM2, a marine sulfate reducer oxidizing organic carbon completely to carbon dioxide. Environ Microbiol 11(5), 1038-1055.

Tabatabai, M.A. (2009) A rapid method for determination of sulfate in water samples. Ecol Lett 7(3), 237-243.

Taubert, M., Vogt, C., Wubet, T., Kleinsteuber, S., Tarkka, M.T., Harms, H., Buscot, F., Richnow, H.H., von Bergen, M. and Seifert, J. (2012) Protein-SIP enables time-resolved analysis of the carbon flux in a sulfate-reducing, benzene-degrading microbial consortium. ISME J 6(12), 2291-2301.

Thauer, R.K., Jungermann, K. and Decker, K. (1977) Energy conservation in chemotrophic anaerobic bacteria. Bacteriol Rev 41(1), 100-180.

Tremblay, P.L., Zhang, T., Dar, S.A., Leang, C. and Lovley, D.R. (2012) The Rnf complex of *Clostridium ljungdahlii* is a proton-translocating ferredoxin:NAD^+ oxidoreductase essential for autotrophic growth. mBio 4(1), e00406-00412.

Tyanova, S., Temu, T., Sinitcyn, P., Carlson, A., Hein, M.Y., Geiger, T., Mann, M. and Cox, J. (2016) The Perseus computational platform for comprehensive analysis of (prote)omics data. Nat Methods 13(9), 731-740.

Ulrich, A.C. and Edwards, E.A. (2003) Physiological and molecular characterization of anaerobic benzene-degrading mixed cultures. Environ Microbiol 5(2), 92-102.

Vallenet, D., Belda, E., Calteau, A., Cruveiller, S., Engelen, S., Lajus, A., Le Fevre, F., Longin, C., Mornico, D., Roche, D., Rouy, Z., Salvignol, G., Scarpelli, C., Thil Smith, A.A., Weiman, M. and Medigue, C. (2013) MicroScope--an integrated microbial resource for the curation and comparative analysis of genomic and metabolic data. Nucleic Acids Res 41(Database issue), D636-647.

Vallenet, D., Labarre, L., Rouy, Z., Barbe, V., Bocs, S., Cruveiller, S., Lajus, A., Pascal, G., Scarpelli, C. and Medigue, C. (2006) MaGe: a microbial genome annotation system supported by synteny results. Nucleic Acids Res 34(1), 53-65.

van der Waals, M.J., Atashgahi, S., da Rocha, U.N., van der Zaan, B.M., Smidt, H. and Gerritse, J. (2017) Benzene degradation in a denitrifying biofilm reactor: activity and microbial community composition. Appl Microbiol Biotechnol, 1-14.

van der Zaan, B.M., Saia, F.T., Stams, A.J., Plugge, C.M., de Vos, W.M., Smidt, H., Langenhoff, A.A. and Gerritse, J. (2012) Anaerobic benzene degradation under denitrifying conditions: *Peptococcaceae* as dominant benzene degraders and evidence for a syntrophic process. Environ Microbiol 14(5), 1171-1181.

van Geldern, R., Nowak, M.E., Zimmer, M., Szizybalski, A., Myrttinen, A., Barth, J.A. and Jost, H.J. (2014) Field-based stable isotope analysis of carbon dioxide by mid-infrared laser spectroscopy for carbon capture and storage monitoring. Anal Chem 86(24), 12191-12198.

Velten, S., Boller, M., Koster, O., Helbing, J., Weilenmann, H.U. and Hammes, F. (2011) Development of biomass in a drinking water granular active carbon (GAC) filter. Water Res 45(19), 6347-6354.

Velten, S., Hammes, F., Boller, M. and Egli, T. (2007) Rapid and direct estimation of active biomass on granular activated carbon through adenosine tri-phosphate (ATP) determination. Water Res 41(9), 1973-1983.

Vizcaino, J.A., Csordas, A., del-Toro, N., Dianes, J.A., Griss, J., Lavidas, I., Mayer, G., Perez-Riverol, Y., Reisinger, F., Ternent, T., Xu, Q.W., Wang, R. and Hermjakob, H. (2016) 2016 update of the PRIDE database and its related tools. Nucleic Acids Res 44(D1), D447-456.

Vogt, C., Kleinsteuber, S. and Richnow, H.H. (2011) Anaerobic benzene degradation by bacteria. Microb Biotechnol 4(6), 710-724.

von Toerne, C., Kahle, M., Schafer, A., Ispiryan, R., Blindert, M., Hrabe De Angelis, M., Neschen, S., Ueffing, M. and Hauck, S.M. (2013) Apoe, Mbl2, and Psp plasma protein levels correlate with diabetic phenotype in NZO mice--an optimized rapid workflow for SRM-based quantification. J Proteome Res 12(3), 1331-1343.

Wahl, E.H., Fidric, B., Rella, C.W., Koulikov, S., Kharlamov, B., Tan, S., Kachanov, A.A., Richman, B.A., Crosson, E.R., Paldus, B.A., Kalaskar, S. and Bowling, D.R. (2006) Applications of cavity ring-down spectroscopy to high precision isotope ratio measurement of $^{13}C/^{12}C$ in carbon dioxide. Isotopes Environ Health Stud 42(1), 21-35.

Wasmund, K., Mußmann, M. and Loy, A. (2017) The life sulfuric: microbial ecology of sulfur cycling in marine sediments. Environmental Microbiology Reports, DOI: 10.1111/1758-2229.12538.

Weelink, S.A., Tan, N.C., ten Broeke, H., van den Kieboom, C., van Doesburg, W., Langenhoff, A.A., Gerritse, J., Junca, H. and Stams, A.J. (2008) Isolation and characterization of *Alicycliphilus denitrificans* strain BC, which grows on benzene with chlorate as the electron acceptor. Appl Environ Microbiol 74(21), 6672-6681.

Wen, G., Kotzsch, S., Vital, M., Egli, T. and Ma, J. (2015) BioMig--a method to evaluate the potential release of compounds from and the formation of biofilms on polymeric materials in contact with drinking water. Environ Sci Technol 49(19), 11659-11669.

Wessel, D. and Flugge, U.I. (1984) A method for the quantitative recovery of protein in dilute solution in the presence of detergents and lipids. Anal Biochem 138(1), 141-143.

Widdel, F. and Bak, F. (1992) The prokaryotes, pp. 3352-3378, Springer.

Widdel, F. and Rabus, R. (2001) Anaerobic biodegradation of saturated and aromatic hydrocarbons. Curr Opin Biotechnol 12(3), 259-276.

Wischgoll, S., Heintz, D., Peters, F., Erxleben, A., Sarnighausen, E., Reski, R., Van Dorsselaer, A. and Boll, M. (2005) Gene clusters involved in anaerobic benzoate degradation of *Geobacter metallireducens*. Mol Microbiol 58(5), 1238-1252.

Wisniewski, J.R., Zougman, A., Nagaraj, N. and Mann, M. (2009) Universal sample preparation method for proteome analysis. Nat Methods 6(5), 359-362.

Wohlbrand, L., Jacob, J.H., Kube, M., Mussmann, M., Jarling, R., Beck, A., Amann, R., Wilkes, H., Reinhardt, R. and Rabus, R. (2013) Complete genome, catabolic sub-proteomes and key-metabolites of *Desulfobacula toluolica* Tol2, a marine, aromatic compound-degrading, sulfate-reducing bacterium. Environ Microbiol 15(5), 1334-1355.

Wolf, P.G., Biswas, A., Morales, S.E., Greening, C. and Gaskins, H.R. (2016) H_2 metabolism is widespread and diverse among human colonic microbes. Gut Microbes 7(3), 235-245.

Wrighton, K.C., Castelle, C.J., Wilkins, M.J., Hug, L.A., Sharon, I., Thomas, B.C., Handley, K.M., Mullin, S.W., Nicora, C.D., Singh, A., Lipton, M.S., Long, P.E., Williams, K.H. and Banfield, J.F. (2014) Metabolic interdependencies between phylogenetically novel fermenters and respiratory organisms in an unconfined aquifer. ISME J 8(7), 1452-1463.

Wu, J.H., Wu, F.Y., Chuang, H.P., Chen, W.Y., Huang, H.J., Chen, S.H. and Liu, W.T. (2013) Community and proteomic analysis of methanogenic consortia degrading terephthalate. Appl Environ Microbiol 79(1), 105-112.

Wu, M. and Scott, A.J. (2012) Phylogenomic analysis of bacterial and archaeal sequences with AMPHORA2. Bioinformatics 28(7), 1033-1034.

Yin, Y., Mao, X., Yang, J., Chen, X., Mao, F. and Xu, Y. (2012) dbCAN: a web resource for automated carbohydrate-active enzyme annotation. Nucleic Acids Res 40(Web Server issue), W445-451.

Zanasi, R., Alfano, D., Scarabino, C., Motta, O., Viglione, R.G. and Proto, A. (2006) Determination of $^{13}C/^{12}C$ carbon isotope ratio. Anal Chem 78(9), 3080-3083.

Zare, R.N., Kuramoto, D.S., Haase, C., Tan, S.M., Crosson, E.R. and Saad, N.M. (2009) High-precision optical measurements of $^{13}C/^{12}C$ isotope ratios in organic compounds at natural abundance. Proc Natl Acad Sci U S A 106(27), 10928-10932.

Zhang, T., Bain, T.S., Nevin, K.P., Barlett, M.A. and Lovley, D.R. (2012) Anaerobic benzene oxidation by *Geobacter* species. Appl Environ Microbiol 78(23), 8304-8310.

Zhang, T., Tremblay, P.L., Chaurasia, A.K., Smith, J.A., Bain, T.S. and Lovley, D.R. (2013) Anaerobic benzene oxidation via phenol in *Geobacter metallireducens*. Appl Environ Microbiol 79(24), 7800-7806.

Zhang, T., Tremblay, P.L., Chaurasia, A.K., Smith, J.A., Bain, T.S. and Lovley, D.R. (2014) Identification of genes specifically required for the anaerobic metabolism of benzene in *Geobacter metallireducens*. Front Microbiol 5, 245.

Zhou, J., Bruns, M.A. and Tiedje, J.M. (1996) DNA recovery from soils of diverse composition. Appl Environ Microbiol 62(2), 316-322.

Zhu, B., Bradford, L., Huang, S., Szalay, A., Leix, C., Weissbach, M., Tancsics, A., Drewes, J.E. and Lueders, T. (2017) Unexpected diversity and high abundance of putative nitric oxide dismutase (Nod) genes in contaminated aquifers and wastewater treatment systems. Appl Environ Microbiol 83(4).

Authorship Clarification

I) Reconstructing metabolic pathways of a member of the genus *Pelotomaculum* suggesting its potential to oxidize benzene to carbon dioxide with direct reduction of sulfate

In Part I, metaproteogenomic analysis was performed on an enrichment culture BPL which carried out benzene oxidation coupled with sulfate reduction. The PhD candidate together with Rainer U. Meckenstock developed the concept of this study and planned laboratory experiments. Kerstin Nicolaisen extracted DNA for the metagenome and protein for one of the metaprotemic analyses (the other one done by the PhD candidate). Thomas Weinmaier conducted initial analyses of the metagenome and Johannes Dröge finished follow-up bioinformatics analysis, including binning process and phylogenetic analysis. Proteins identification was done by Christine von Toerne. The PhD candidate performed data processing with both metagenome and metaproteome. Sviatlana Marozava provided help with metaproteomic analysis. The work was published in FEMS Microbiology Ecology (Dong et al. 2017). The original manuscript draft for Part I was developed by the PhD candidate. All co-authors in this article contributed to writing, reviewing and editing of the manuscript.

Dong X, Dröge J, von Toerne C, Marozava S, McHardy AC, Meckenstock RU (2017). Reconstructing metabolic pathways of a member of the genus *Pelotomaculum* suggesting its potential to oxidize benzene to carbon dioxide with direct reduction of sulfate. *FEMS Microbiology Ecology* **93:** fiw254-fiw254.

II) Fermentative Spirochaetes drive nutrient cycling by a subsurface microbial loop in hydrocarbon-contaminated habitats

In Part II, the functional role of Spirochaetes was explored in contaminated habitats. The PhD candidate together with Rainer U. Meckenstock developed the concept of this study and planned laboratory experiments. The PhD candidate conducted the experiments and data analyses. Chris Greening performed phylogenetic analysis of hydrogenases and revised 16S rRNA gene sequences analysis of Spirochaetes. Ralf

Conrad contributed to gas chromatography analysis of hydrogen concentrations. Thomas Brüls contributed to the part of sequencing and reconstruction of Spirochaetes genomes. Svenja Blaskowski, Farnusch Kaschani, and Markus Kaiser contributed to mass spectrometry-based proteome analyses. The original manuscript draft for Part II was developed by the PhD candidate. All co-authors contributed to writing, reviewing and editing of the manuscript.

Dong X, Greening C, Brüls T, Conrad R, Blaskowski S, Kaschani F, Kaiser M, Meckenstock RU (2017) Fermentative Spirochaetes drive nutrient cycling by a subsurface microbial loop in hydrocarbon-contaminated habitats. *Submitted to the ISME Journal*.

III) Monitoring microbial mineralization using reverse stable isotope labelling analysis by mid-infrared laser spectroscopy

In Part III, a novel method was developed with the name of reverse stable isotope labelling analysis. The PhD candidate together with Rainer U. Meckenstock developed the concept of this study and planned laboratory experiments. Maik A. Jochmann, Martin Elsner, and Armin H. Meyer contributed to experimental parts of Isotope Ratio Mass Spectrometry analyses. The experiments for applying RIL method to determine aerobic mineralization rates were conducted by the bachelor students Leonard E. Bäcker and Mona Rahmatullah. They were supervised by Rainer U. Meckenstock and the PhD candidate. Daniel Schunk and Guido Lens provided the pilot plant used for drinking water production and helped design the experiments for DOC removal. All other experiments were conducted and analyzed by the PhD candidate. The original manuscript draft for Part III was developed by the PhD candidate. All co-authors contributed to writing, reviewing and editing of the manuscript.

Dong X, Jochmann MA, Elsner M, Meyer AH, Bäcker L, Rahmatullah M, Schunk D, Lens G, Meckenstock RU (2017) Monitoring microbial mineralization using reverse stable isotope labelling analysis by mid-infrared laser spectroscopy. *Environmental Science & Technology*. ***Accepted.*** DOI: 10.1021/acs.est.7b02909.

IV) Anaerobic degradation of benzene and polycyclic aromatic hydrocarbons

This is a review article (Meckenstock et al. 2017) published in a special issue of Journal of Molecular Microbiology and Biotechnology. The outline of it was developed by Rainer U. Meckenstock. The PhD candidate wrote “Table 1” and the Section “Stable Isotope Fractionation to Assess Biodegradation of Benzene and PAHs”, which are parts of the introduction of the current PhD thesis (Table 1 in Chapter 1.1 and Chapter 1.6.1). They were revised and edited by Rainer U. Meckenstock.

Meckenstock RU, Boll M, Mouttaki H, Koelschbach JS, Cunha Tarouco P, Weyrauch P, **Dong, X**, Himmelberg AM (2016). Anaerobic degradation of benzene and polycyclic aromatic hydrocarbons. *Journal of Molecular Microbiology and Biotechnology* **26:** 92-118.

CURRICULUM VITAE

Name:	Xiyang Dong
Address:	Bäuminghausstr. 150, 45326 Essen, Germany
Telephone no.:	+49 17661433583
E-Mail:	xiyang.dong@uni-due.de, thegreatlake@126.com
Date of birth:	Jan 3rd,1988
Place of birth:	Shandong, China
Nationality:	Chinese

Education

Mar 2015 – Sep 2017	Guest PhD student at Fakultät für Chemie - Biofilm Centre, University of Duisburg-Essen, Germany Supervisor: Prof. Rainer Meckenstock
Oct 2013 – Sep 2017	PhD student at Institute of Groundwater Ecology, Helmholtz Zentrum München, Germany Supervisor: Prof. Rainer Meckenstock
Sep 2010 – Jun 2013	Master of engineering in Environmental Engineering, Dalian University of Technology, China Supervisor: Prof. Jiti Zhou and Associate Prof. Yu Zhang
Sep 2006 – Jul 2010	Bachelor of engineering in Environmental Engineering, Nanjing Normal University, China

List of Scientific Communications

Scientific Communications Related to the Dissertation

Peer-reviewed publications

1. **Dong X**, Jochmann MA, Elsner M, Meyer AH, Bäcker LE, Rahmatullah M, Schunk D, Lens G, Meckenstock RU (2017) Monitoring microbial mineralization using reverse stable isotope labelling analysis by mid-infrared laser spectroscopy. *Environmental Science & Technology*. ***Accepted.*** DOI: 10.1021/acs.est.7b02909.
2. **Dong X**, Dröge J, von Toerne C, Marozava S, McHardy AC, Meckenstock RU (2017). Reconstructing metabolic pathways of a member of the genus *Pelotomaculum* suggesting its potential to oxidize benzene to carbon dioxide with direct reduction of sulfate. *FEMS Microbiology Ecology* **93:** fiw254-fiw254.
3. Meckenstock RU, Boll M, Mouttaki H, Koelschbach JS, Cunha Tarouco P, Weyrauch P, **Dong, X**, Himmelberg AM (2016). Anaerobic degradation of benzene and polycyclic aromatic hydrocarbons. *Journal of Molecular Microbiology and Biotechnology* **26:** 92-118.

Submitted manuscripts for peer-review

1. **Dong X**, Greening C, Brüls T, Conrad R, Blaskowski S, Kaschani F, Kaiser M, Meckenstock RU (2017) Fermentative Spirochaetes drive nutrient cycling by a subsurface microbial loop in hydrocarbon-contaminated habitats. *Submitted to the ISME Journal*.

Selected conference contributions

1. **Dong X** (2017) The functional role of environmental spirochetes at contaminated sites. **Oral presentation** at Microbiology and Infection 2017 - 5th Joint Conference of the German Society for Hygiene and Microbiology (DGHM) and the Association for General and Applied Microbiology (VAAM), Würzburg, Germany.

2. **Dong X** (2017) Sensitive quantification of microbial mineralization rates using reverse stable isotope labelling analysis of dissolved inorganic carbon by mid-infrared laser spectroscopy. **Oral presentation** at Neujahrskolloquium der Fakultät für Chemie und des Ortsverbandes Essen-Duisburg der GDCh, Essen, Germnay.
3. **Dong X** (2016) Metaproteogenomic analysis revealed a member of the genus *Pelotomaculum* completely oxidizing benzene to carbon dioxide with direct reduction of sulfate. **Poster presentation** at the Annual Conference 2016 of the Association for General and Applied Microbiology (VAAM), Jena, Germany.

Other Scientific Communications Not Related to the Dissertation

Peer-reviewed publications

1. Sun J, Zhang Y, **Dong X**, Chen M, Zhou J (2015). Regeneration of spent NOx scrubber liquor using a dual-chamber microbial fuel cell. *Journal of Chemical Technology & Biotechnology* **90:** 1692-1698.
2. Zhang Y, Shi Z, Chen M, **Dong X**, Zhou J (2015). Evaluation of simultaneous nitrification and denitrification under controlled conditions by an aerobic denitrifier culture. *Bioresource Technology* **175:** 602-605.
3. **Dong X**, Zhang Y, Zhou J, Li H, Wang X, Chen M (2014). Evaluation of simultaneous reduction of Fe(II)EDTA-NO and Fe(III)EDTA by a bacterial pure culture. *Journal of Chemical Technology & Biotechnology* **89:** 111-116.
4. **Dong X**, Zhang Y, Zhou J, Chen M, Wang X, Shi Z (2013). Fe(II)EDTA-NO reduction coupled with Fe(II)EDTA oxidation by a nitrate- and Fe(III)-reducing bacterium. *Bioresource Technology* **138:** 339-344.
5. Chen M, Zhang Y, Zhou J, **Dong X**, Wang X, Shi Z (2013). Sulfate removal by *Desulfovibrio* sp. CMX in chelate scrubbing solutions for NO removal. *Bioresource Technology* **143:** 455-460.
6. Li N, Zhang Y, Li Y, Chen M, **Dong X**, Zhou J (2013). Reduction of Fe(II)EDTA-NO using *Paracoccus denitrificans* and changes of Fe(II)EDTA in the system. *Journal of Chemical Technology & Biotechnology* **88:** 311-316.

7. Wang X, Zhang Y, **Dong X**, Chen M, Shi Z, Zhou J (2013). Fe(II)EDTA-NO reduction by sulfide in the anaerobic aqueous phase: stoichiometry and kinetics. *Energy & Fuels* **27:** 6024-6030.
8. Zhang X, Jin R, Liu G, **Dong** X, Zhou J, Wang A (2013). Removal of nitric oxide from simulated flue gas via denitrification in a hollow-fiber membrane bioreactor. *Journal of Environmental Sciences* **25:** 2239-2246.
9. **Dong X**, Zhang Y, Zhou J, Li N, Chen M (2012). Reduction of Fe(III)EDTA in a NOx scrubber liquor by a denitrifying bacterium and the effects of inorganic sulfur compounds on this process. *Bioresource Technology* **120:** 127-132.

Acknowledgments

First and foremost, I would like to express my deepest gratitude to my supervisor Prof. Rainer Meckenstock. Being a great mentor, he was always willing to assist and provide support and guidance whenever it was needed. He also gave me opportunities to grow skills. His passion and motivation in science greatly inspired me. More importantly, he provided career advice and facilitated opportunities on my career development.

I would like to thank Dr. Tillmann Lüders for being my official supervisor at TUM after Rainer moved to UDE and providing very helpful suggestions on my thesis. I am very grateful to Prof. Wolfgang Liebl for taking over the chair of my doctoral examination committee. Thanks also go to Prof. Siegfried Scherer for being the second examiner. And special thanks to Dr. Maik Jochmann for being a member of my personal Thesis Committee. Much gratitude to Dr. Alfredo Perez de Mora for taking care of me during my first several months in Germany.

Much gratitude to Dr. Johannes Dröge for binning process, Dr. Chris Greening for hydrogenase analysis, and Dr. Thomas Brüls for bioinformatics analysis. Special thanks to the following people for proteome analyses: Dr. Christine von Toerne, Dr. Sviatlana Marozava, Svenja Blaskowski and Dr. Farnusch Kaschani. Many thanks to Prof. Ralf Conrad and Melanie Klose for hydrogen measurement. Thanks Dr. Martin Elsner and Dr. Armin Meyer for IRMS analysis. Thanks also goes to Leonard Bäcker and Mona Rahmatullah for their work on DOC removal project.

I would like to thank Dr. Verena Brauer for translating the abstract into German, and Dr. Hubert Müller for proof-reading my thesis. My gratitude also goes to all group members in the lab of Meckenstock for creating a positive working environment.

I dedicate this thesis to my parents for their unconditional love and support, and to my beloved girlfriend Qing for her love, friendship, help, understanding and patience. Finally, I would acknowledge the Chinese Scholarship Council for financial support.

Appendix

Supporting Tables

Table A1 Expressed genes belonging to *Pelotomaculum* candidate BPL during anaerobic degradation of benzene.

Table A2 List of genes identified in the genomes and used for metabolic pathway reconstruction for Spirochaetes in hydrocarbon- and organohalide-contaminated environments shown in Figure 11. Genes for the illustrated pathways were detected in the genomes of *Rectinema cohabitans* HM, uncultured Spirochaetes bacterium bdmA 4, and uncultured Spirochaetes bacterium SA-8.

Table A3 Proteomic analysis of *R. cohabitans* grown on glucose. Four cultures of *R. cohabitans* strain HM were grown with 10 mM glucose and 0.1% yeast extract. Considering the size is too large to include here, the mass spectrometry proteomics data have been deposited to the ProteomeXchange Consortium via the PRIDE partner repository (https://www.ebi.ac.uk/pride/archive/) with the dataset identifier PXD005624.

Table A4 List of identified proteins for *R. cohabitans* HM as shown in Figure 14. The mass spectrometry proteomics data have been deposited to the ProteomeXchange Consortium via the PRIDE partner repository (https://www.ebi.ac.uk/pride/archive/) with the dataset identifier PXD005624.

Table A1 Expressed genes belonging to *Pelotomaculum* candidate BPL during anaerobic degradation of benzene.

Gene ID in Pelotomaculum spp. Genome	IMG product name
sulfate reduction	
2617919556	putative adenylylsulfate reductase-associated electron transfer protein QmoB
2617919557	putative adenylylsulfate reductase-associated electron transfer protein QmoA
2617919558	adenylylsulfate reductase subunit A
2617919559	dissimilatory adenylylsulfate reductase beta subunit (EC 1.8.99.2)
2617919560	ATP sulfurylase (sulfate adenylyltransferase)
2617919937	K(+)-stimulated pyrophosphate-energized sodium pump
2617920254	Dissimilatory sulfite reductase (desulfoviridin), gamma subunit
2617920256	Nitrate reductase gamma subunit
2617920264	dissimilatory sulfite reductase beta subunit
2617920265	dissimilatory sulfite reductase alpha subunit (EC 1.8.99.1)
2617921751	NADH:ubiquinone oxidoreductase subunit 2 (chain N)
2617921752	NADH:ubiquinone oxidoreductase subunit 4 (chain M)
2617921753	NADH-quinone oxidoreductase subunit L
2617921755	NADH:ubiquinone oxidoreductase subunit 6 (chain J)
2617921756	NADH-quinone oxidoreductase subunit I
2617921757	NADH:ubiquinone oxidoreductase subunit 1 (chain H)
2617921758	NADH-quinone oxidoreductase subunit D
2617921761	NADH-quinone oxidoreductase subunit A
Wood-Ljungdahl pathway	
2617920380	5,10-methylene-tetrahydrofolate dehydrogenase/Methenyl tetrahydrofolate cyclohydrolase
2617920888	Ni-dependent carbon monoxide dehydrogenase precursor
2617921113	methyltetrahydrofolate--corrinoid iron-sulfur protein Co-methyltransferase
2617921126	5,10-methylenetetrahydrofolate reductase
2617921323	Formyltetrahydrofolate synthetase
2617921376	CO dehydrogenase/acetyl-CoA synthase delta subunit (corrinoid Fe-S protein)
2617921377	CO dehydrogenase maturation factor
2617921378	CO dehydrogenase/acetyl-CoA synthase gamma subunit (corrinoid Fe-S protein)
2617922225	formate dehydrogenase, alpha subunit
benzoyl-CoA degradation pathway	
2617919856	6-ketocyclohex-1-ene-1-carbonyl-CoA hydrolase
2617919857	cyclohexa-1,5-dienecarbonyl-CoA hydratase
2617919858	6-hydroxycyclohex-1-ene-1-carbonyl-CoA dehydrogenase
2617919859	Acyl-CoA dehydrogenases
2617921884	tungsten-dependent benzoyl-CoA reductase subunit bamB
2617921892	acetyl-CoA synthetase
2617921893	Enoyl-CoA hydratase/carnithine racemase
2617921894	3-hydroxyacyl-CoA dehydrogenase

2617921895	Acyl dehydratase
2617921991	tungsten-dependent benzoyl-CoA reductase-related protein bamD
unclassfied enzymes	
2617919427	Hemerythrin HHE cation binding domain-containing protein
617921157	Putative zinc-finger
2617919439	TusA-related sulfurtransferase
2617919500	Oxygen-sensitive ribonucleoside-triphosphate reductase
2617919503	S-adenosylhomocysteine hydrolase
2617919510	Acyl carrier protein
2617919522	hypothetical protein
2617919530	large subunit ribosomal protein L28
2617919532	6,7-dimethyl-8-ribityllumazine synthase
2617919573	Aspartokinases
2617919577	Stage IV sporulation protein A (spore_IV_A)
2617919589	4-hydroxy-3-methylbut-2-enyl diphosphate reductase
2617919592	3-phosphoshikimate 1-carboxyvinyltransferase
2617919594	-deoxy-D-arabinoheptulosonate-7-phosphate synthase
2617919604	Protein of unknown function (DUF1657)
2617919613	Pyruvate kinase
2617919632	homocitrate synthase NifV
2617919635	aspartyl/glutamyl-tRNA(Asn/Gln) amidotransferase subunit C
2617919637	hypothetical protein
2617919644	Copper amine oxidase N-terminal domain
2617919645	Copper amine oxidase N-terminal domain
2617919656	YeeE/YedE family (DUF395)
2617919662	hypothetical protein
2617919670	RND family efflux transporter, MFP subunit
2617919674	Predicted Fe-Mo cluster-binding protein, NifX family
2617919678	Subtilisin-like serine proteases
2617919680	Cell fate regulator YlbF, YheA/YmcA/DUF963 family (controls sporulation, competence, biofilm development
2617919682	Cell wall-associated hydrolases (invasion-associated proteins)
2617919702	hypothetical protein
2617919703	Molybdopterin biosynthesis enzyme
2617919704	Molybdopterin biosynthesis enzyme
2617919705	S-layer homology domain
2617919708	molybdopterin adenylyltransferase
2617919709	Co-chaperonin GroES (HSP10)
2617919710	Chaperonin GroEL (HSP60 family)
2617919717	Benzoyl-CoA reductase/2-hydroxyglutaryl-CoA dehydratase subunit, BcrC/BadD/HgdB
2617919759	hypothetical protein
2617919780	dTDP-4-dehydrorhamnose 3,5-epimerase and related enzymes
2617919818	hypothetical protein

2617919824	ABC-type phosphate transport system, periplasmic component
2617919828	phosphate uptake regulator, PhoU
2617919842	Predicted DNA-binding protein with PD1-like DNA-binding motif - COG1661
2617919843	hypothetical protein
2617919851	Sporulation and spore germination
2617919853	3-oxoacyl-[acyl-carrier protein] reductase
2617919854	Acetyl-CoA acetyltransferase
2617919855	Predicted nucleic-acid-binding protein containing a Zn-ribbon - COG1545
2617919865	membrane fusion protein, cobalt-zinc-cadmium efflux system
2617919870	hypothetical protein
2617919871	Transcriptional regulator
2617919884	Nucleoside-diphosphate-sugar epimerases
2617919891	S-adenosylmethionine synthetase
2617919895	Cold shock proteins
2617919896	putative sigma-54 modulation protein
2617919902	Transketolase, C-terminal subunit
2617919903	hypothetical protein
2617919910	Predicted RNA-binding protein - COG1532
2617919923	bifunctional phosphoglucose/phosphomannose isomerase
2617919931	Glyceraldehyde-3-phosphate dehydrogenase/erythrose-4-phosphate dehydrogenase
2617919932	3-phosphoglycerate kinase
2617919933	Triosephosphate isomerase
2617919935	Enolase
2617919952	Small-conductance mechanosensitive channel
2617919957	Phosphoribosylformimino-5-aminoimidazole carboxamide ribonucleotide (ProFAR) isomerase
2617919966	AICAR transformylase/IMP cyclohydrolase PurH (only IMP cyclohydrolase domain in Aful)
2617919972	Phosphoribosylcarboxyaminoimidazole (NCAIR) mutase
2617919980	S-layer homology domain
2617919989	hypothetical protein
2617919992	Rhodanese-related sulfurtransferase
2617919993	Chitobiase/beta-hexosaminidase C-terminal domain
2617919996	Ig-like domain-containing protein
2617919997	hypothetical protein
2617919998	Cohesin domain
2617919999	hypothetical protein
2617920000	hypothetical protein
2617920001	Chitobiase/beta-hexosaminidase C-terminal domain
2617920002	S-layer homology domain
2617920003	hypothetical protein
2617920007	Ribosomal protein S9
2617920017	Uncharacterized protein conserved in bacteria
2617920021	Acyl-CoA dehydrogenases

2617920032	Protein of unknown function (DUF2680)
2617920037	Serine-pyruvate aminotransferase/archaeal aspartate aminotransferase
2617920039	Pyridoxine biosynthesis enzyme
2617920046	DNA polymerase sliding clamp subunit (PCNA homolog)
2617920084	hypothetical protein
2617920087	Aspartyl aminopeptidase
2617920092	Uncharacterized conserved protein - COG3874
2617920122	Uncharacterized conserved protein - COG0432
2617920126	DNA-binding transcriptional regulator, Lrp family
2617920143	LysM domain
2617920195	NADPH-dependent 2,4-dienoyl-CoA reductase, sulfur reductase
2617920210	F0F1-type ATP synthase, epsilon subunit (mitochondrial delta subunit)
2617920211	F0F1-type ATP synthase, beta subunit
2617920212	F0F1-type ATP synthase, gamma subunit
2617920213	F0F1-type ATP synthase, alpha subunit
2617920214	F0F1-type ATP synthase, delta subunit (mitochondrial oligomycin sensitivity protein)
2617920215	F0F1-type ATP synthase, subunit b
2617920216	F0F1-type ATP synthase, subunit a
2617920236	Transaldolase
2617920237	Fructose/tagatose bisphosphate aldolase
2617920239	Response regulator containing CheY-like receiver, AAA-type ATPase, and DNA-binding domains
2617920245	prevent-host-death family protein
2617920247	Transcriptional regulators
2617920255	Fe-S oxidoreductase
2617920257	4Fe-4S dicluster domain-containing protein
2617920270	UDP-N-acetylglucosamine enolpyruvyl transferase
2617920279	Adenylosuccinate synthase
2617920283	Ribosomal protein L9
2617920287	Single-stranded DNA-binding protein
2617920289	Regulators of stationary/sporulation gene expression
2617920301	Ribosomal protein L17
2617920302	DNA-directed RNA polymerase, alpha subunit/40 kD subunit
2617920304	Ribosomal protein S11
2617920312	Ribosomal protein S5
2617920314	large subunit ribosomal protein L6
2617920315	Ribosomal protein S8
2617920324	Ribosomal protein L22
2617920330	Ribosomal protein S10
2617920332	type IV pilus assembly protein PilA
2617920353	Predicted Zn-dependent proteases and their inactivated homologs - COG0312
2617920358	elongation factor P
2617920361	NADPH-dependent 2,4-dienoyl-CoA reductase, sulfur reductase

2617920371	oxaloacetate decarboxylase, alpha subunit
2617920373	Uncharacterized conserved protein YloU, alkaline shock protein (Asp23) family
2617920377	ferredoxin--NADP+ reductase
2617920378	glutamate synthase (NADPH/NADH) small chain
2617920381	Formiminotetrahydrofolate cyclodeaminase
2617920382	Exonuclease VII small subunit
2617920414	Uncharacterized conserved protein - COG3360
2617920427	Putative sterol carrier protein
2617920434	Aspartate-semialdehyde dehydrogenase
2617920436	Dihydrodipicolinate synthase/N-acetylneuraminate lyase
2617920444	hypothetical protein
2617920456	stage V sporulation protein S
2617920469	IMP dehydrogenase/GMP reductase
2617920539	S-layer homology domain
2617920542	Negative regulator of flagellin synthesis (anti-sigma28 factor)
2617920549	Flagellar capping protein
2617920552	Flagellin and related hook-associated proteins
2617920568	hypothetical protein
2617920570	Stress response protein SCP2
2617920571	tellurium resistance protein TerD
2617920573	tellurium resistance protein TerD
2617920589	Superoxide dismutase
2617920615	Electron transfer flavoprotein, alpha subunit
2617920616	Electron transfer flavoprotein, beta subunit
2617920631	Cell division GTPase
2617920668	NADH-quinone oxidoreductase subunit F
2617920708	Outer membrane efflux protein
2617920709	Copper amine oxidase N-terminal domain
2617920710	Copper amine oxidase N-terminal domain
2617920712	hypothetical protein
2617920728	NifU homolog involved in Fe-S cluster formation
2617920742	precorrin-2/cobalt-factor-2 C20-methyltransferase
2617920747	Uncharacterized conserved protein
2617920779	Predicted periplasmic solute-binding protein - COG1427
2617920796	Uncharacterized protein conserved in bacteria
2617920806	FOG: LysM repeat
2617920807	hypothetical protein
2617920823	stage V sporulation protein G
2617920835	Parvulin-like peptidyl-prolyl isomerase
2617920838	Bacterial nucleoid DNA-binding protein
2617920844	Methyl-accepting chemotaxis protein
2617920854	prevent-host-death family protein

2617920867	2,4-dienoyl-CoA reductase, NADH:flavin oxidoreductases, Old Yellow Enzyme family
2617920868	S-layer homology domain
2617920891	hypothetical protein
2617920910	hypothetical protein
2617920940	hypothetical protein
2617920966	Methyl-accepting chemotaxis protein
2617920969	Methyl-accepting chemotaxis protein
2617920990	NADPH-dependent FMN reductase
2617920998	rod shape-determining protein MreB
2617921007	arginine decarboxylase
2617921008	Spermidine synthase
2617921016	hypothetical protein
2617921017	Predicted membrane protein - COG2855
2617921019	N-acetylglutamate synthase (N-acetylornithine aminotransferase)
2617921020	Acetylglutamate kinase
2617921021	Ornithine/acetylornithine aminotransferase
2617921024	Ornithine carbamoyltransferase
2617921025	argininosuccinate synthase
2617921045	Branched-chain amino acid aminotransferase/4-amino-4-deoxychorismate lyase
2617921047	acetolactate synthase, large subunit
2617921048	Acetolactate synthase, small (regulatory) subunit
2617921049	Ketol-acid reductoisomerase
2617921051	2-isopropylmalate synthase
2617921052	3-isopropylmalate dehydratase large subunit
2617921054	Isocitrate/isopropylmalate dehydrogenase
2617921056	NifU-like domain-containing protein
2617921084	Ribosomal protein S2
2617921085	Translation elongation factor Ts
2617921087	Ribosome recycling factor
2617921114	Heterodisulfide reductase, subunit A and related polyferredoxins
2617921115	CoB--CoM heterodisulfide reductase subunit C
2617921116	Heterodisulfide reductase, subunit B
2617921119	4Fe-4S dicluster domain-containing protein
2617921120	4Fe-4S dicluster domain-containing protein
2617921121	NAD(P)H-flavin reductase
2617921123	heterodisulfide reductase subunit A
2617921133	FKBP-type peptidyl-prolyl cis-trans isomerase (trigger factor)
2617921134	Protease subunit of ATP-dependent Clp proteases
2617921139	Rubrerythrin
2617921145	Zn-dependent alcohol dehydrogenases
2617921178	Glutamate synthase domain 2
2617921183	Clostridium P-47 protein

2617921188	Clostridium P-47 protein
2617921189	Clostridium P-47 protein
2617921206	Universal stress protein UspA and related nucleotide-binding proteins
2617921225	ABC-type molybdate transport system, periplasmic component
2617921237	ABC-type Fe3+-hydroxamate transport system, periplasmic component
2617921239	Cobalamin biosynthesis protein CobN and related Mg-chelatases
2617921243	protoporphyrin IX magnesium-chelatase (EC 6.6.1.1)
2617921245	Copper amine oxidase N-terminal domain
2617921249	protein of unknown function (DUF4198)
2617921251	Methylase involved in ubiquinone/menaquinone biosynthesis, UbiE
2617921252	peptide/nickel transport system substrate-binding protein
2617921263	Prenyltransferase and squalene oxidase repeat-containing protein
2617921272	Uncharacterized protein probably involved in high-affinity Fe2+ transport
2617921288	Pyruvate:ferredoxin oxidoreductase and related 2-oxoacid:ferredoxin oxidoreductases, alpha subunit
2617921314	S-layer homology domain-containing protein
2617921321	cell division protease FtsH
2617921327	Dihydroneopterin aldolase
2617921335	Predicted oxidoreductase, contains short-chain dehydrogenase (SDR) and DUF2520 domains
2617921338	Aspartate 1-decarboxylase
2617921339	quinolinate synthetase
2617921350	Phosphoenolpyruvate synthase/pyruvate phosphate dikinase
2617921361	probable rRNA maturation factor
2617921370	Predicted Fe-Mo cluster-binding protein, NifX family
2617921373	hypothetical protein
2617921374	Uncharacterized conserved protein - COG1433
2617921379	CO dehydrogenase/acetyl-CoA synthase beta subunit
2617921380	Ni-dependent carbon monoxide dehydrogenase precursor
2617921406	Uncharacterized conserved protein
2617921411	perosamine synthetase
2617921413	GDPmannose 4,6-dehydratase
2617921451	Uncharacterized conserved protein YloU, alkaline shock protein (Asp23) family
2617921459	Cell fate regulator YlbF, YheA/YmcA/DUF963 family (controls sporulation, competence, biofilm development)
2617921466	RNA-binding protein Hfq
2617921504	Protein of unknown function (DUF1292)
2617921510	hypothetical protein
2617921525	Predicted membrane GTPase involved in stress response - COG1217
2617921570	Chaperonin GroEL (HSP60 family)
2617921571	Molecular chaperone GrpE (heat shock protein)
2617921572	Molecular chaperone
2617921578	Ribosomal protein S21
2617921592	cysteinyl-tRNA synthetase
2617921655	N-formylmethionyl-tRNA deformylase

2617921657	hypothetical protein
2617921662	Uncharacterized protein conserved in bacteria
2617921665	Uncharacterized conserved protein - COG1416
2617921670	ATPase, P-type (transporting), HAD superfamily, subfamily IC
2617921717	Copper chaperone
2617921725	Peptidyl-prolyl cis-trans isomerase (rotamase) - cyclophilin family
2617921733	Benzoyl-CoA reductase/2-hydroxyglutaryl-CoA dehydratase subunit, BcrC/BadD/HgdB
2617921734	Benzoyl-CoA reductase/2-hydroxyglutaryl-CoA dehydratase subunit, BcrC/BadD/HgdB
2617921806	Chorismate mutase
2617921820	Predicted periplasmic protein (DUF2233)
2617921821	Uncharacterized protein containing a ferredoxin domain
2617921825	Di- and tricarboxylate transporters
2617921828	Pyridoxamine 5'-phosphate oxidase
2617921834	Secreted protein containing C-terminal beta-propeller domain distantly related to WD-40 repeats
2617921875	Cold shock proteins
2617921876	Universal stress protein UspA and related nucleotide-binding proteins
2617921886	FAD/FMN-containing dehydrogenases
2617921887	heterodisulfide reductase subunit D
2617921888	FAD/FMN-containing dehydrogenases
2617921889	KamA family protein
2617921890	Enoyl-CoA hydratase/carnithine racemase
2617921891	acetyltransferase
2617921896	Crotonobetainyl-CoA:carnitine CoA-transferase CaiB
2617921897	CoA:oxalate CoA-transferase
2617921905	phosphoenolpyruvate--protein phosphotransferase
2617921910	N-acetylmuramoyl-L-alanine amidase
2617921915	RNAse PH
2617921959	Sporulation protein and related proteins
2617921962	Preprotein translocase subunit YajC
2617921964	Preprotein translocase subunit SecD
2617921965	Preprotein translocase subunit SecF
2617921968	Universal stress protein UspA and related nucleotide-binding proteins
2617921985	carboxyl-terminal processing protease
2617921996	Ribosomal protein L11
2617921997	Ribosomal protein L1
2617921998	Ribosomal protein L10
2617921999	Ribosomal protein L7/L12
2617922000	DNA-directed RNA polymerase, beta subunit/140 kD subunit
2617922002	DNA-directed RNA polymerase subunit beta
2617922005	Ribosomal protein S7
2617922006	translation elongation factor 2 (EF-2/EF-G)
2617922007	GTPases - translation elongation factors

2617922012	RNA recognition motif. (a.k.a. RRM, RBD, or RNP domain)
2617922055	large subunit ribosomal protein L21
2617922070	long-chain acyl-CoA synthetase
2617922073	Rhodanese-related sulfurtransferase
2617922086	HlyD family secretion protein
2617922096	thiazole-phosphate synthase
2617922097	Sulfur transfer protein involved in thiamine biosynthesis
2617922102	Conserved protein/domain typically associated with flavoprotein oxygenases, DIM6/NTAB family
2617922105	Transcription elongation factor
2617922118	hypothetical protein
2617922137	Acetyl-CoA acetyltransferase
2617922161	ABC-type molybdate transport system, periplasmic component
2617922188	Thioredoxin domain-containing protein
2617922218	Uncharacterized conserved protein - COG2442
2617922227	4Fe-4S binding domain-containing protein
2617922233	Formylmethanofuran dehydrogenase subunit E
2617922234	cobalt/nickel transport protein
2617922251	Uncharacterized protein conserved in bacteria
2617922257	adenine phosphoribosyltransferase
2617922283	D-alanine-D-alanine ligase and related ATP-grasp enzymes
2617922285	Translation elongation factors (GTPases)
2617922317	Clp amino terminal domain
unclassfied	hypothetical protein
undefined	Thioredoxin domain-containing protein
undefined	Predicted acid phosphatase - COG0496

Table A2 List of genes identified in the genomes and used for metabolic pathway reconstruction for Spirochaetes in hydrocarbon- and organohalide-contaminated environments shown in Figure 11. Genes for the illustrated pathways were detected in the genomes of *Rectinema cohabitans* HM, uncultured Spirochaetes bacterium bdmA 4, and uncultured Spirochaetes bacterium SA-8.

Glycolysis/Gluconeogenesis					
No.	Enzyme	EC Number(s)	Spirochaetes Bin 1 SA-8	uncultured Spirochaetes bacterium bdmA 4	*R. cohabitans*
G1	glucokinase	2.7.1.2	SPSA8_v1_410004	SPBDM4_v1_70210	SPBIB_v1_120011
G2	glucose-6-phosphate isomerase	5.3.1.9	SPSA8_v1_690007_pgi	SPBDM4_v1_50976 - pgi, SPBDM4_v1_40538 - pgiA	SPBIB_v1_130044 - pgi
G3	6-phosphofructokinase	2.7.1.11	not identified	SPBDM4_v1_40290	SPBIB_v1_350003
G4	fructose-bisphosphate aldolase	4.1.2.13	SPSA8_v1_230024_fba	SPBDM4_v1_50273, SPBDM4_v1_50942 - fba, SPBDM4_v1_40557 - fbaA	SPBIB_v1_140014 - fba
G5	triose-phosphate isomerase	5.3.1.1	SPSA8_v1_560006	SPBDM4_v1_51054 - tpiA	SPBIB_v1_100039 - tpiA
G6	glyceraldehyde-3-phosphate dehydrogenase (phosphorylating)	1.2.1.12	SPSA8_v1_560002	SPBDM4_v1_51050 - gapA	SPBIB_v1_100034 - gapA
G7	phosphoglycerate kinase	2.7.2.3	SPSA8_v1_560003	SPBDM4_v1_51051 - pgk, SPBDM4_v1_41029	SPBIB_v1_100035 - pgk, SPBIB_v1_210059, SPBIB_v1_290179
G8	phosphoglycerate mutase	5.4.2.1	SPSA8_v1_410010_gpmI	SPBDM4_v1_40326, SPBDM4_v1_70215 - gpmI, SPBDM4_v1_40696 - gpmA	SPBIB_v1_90032 - gpmI, SPBIB_v1_270010 - gpmA
G9	phosphopyruvate hydratase	4.2.1.11	not identified	SPBDM4_v1_40824 - eno	SPBIB_v1_280034 - eno
G10	pyruvate kinase	2.7.1.40	SPSA8_v1_280005	SPBDM4_v1_50076 - pyk	SPBIB_v1_290204 - pyk
Pentose phosphate pathway					
No.	Enzyme	EC Number(s)	Spirochaetes Bin 1 SA-8	uncultured Spirochaetes bacterium bdmA 4	*R. cohabitans*
P1	Glucose-6-phosphate dehydrogenase (NADP(+))	1.1.1.49	SPSA8_v1_290001	SPBDM4_v1_50483 - zwf	SPBIB_v1_210196 - zwf
P2	6-phosphogluconolactonase	3.1.1.31	SPSA8_v1_290002	SPBDM4_v1_50484	SPBIB_v1_210195
P3	Phosphogluconate dehydrogenase (decarboxylating)	1.1.1.44	SPSA8_v1_640011	SPBDM4_v1_70232 - gnd	SPBIB_v1_90014 - gnd
P4	D-glyceraldehyde-3-phosphate glycolaldehyde transferase	2.2.1.1	SPSA8_v1_280002	SPBDM4_v1_40259, SPBDM4_v1_40260, SPBDM4_v1_41032 - tkt, SPBDM4_v1_50175 - tkt	SPBIB_v1_10035, SPBIB_v1_10036, SPBIB_v1_250033 - tktB

P5	ribulose-phosphate 3-epimerase	5.1.3.1	SPSA8_v1_330009	SPBDM4_v1_70027 - rpe	SPBIB_v1_100090 - rpe
P6	ribose-5-phosphate isomerase	5.3.1.6	SPSA8_v1_780001	not identified	SPBIB_v1_10034 - rpiB, SPBIB_v1_410042 - rpiB
P7	ribose-5-phosphate diphosphotransferase	2.7.6.1	not identified	SPBDM4_v1_40813	SPBIB_v1_280022
Starch and sucrose metabolism pathway					
No.	Enzyme	EC Number(s)	Spirochaetes Bin 1 SA-8	uncultured Spirochaetes bacterium bdmA 4	*R. cohabitans*
A1	Glucose-1-phosphate adenylyltransferase	2.7.7.27	not identified	SPBDM4_v1_51063 - glgC	SPBIB_v1_100048 - glgC
A2	Glycogen synthase	2.4.1.21	SPSA8_v1_500008	SPBDM4_v1_80030 - glgA	SPBIB_v1_50016 - glgA
A3	1,4-alpha-glucan branching enzyme	2.4.1.18	not identified	not identified	not identified
A4	Glycogen phosphorylase	2.4.1.1	SPSA8_v1_570005-6	SPBDM4_v1_50116 - glgP	SPBIB_v1_250079 - glgP
A5	Phosphoglucomutase	5.4.2.2	SPSA8_v1_410001	SPBDM4_v1_70206 - pgcA	SPBIB_v1_120008 - pgcA
Fermentation					
No.	Enzyme	EC Number(s)	Spirochaetes Bin 1 SA-8	uncultured Spirochaetes bacterium bdmA 4	*R. cohabitans*
F1	pyruvate ferredoxin oxidoreductase	1.2.7.1	SPSA8_v1_240015_ydbK	SPBDM4_v1_40344 - ydbK	SPBIB_v1_340021 - ydbK
F2	multi-enzyme complex pyruvate dehydrogenase	1.2.4.1, 2.3.1.12, 1.8.1.4	SPSA8_v1_670003-6	SPBDM4_v1_40897-9	SPBIB_v1_150091-3
F3	phosphate acetyltransferase (annotated as Phosphate butyryltransferase in the platform)	2.3.1.8	SPSA8_v1_50027	SPBDM4_v1_50824	SPBIB_v1_150125
F4	acetate kinase	2.7.2.1	SPSA8_v1_50028	SPBDM4_v1_40312 - ackA	SPBIB_v1_340053 - ackA
F5	Acetaldehyde dehydrogenase (acetylating)	1.2.1.10	not identified	SPBDM4_v1_50365 - alkH, SPBDM4_v1_30004 - aldA	SPBIB_v1_10033, SPBIB_v1_200018, SPBIB_v1_250096
F6	alcohol dehydrogenase	1.1.1.1	SPSA8_v1_730004	SPBDM4_v1_50015, SPBDM4_v1_41037, SPBDM4_v1_41043	SPBIB_v1_290156
Membrane energization					
No.	Enzyme	EC Number(s)	Spirochaetes Bin 1 SA-8	uncultured Spirochaetes bacterium bdmA 4	*R. cohabitans*
E1	Electron transport complex, RnfABCDGE-type		SPSA8_v1_380010-15	SPBDM4_v1_40884-9	SPBIB_v1_290012-7
E2	V-type ATP synthase	3.6.1.14	SPSA8_v1_40015-21	SPBDM4_v1_40178-84, SPBDM4_v1_70188-94	SPBIB_v1_370004-10, SPBIB_v1_110048-54
E3	Pyrophosphate-energized proton pump		SPSA8_v1_180025	SPBDM4_v1_40486	SPBIB_v1_260006
Protein degradation					

N1	extracellular peptidases (M23B, S8A, S26A, S33)		Database A5	Database A4	Database A3
N2	oligo/dipeptide and amino acid transoprters		Database A5	Database A4	Database A3
N3	intracellular peptidases		Database A5	Database A4	Database A3
N4	Aminotranferases		Database A5	Database A4	Database A3
N5	Indolepyruvate ferredoxin oxidoreductase	1.2.7.8	SPSA8_v1_30002-3	SPBDM4_v1_40271-2	SPBIB_v1_350033-4
N5	pyruvate/ketoisovalerate oxidoreductase	1.2.7.7	SPSA8_v1_50024-6	SPBDM4_v1_50825-8	SPBIB_v1_150121-4
N5	2-oxoglutarate synthase subunit	1.2.7.3	SPSA8_v1_220016-9	SPBDM4_v1_50767-70	SPBIB_v1_150177-80
N5	Tungsten-containing aldehyde ferredoxin oxidoreductase	1.2.7.5	SPSA8_v1_700003-4	not identified	not identified
N5	pyruvate ferredoxin oxidoreductase	1.2.7.1	SPSA8_v1_240015_ydbK	SPBDM4_v1_40344 - ydbK	SPBIB_v1_340021 - ydbK
Hydrogen metabolism					
No.	Enzyme	EC Number(s)	Spirochaetes Bin 1 SA-8	uncultured Spirochaetes bacterium bdmA 4	*R. cohabitans*
H1	FeFe A1 hydrogenase		not identified	SPBDM4_v1_80097	SPBIB_v1_20025
H2	FeFe A3 hydrogenase		SPSA8_v1_300018	SPBDM4_v1_40494	SPBIB_v1_260013, SPBIB_v1_210130
H3	FeFe B hydrogenase		SPSA8_v1_810002	not identified	SPBIB_v1_290056, SPBIB_v1_360015
H4	FeFe C hydrogenase		SPSA8_v1_270001, SPSA8_v1_810005	SPBDM4_v1_40759	SPBIB_v1_360012, SPBIB_v1_280015
Secretion systems					
No.	Enzyme				
	Preprotein translocase, SecG subunit				SPBIB_v1_100040
	Protein translocase subunit SecA				SPBIB_v1_110017
	Protein-export membrane protein SecF				SPBIB_v1_210207
	Protein translocase subunit SecD				SPBIB_v1_210208
	putative SEC-C motif domain protein				SPBIB_v1_280056
	Protein translocase subunit SecE				SPBIB_v1_310045
	preprotein translocase membrane subunit				SPBIB_v1_370006
Carbohydrate-active enzymes (polysaccharide degradation)					
S1	hydrolases and extracelluar binding proteins		Database A5	Database A4	Database A3
S2	ABC tranporters		Database A5	Database A4	Database A3

S3	Hydrolases		Database A5	Database A4	Database A3

Table A4 List of identified proteins for *R. cohabitans* HM as shown in Figure 14.

Gene	Function	Classification
SPBIB_v1_250074	2,3-cyclic-nucleotide 2-phosphodiesterase	purine metabolism and pyrimidine metabolism.
SPBIB_v1_150165	31 kDa immunogenic protein	
SPBIB_v1_350024	5-nucleotidase/2,3-cyclic phosphodiesterase-like hydrolase	purine metabolism and pyrimidine metabolism.
SPBIB_v1_150087	ABC sugar transporter, periplasmic ligand binding protein	sugar metabolism
SPBIB_v1_260060	ABC sugar transporter, periplasmic ligand binding protein	sugar metabolism
SPBIB_v1_250100	ABC transporter substrate binding protein	malto-oligosaccharides, multiple oligosaccharides, glycerol 3-phosphate, and iron
SPBIB_v1_330021	ABC-type dipeptide transport system, periplasmic component	oligo/dipeptide and amino acid transoprters
SPBIB_v1_210094	ABC-type transporter, periplasmic subunit	
SPBIB_v1_210125	ABC-type transporter, periplasmic subunit	oligo/dipeptide and amino acid transoprters
SPBIB_v1_290103	Aconitate hydratase	
SPBIB_v1_20007	Basic membrane lipoprotein	
SPBIB_v1_240055	Basic membrane lipoprotein	
SPBIB_v1_310088	Branched-chain amino acid ABC transporter substrate-binding protein	oligo/dipeptide and amino acid transoprters
SPBIB_v1_150042	conserved exported protein of unknown function	
SPBIB_v1_210118	conserved exported protein of unknown function	
SPBIB_v1_210161	conserved exported protein of unknown function	
SPBIB_v1_270015	conserved exported protein of unknown function	
SPBIB_v1_350064	conserved exported protein of unknown function	
SPBIB_v1_310019	Desulfoferrodoxin	
SPBIB_v1_100150	DNA-binding protein HRL18	
SPBIB_v1_80014	D-ribose-binding protein	
SPBIB_v1_250059	exported protein of unknown function	
SPBIB_v1_340054	exported protein of unknown function	
SPBIB_v1_380039	exported protein of unknown function	
SPBIB_v1_240026	Extracellular ligand-binding receptor	oligo/dipeptide and amino acid transoprters

SPBIB_v1_150035	Extracellular solute-binding protein	
SPBIB_v1_10042	Extracellular solute-binding protein family 1	malto-oligosaccharides, multiple oligosaccharides, glycerol 3-phosphate, and iron
SPBIB_v1_380003	Extracellular solute-binding protein family 1	malto-oligosaccharides, multiple oligosaccharides, glycerol 3-phosphate, and iron
SPBIB_v1_400009	Extracellular solute-binding protein family 1	malto-oligosaccharides, multiple oligosaccharides, glycerol 3-phosphate, and iron
SPBIB_v1_60010	Extracellular solute-binding protein family 1	malto-oligosaccharides, multiple oligosaccharides, glycerol 3-phosphate, and iron
SPBIB_v1_290108	Extracellular solute-binding protein family 5	oligo/dipeptide and amino acid transoprters
SPBIB_v1_250085	FAD-dependent pyridine nucleotide-disulfide oxidoreductase	
SPBIB_v1_270007	Gamma-glutamyltranspeptidase	intracellular peptidases
SPBIB_v1_290147	Gamma-glutamyltranspeptidase	intracellular peptidases
SPBIB_v1_80037	glutamate dehydrogenase, NADP-specific	Amino acid degradation
SPBIB_v1_100034	glyceraldehyde-3-phosphate dehydrogenase A	glycerol fermentation
SPBIB_v1_380029	glycerol-3-phosphate transporter subunit;periplasmic-binding component of ABC superfamily	
SPBIB_v1_340036	Iron ABC transporter, substrate binding protein	
SPBIB_v1_210026	Leucine-, isoleucine-, valine-, threonine-, and alanine-binding protein	oligo/dipeptide and amino acid transoprters
SPBIB_v1_290158	oligopeptide transporter subunit;periplasmic-binding component of ABC superfamily	oligo/dipeptide and amino acid transoprters
SPBIB_v1_50038	Oligopeptide-binding protein AliB	oligo/dipeptide and amino acid transoprters
SPBIB_v1_150028	Periplasmic binding protein/LacI transcriptional regulator	
SPBIB_v1_10062	Periplasmic sugar-binding protein	
SPBIB_v1_410087;SPBIB_v1_10012	Plasmid stabilization system protein;Plasmid stabilization system protein	
SPBIB_v1_110024	protease, ATP-dependent zinc-metallo (M41)	Type II sectroy system
SPBIB_v1_310056	protein chain elongation factor EF-Tu (duplicate of tufB)	
SPBIB_v1_110017	Protein translocase subunit SecA	Protease
SPBIB_v1_150059	Purine-binding protein BAB2_0673	
SPBIB_v1_340021	putative 2-oxoacid-flavodoxin fused oxidoreductase:conserved protein;4Fe-4S cluster binding protein	Amino acid degradation
SPBIB_v1_210218	putative ABC-type transport system, periplasmic component/surface lipoprotein	
SPBIB_v1_100146	putative basic membrane lipoprotein	
SPBIB_v1_260082	putative cation ABC transporter, periplasmic binding protein	

SPBIB_v1_310055	putative Elongation factor G	
SPBIB_v1_350021	putative Extracellular solute-binding protein family 1	malto-oligosaccharides, multiple oligosaccharides, glycerol 3-phosphate, and iron
SPBIB_v1_210067	putative Periplasmic sugar binding protein-like protein	
SPBIB_v1_340064	Split soret cytochrome c	
SPBIB_v1_260025	Sugar ABC transporter substrate-binding protein	
SPBIB_v1_100013	TRAP dicarboxylate transporter, DctP subunit	
SPBIB_v1_380022	TRAP dicarboxylate transporter, DctP subunit	

Supporting Figures

Figure A1 Identity dot plot between *Pelotomaculum* candidate BPL (contigs on the y axis) and *Pelotomaculum thermopropionicum* SI (full genome sequence on the x axis) generated using MUMmer (http://mummer.sourceforge.net/). Red dots indicate stretches of nucleotide identity and blue dots reverse complementary matches. Grey horizontal lines separate the individual contigs on the y axis.

Figure A2 Gene count of COG functional categories for *Pelotomaculum* candidate BPL and *Pelotomaculum thermopropionicum* SI.

Figure A3 Full phylogenetic tree showing the phylogeny of the [FeFe]-hydrogenase catalytic subunit sequences detected in *R. cohabitans* HM, uncultured Spirochaetes bacterium bdmA 4, and uncultured Spirochaetes bacterium SA-8.

Figure A4 Expanded maximum likelihood tree of partial 16S rRNA gene sequences of Spirochaetes. This shows the phylogenetic affiliation of *R. cohabitans*, uncultured Spirochaetes bacterium bdmA 4, and uncultured Spirochaetes bacterium SA-8.

Figure A5 Mass spectrum of CO_2 obtained via Isotope Ratio Mass Spectrometry: (a) natural sample with a low ^{13}C abundance ($\delta^{13}C$ = -9.7 ‰); (b) ^{13}C-enriched sample ($x(^{13}C)$ = 10.0 %). CO_2 samples are firstly ionized to different ions mass-to-charge ratios (m/z) at 44, 45 and 46. The first three peaks (square-shaped) belong to working gas while the last one to the sample.

Figure A6 Normalized transmission spectrum of air containing 380 ppm CO_2 obtained via Isotope Ratio Mid-Infrared Spectroscopy: (a) natural sample with a low ^{13}C abundance ($\delta^{13}C$ = -9.7 ‰); (b) ^{13}C-enriched sample ($x(^{13}C)$ = 10.0 %). The peak areas labeled as $(13)CO_2(1)$ and $CO_2(1)$ were used to determine the $^{13}C/^{12}C$ isotopic ratios in this study.

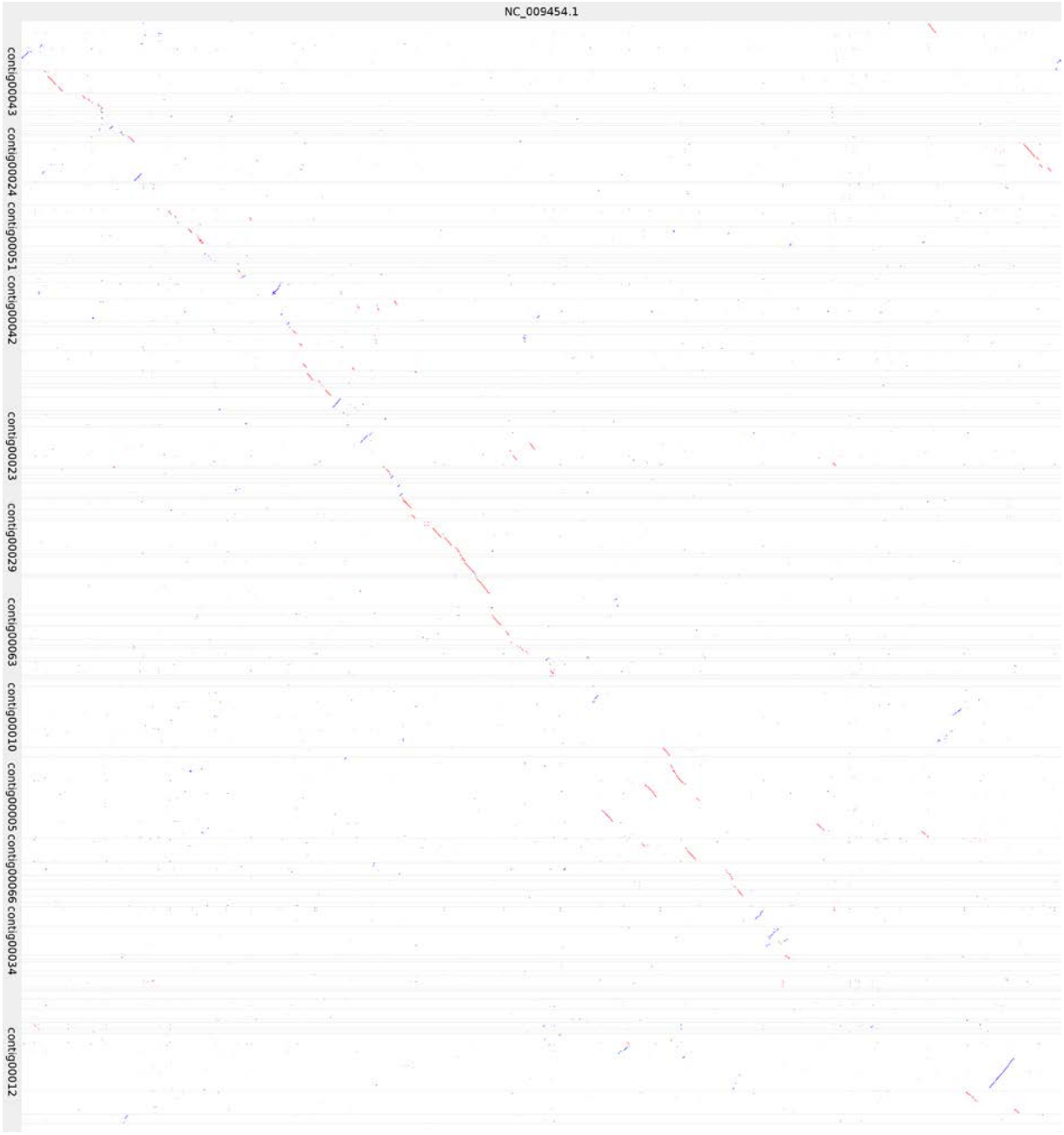

Figure A1 Identity dot plot between *Pelotomaculum* candidate BPL (contigs on the y axis) and *Pelotomaculum thermopropionicum* SI (full genome sequence on the x axis) generated using MUMmer (http://mummer.sourceforge.net/). Red dots indicate stretches of nucleotide identity and blue dots reverse complementary matches. Grey horizontal lines separate the individual contigs on the y axis.

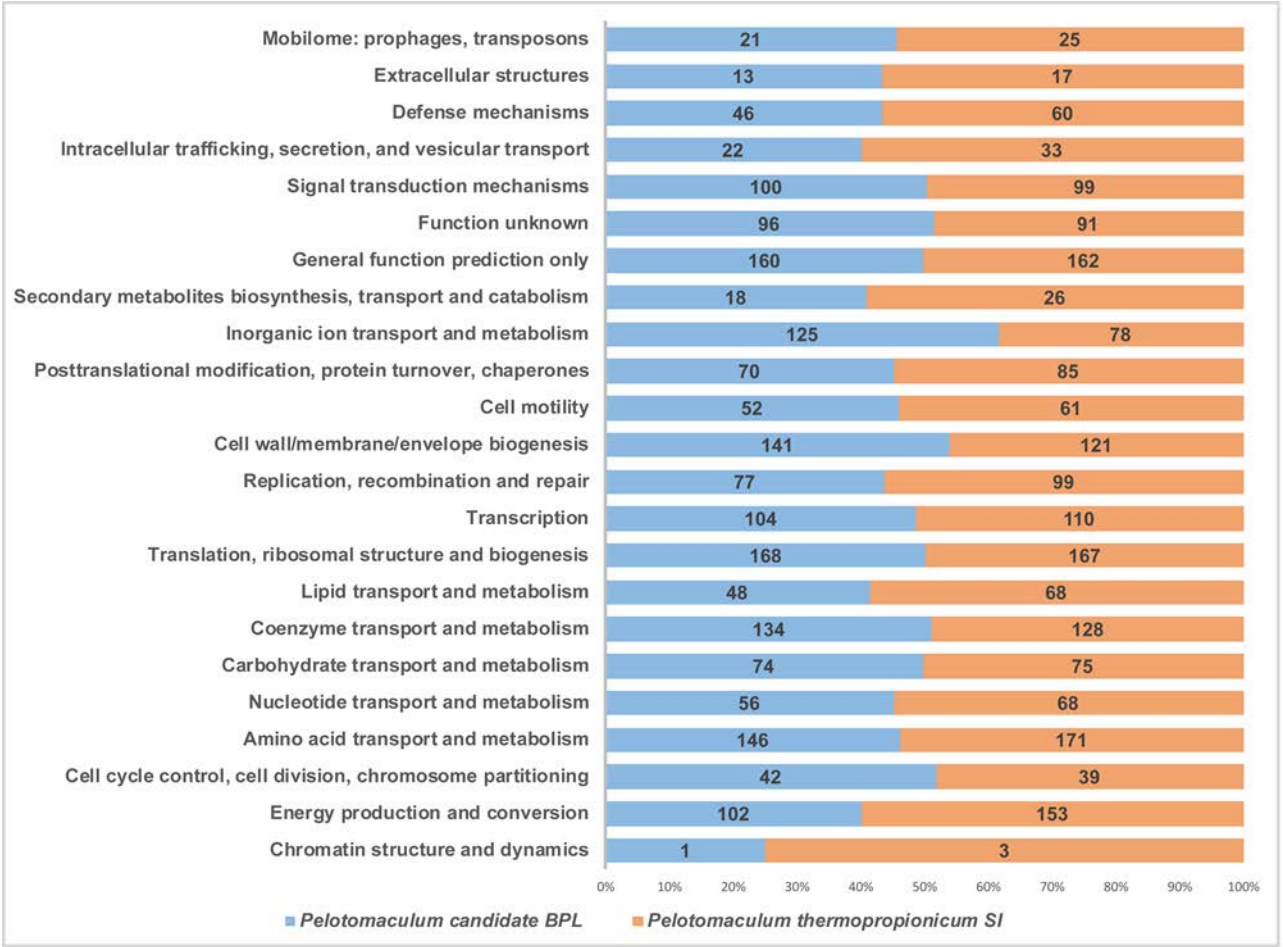

Figure A2 Gene count of COG functional categories for *Pelotomaculum* candidate BPL and *Pelotomaculum thermopropionicum* SI.

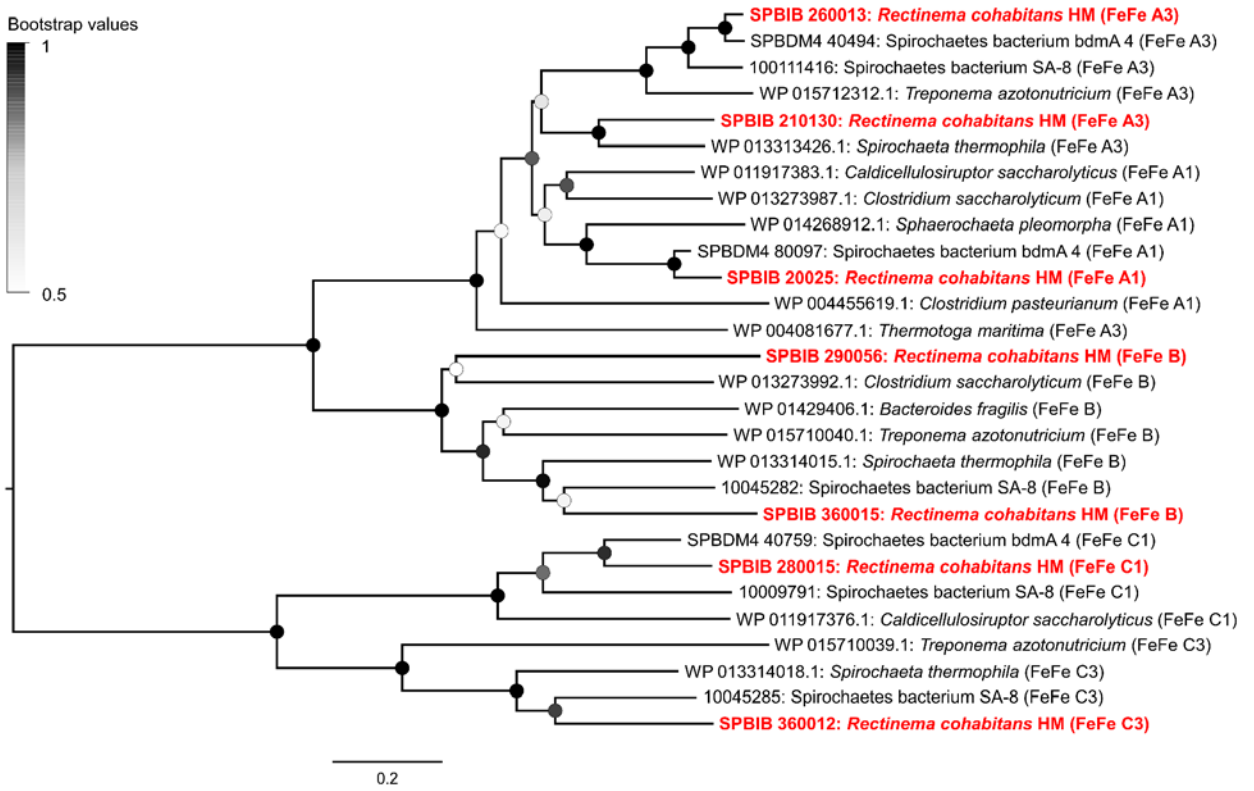

Figure A3 Full phylogenetic tree showing the phylogeny of the [FeFe]-hydrogenase catalytic subunit sequences detected in *R. cohabitans* HM, uncultured Spirochaetes bacterium bdmA 4, and uncultured Spirochaetes bacterium SA-8.

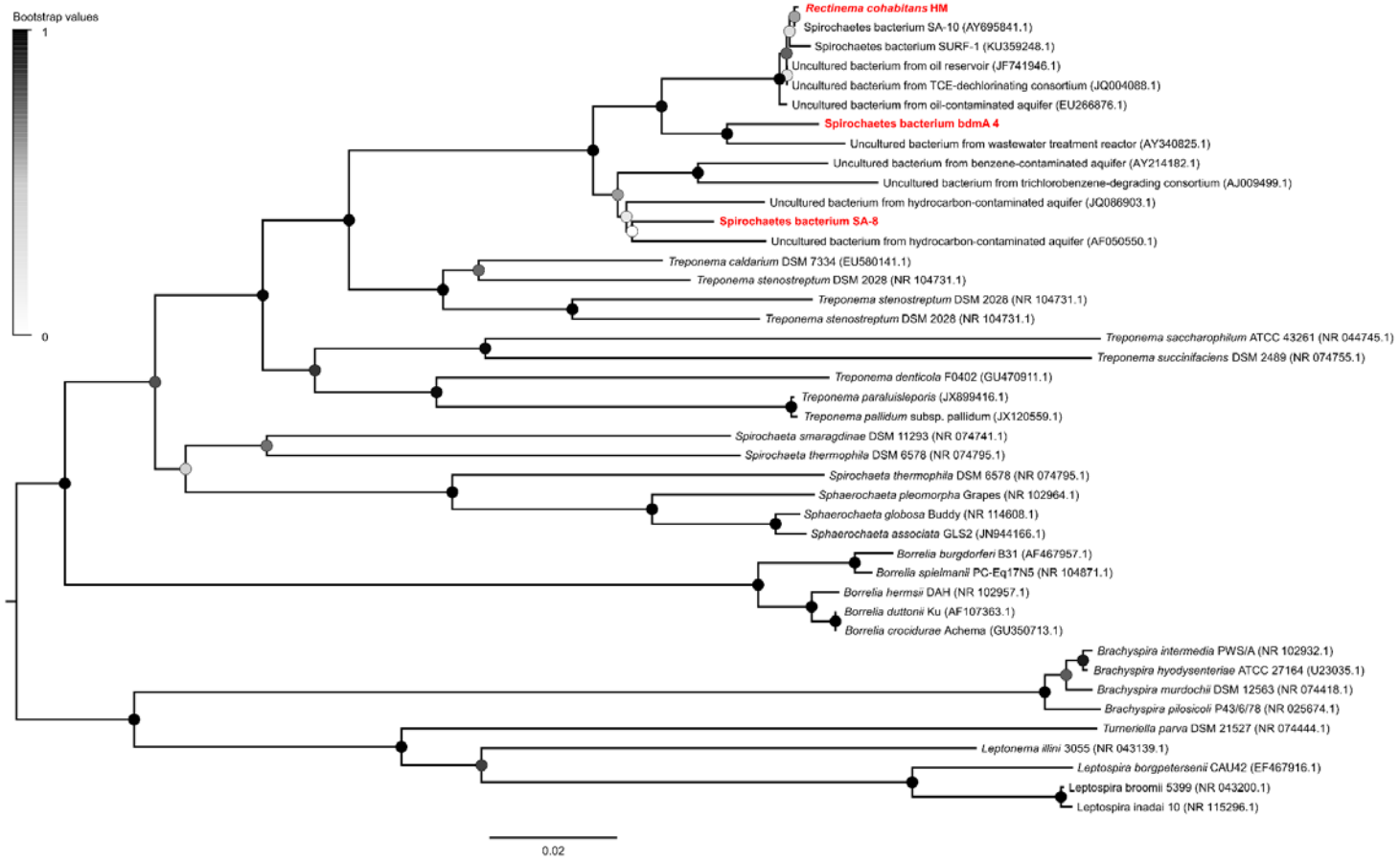

Figure A4 Expanded maximum likelihood tree of partial 16S rRNA gene sequences of Spirochaetes. This shows the phylogenetic affiliation of *R. cohabitans*, uncultured Spirochaetes bacterium bdmA 4, and uncultured Spirochaetes bacterium SA-8.

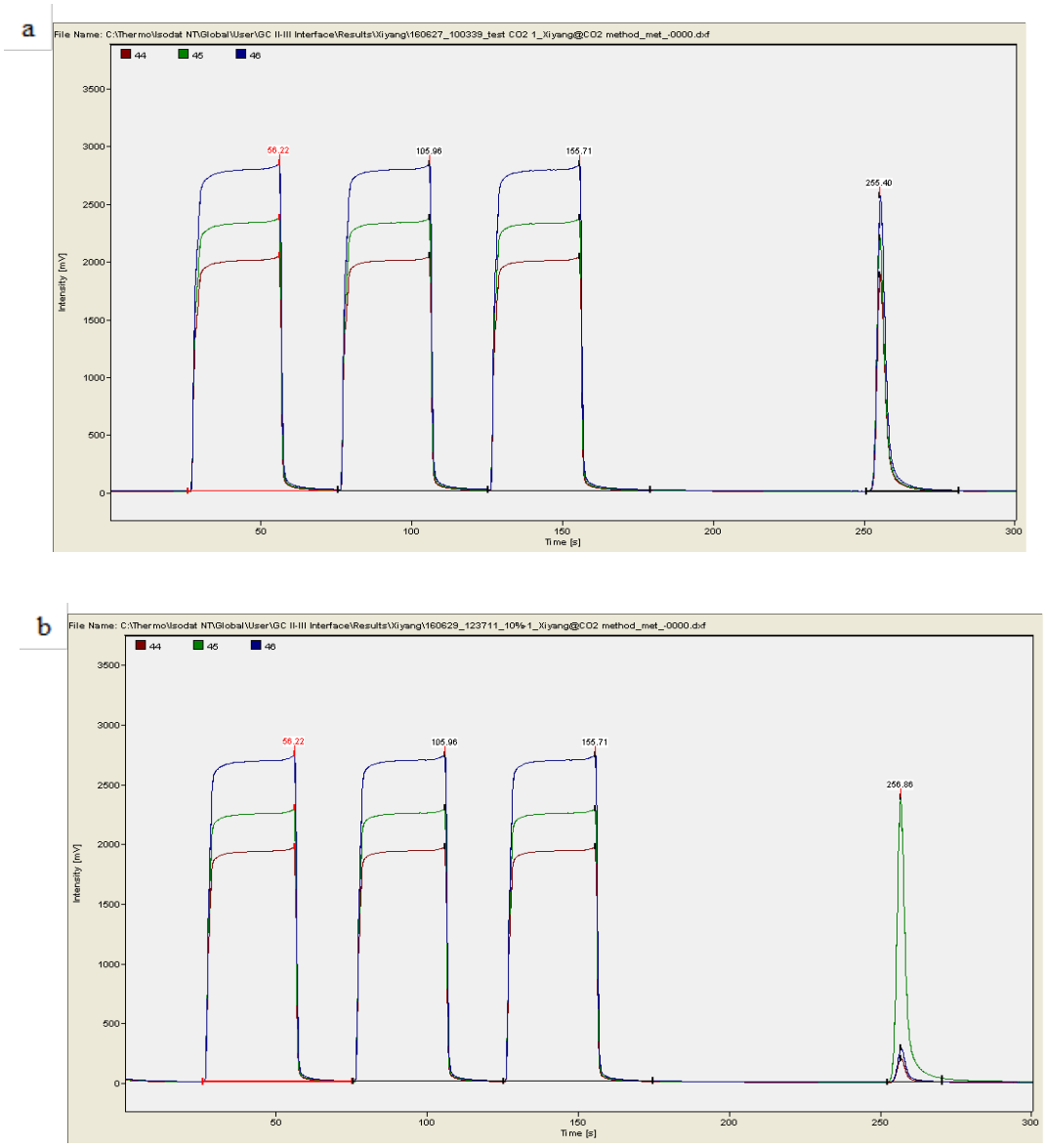

Figure A5 Mass spectrum of CO_2 obtained via Isotope Ratio Mass Spectrometry: (a) natural sample with a low ^{13}C abundance ($\delta^{13}C$ = -9.7 ‰); (b) ^{13}C-enriched sample ($x(^{13}C)$ = 10.0 %). CO_2 samples are firstly ionized to different ions mass-to-charge ratios (m/z) at 44, 45 and 46. The first three peaks (square-shaped) belong to working gas while the last one to the sample.

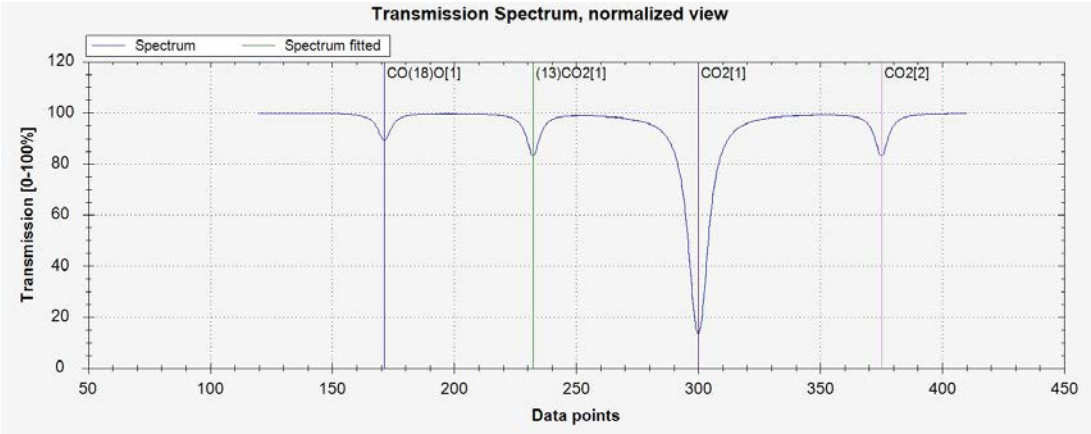

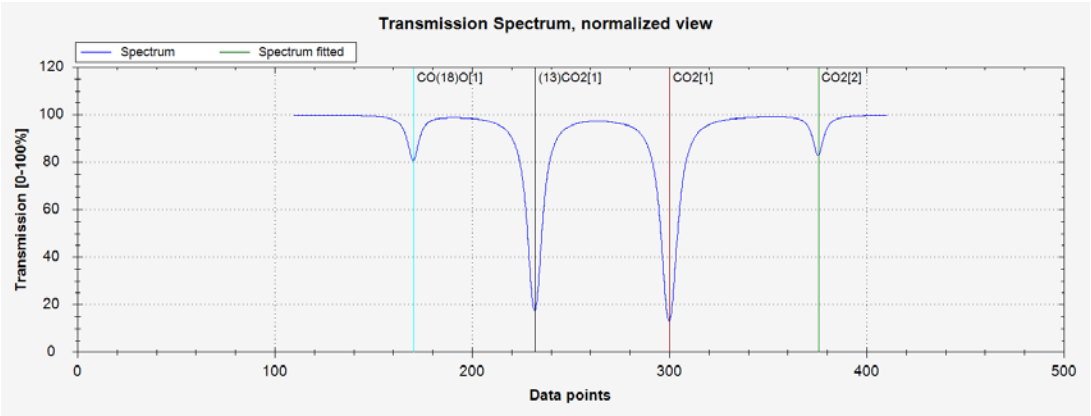

Figure A6 Normalized transmission spectrum of air containing 380 ppm CO_2 obtained via Isotope Ratio Mid-Infrared Spectroscopy: (a) natural sample with a low ^{13}C abundance ($\delta^{13}C$ = -9.7 ‰); (b) ^{13}C-enriched sample ($x(^{13}C)$ = 10.0 %). The peak areas labeled as $(13)CO_2(1)$ and $CO_2(1)$ were used to determine the $^{13}C/^{12}C$ isotopic ratios in this study.

Supporting Databases

Database A1 FASTA-formatted sequences for 16S rRNA genes of *Pelotomaculum* candidate BPL.

Database A2 FASTA Amino Acid format for protein coding genes in the genome of *Pelotomaculum* candidate BPL. Considering the size is too large to include here, it can be found at Integrated Microbial Genomes (IMG) system. GOLD Study ID: Gs0114392, GOLD Project ID: Gp0111374, GOLD Analysis Project Id: Ga0073689.

Database A3 FASTA Amino Acid format for protein coding genes in the genome of *R. cohabitans* HM. Considering the size is too large to include here, it can be found at Microbial Genome Annotation & Analysis Platform (MicroScope) with name of *Uncultured spirochete bib* (WGS SPIROBIBN47.1). It was submitted to European Nucleotide Archive under study identifier PRJEB19364.

Database A4 FASTA Amino Acid format for protein coding genes in the genome of uncultured Spirochaetes bacterium SA-8. Considering the size is too large to include here, it can be found at Microbial Genome Annotation & Analysis Platform (MicroScope) with name of *Spirochaetes Bin 1 SA-8* (WGS SPSA8.1). It was submitted to European Nucleotide Archive under study identifier PRJEB19364.

Database A5 FASTA Amino Acid format for protein coding genes in the genome of uncultured Spirochaetes bacterium bdmA 4. Considering the size is too large to include here, it can be found at Microbial Genome Annotation & Analysis Platform (MicroScope) with name of *Uncultured spirochete bdmA 4* (WGS SPIRO4BDMA.1). It was submitted to It can be found at European Nucleotide Archive under study identifier PRJEB19364.

Database A6 Amino Acid format for hydrogenase sequences used for Figures 12 and A3.

Database A1 FASTA-formatted sequences for 16S rRNA genes of *Pelotomaculum* candidate BPL.

>bpl_candidate_16S@contig01451_113_1661

TCATAGAAGATTTTATGGAGAGTTTGATCCTGGCTCAGGACGAACGCTGGCGGCGTGCTTAAC
ACATGCAAGTCGAACGGAGGTTTAAGAGGAAGCTTGCGAATCTTGAACCTTAGTGGCGGACG
GGTGAGTAACGCGTGGATAACCTGCCTGACTGACCGGGACAACACCGGGAAACTGGCGCTA
ATACCGGATACGCTCATTTATGCGCAAGCGTGGATGAGGAAAGGGGCAACCCGCAGACAGAT
GGGTCCGCGTCCCATTAGCTAGTTGGAGGTGTAAGAGACCCCCAAGGCGACGATGGGTAGC
CGGCCTGAGAGGGTGGACGGCCACACTGGAACTGAGACACGGTCCAGACTCCTACGGGAGG
CAGCAGTGGGGAATCTTCCGCAATGGGCGCAAGCCTGACGGAGCAACGCCGCGTGAGTGAC
GAAGGCCTTCGGGTTGTAAAACTCTGTCTTCGGGGAAGAAGAAAGTGACGGTACCCGAGGAG
GAAGCCCCGGCTAACTACGTGCCAGCAGCCGCGGTAAAACGTAGGGGGCGAGCGTTGTCCG
GAATTACTGGGCGTAAAGGGCGCGTAGGCGGTTTACcAAGTGAGGggTGAAAACTaaCGGCTC
AACCGtGaGAgTGCCTcTGAAACTGGTAGACTTGAGggCAGGAGAGGGGAGTGGAATTCCCaGT
GTAGCGGTGAAATGCGTAGATATTGGGAGGAACACCAGTGGCGAAGGCGACTCTCTGGCCTG
TTACTGACGCTGAGGCGCGAAAGCGTGGGGAGCGAACGGGATTAGATACCCCGGTAGTCCA
CGCCGTAAACGATGGGTGCTAGGTGTAGGAGGTATCGACCCCTTCTGTGCCGTAGTTAACAC
AATAAGCACCCCGCCTGGGGAGTACGGCCGCAAGGTTGAAACTCAAAGGAATTGACGGGGG
CCCGCACAAGCGGTGGAGCATGTGGTTTAATTCGACGCAACGCGAAGAACCTTACCAGGGTT
TGACATCCCCTGACAGCTGTGGAAACACAGAATTTTACCTTCGGGTAGACAGGGAGACAGGT
GGTGCATGGTTGTCGTCAGCTCGTGTCGTGAGATGTTGGGTTAAGTCCCGCAACGAGCGCAA
CCCCTACGTTTAGTTGCTAACGGGTGGAGCCGAGCACTCTAGACGAACTGCCGTTGACAAAA
CGGAGGAAGGTGGGGATGACGTCAAATCATCATGCCCCTTATGTCCTGGGCCACACACGTGC
TACAATGGCCGGTACAGAGGGAAGCGAAGCCGTGAGGTGGAGCAAATCCCAAAAAGCCGGT
CTCAGTTCGGATTGCAGGCTGCAACCCGCCTGCATGAAGTCGGAATCGCTAGTAATCGCAGG
TCAGCATACTGCGGTGAATACGTTCCCGGGCCTTGTACACACCGCCCGTCACACCACGAAAG
CTGACAACACCCGAAGCCGGTGACTTAACCGCAAGGAGAGAGCCGTCGAAGGTGGGGTTGG
TGATTGGGGTGAAGTCGTAACAAGGTAGCCGTATCGGAAGGTGCGGCTGGATCACCTCCTTT
CTAA

Database A6 Amino Acid format for hydrogenase sequences used for Figures 12 and A3.

SPBIB_v1_260013|ID:27163327|hndD| FeFe Group A3 hydrogenase catalytic subunit [Uncultured spirochete bib]

MVNVKVNGIPVQVAEGSTVLEAAKKANVKIPTLCYNPDLSPWASCGICVVKIEGSNKMLRSCCTPV
SEGMSIISNDPDLVQTRKTVIELILSTHPDDCLACPRNQACELQTLAQEFGIREQPYKKMVRDIPQD
TSTGSLILNPSKCIRCGRCVEVCQEMQGVWAVEFLGRGESIRIAPAADVKLGDSPCIKCGQCSAHC
PVGAIYENDQTKLVWDALMKEGPEAKTCAVQIAPAVRVALAESFGLPPGTDLTGKIYTALRRLGFD
AVFDTNFSADLTIMEEGTEFVHRLTGALKAGMQQATADKSMPLITSCCPAWVDYMEKYYPDMIPN
FSTAKSPQQMMGAMIKTYWAAKAKVDPAKIYSVSIMPCTAKKFENSRDESMYSSGYKDVDVTLTT
RELARMIKQAGIDFLNLPESEPDSPLGPYSGAGVIFGATGGVMEAALRTAYFLVTKEELKDVNFTA
VRGLSGIKEATVHINGIELRVAAAHQMGNIATVLDQVRKAREEGRETPWHFIEVMACRGGCIGGG
GQPYGATDEVRKLRMRGIYDNDEKQEYRCSHDNPYIKQIYAEFLQKPASHKAHELLHTQYKERPL
YLK*

SPBIB_v1_20025|ID:27161852|hndD| FeFe Group A1 hydrogenase catalytic subunit [Uncultured spirochete bib]

MEEQLIEITIDGQNVRVDPSANIVEACAHAGVKIPTLCYLKGISQNASCGVCVVEVEGAKSLVRSCV
QKPVPGMKIRTSSPRVIRARKTAVELLLANHPDDCLSCIRSDTCELHTIANILEVRADRFPGYKKYP
MPDTTSEGIVRDDSKCILCGRCVAVCEETQGVHAIAFSGRGARTRVSTFLDRGLAQSACVQCGQC
SVVCPTGAITEKDESREVFSAIEDPRLTVVVQTAPAIRASLGEALGLPAGSLVTGQMVAALRRLGFN
RVFDTQFTADLTIMEEGSELLERLSKGGTLPMITSCSPGWINFIEGFYPDLLSHLSTCKSPQQMFGS
VAKTYYAKKAGLTPDHMRVVSIMPCTAKKYEARRKEMDGAWGWWKEQDPGKVPARPFFDVDW
ALTTRELARMIKLAGIDISRLPEEEFDDPLGQSTGAGTIFGTTGGVMEAALRTVYELVEKKPLENIEF
TKVRGFEAIKTAEVVVGGSPVRVAVAHGLANARVLLDEIRAGKSPYHFIEIMSCPGGCVGGGGQP
VLADLEKKLARSQALYEEDRKLAIRKSHENPAVRALYQEFLGKPLGHLSHELLHTSYKARVF*

SPBIB_v1_210130|ID:27163022|hndD| FeFe Group A3 hydrogenase catalytic subunit [Uncultured spirochete bib]

MKNVTLTINGKKISVPEHTTVFSAAEKAGISIPALCRHEDLEPKGACGMCIVKIEGQPGYKRSCVTA
VEEGMEVLTSTAEIRDIRRGILELVLAAHPADCLQCIKHGKCELQTLAERFEIRDLRYDRYTRGLPV
DRSSFGIVRDMNKCIGCGRCVQVCNEVQTVASIFFHGRGSNTIVSPAYGTTMGDSVCVNCGQCIV
YCPVGALYEKEAIEEVWKAIDDPDKVVVAQIAPAVRVAIGEEFGLEPGELSIGKLYSALKALGIDVVF
DTNFSADLTIVEEATEFLERLKESGPFPLITSCSPGWIKFGETFYPELLENVSSCKSPQQMLGALIKT
HYAESRGLDRNNIVSLSIMPCTAKKFEAGRPEMRSSGARDVDYVLTTREIARMIRQVGIDFRNLPD
GTPDPLLSRYSGAATIFGASGGVMEAALRTAYELATGKALEKVDFVDVRGMTGVKEAEIDVDGTPI
KVAVTNGLANARKILDRVAEDKRRGRSSYHFIEIMACAGGCVGGGGQPIPNTLARRARRIEGLYRE
DRSLPLRKSHENPEIRALYAEFLGSPGSEKAHALLHTKYSPREQYQFSE*

SPBIB_v1_290056|ID:27163581| FeFe Group B hydrogenase catalytic subunit [Uncultured spirochete bib]

VPEVFERMRGLYTPCTDIRRKIFVGVTRFVLAGKKPEDIDYLPFDIIDMGKPTYRCCSYRELSIVKQR
IRLAFGLPLIEERDNTPVSAGIGEAFTDRKVISAPLVNVIRAACEKCPEDKVIVTDMCQSCMAHPCSI
VCPVNAISFPNGGKAFIDQKKCVKCMKCVKACPYQSITRMVRPCAAACGVDAIHSDPDGYATIDQ
DKCVNCGLCTVSCPFAAISDKTELVQILHQLMGPEDRRPYAILAPSFVGQFGRLASPGAIVAGLRA
VGFRGVREVALGADCDTLLLAKRLAEKSSPDNPQHKTFLGTSCCPSWVKTARRHFPEFADNIAES
FTPMVETAKIIKDQDPSARVVFIGPCIAKKAEALEPEMQPYVDHVLTFEELAAIFVAKDIDLAEITPVE
FPDEASALGRGYAVAGGVATAIAETARQKYGKENIAVARADTLRNCRAMLADIKSGKTSPELVEG
MACPGGCVGGPGTLIGLLSARNEVGKFAGLAPKNPATLTK*

SPBIB_v1_360012|ID:27164068| FeFe Group C3 hydrogenase catalytic subunit [Uncultured spirochete bib]

MNRQVIYTETMRCQDCYKCVRECPVKAIQILDGHARVVEDICILCGHCVMVCPQSAKKVRSDVER
VRRLLELKPVAVASLAPSFAAEFSGCTAGQLIASIRKLGFAAVSETALGADLVSSAMRNELGQLAD
NGRNFLIGAACPAVVRYVSFYRPDLVPFLSENGSPMIAHARYLRSRFGENALVVFIGPCIAKKKEAD
ESGGLVNAVLTFAELRQLFEEENIDPSAEKPTSNDTFFPQRPSKGELYPIEGGMIASIKQHGSTDVP
CMSFSGMGHIQAALRDLPDGIPETGIFLELLACEGGCINGPCSDASRGTVSKRMQILLYEKQGESE
PFNTEIACQVKHSAAKPVQRQVREEEIRAALALVGKKEPSDELNCSGCGYDSCREFAKAIVIGHAE
PTMCLSYMRNLAQKKANALLRAMPSAAVVVNADLKVIECNEPFVRILEKDAQFVAEAKPTLEGADL
RKLLPFWERFNDVLHHSPGDAFIESDFRCGERILHGTIFSIEKQMIAGGLFQDITAPWIQKDRVIKEA
KKVIRQNVRTVQKIAYLLGENAAESEAALRSIIESFGGEVGQ*

SPBIB_v1_280015|ID:27163481| FeFe Group C1 hydrogenase catalytic subunit [Uncultured spirochete bib]

VNNKTLQNQENNIRTFHSVQLDADLCVGCTTCIKFCPTKAIRVRDGKAKIFEDRCIDCGECIRRCPK
GAKKAISDPLFILDGYDLKVALPAPSLYAQFGTRYSQSDIFAALHHMGFDEVFDVAWGAIVATEITR
SILAKPGPAPRISSACPVIVRLIQQRFPSLIPNLMPILPPSEIAAREARKRLSEISRKIGIFFLSPCTAKV
TAVRMPLGYSQSSIDAVISFSDIFLPLKRALEERKPLSPKKGFKSSVPQASSGHSPILPMMDNLEPG
MGWARSDGELDALRIPDSVSVDGISNVIDLFEAIENGNIESIQYIEALACPGGCVGGPMAVENPHIA
RSNMRQRCQKDNLAAEASSSPMKAIKPPSPKLPEQEELPSYIWTEQVSPKPVLVLDADLSKALEM
AEKIDTIHAQLPGIDCGACGAPDCDCLAEDIVRGFASIEDCRLLEHPYSKGTKENIHSEGLST*

SPBIB_v1_360015|ID:27164071| FeFe Group B hydrogenase catalytic subunit [Uncultured spirochete bib]

MPREDNTTRIRRELLVRLGRLALEGTLADSIDDVPFDMTAEGWETMRCCVHHDRAILRLRSYALLG
GDVRGMDDVRKPLSVLAEGFQNSRCQDGAELGESGRFPLQVLGEACNACAKSRYVVTDACQAC
VARPCKVNCPKGAVTVNGRSHIDPDKCVNCGLCEKSCPFHAIVKVPVPCEEVCPTGAISKGEDGIA
RIDEAKCILCGKCLRACPFGAPIEQTQYLEAASWLREQARPLIALVAPATMAQFPVSSGKFMAGLY
RLGFAAVAEVAEAACATAEREAAELRERMHRSEGFLATSCCPSWVLASKALGDVAGHVLHTPSP
MAIAAKWARKRYPEARIVFIGPCLAKRAEARGFPGEDGRKLVDAVLSAEEIGALFTAKDIQLQALEE
ARAVQLAEQGSSLDLCYGRGFAQSGGVAASVQSVLENENSRIEVGSSWTIRTLVIQGLSKQVLAL
AALWNKQAPDADLVEVMACEGGCIGGPLAIAQAKSAAVFLQRYMSEPPPEAKVASSSEAVEKAV*

SPBDM4_v1_80097|ID:27159873| FeFe Group A1 hydrogenase catalytic subunit (fragment) [Uncultured spirochete bdmA 4]

VCEETQGVNAIAFTGRGARTRVATFMDRGLAQSACVQCGQCSVVCPTGAITEKDESRDVFDALR
DSKLSVVVQTAPAIRASLGEALGLPAGSLVTGQMVAALRRLGFAKVFDTQFTADLTIMEEGSELLE
RLSHGGTTPMITSCSPGWINFIEGFYPDLLGHVSTCKSPQQMFGAVAKTYYAQAAGIAPDKMRVV
SIMPCTAKKYEARRKEMDGAWGWWKEQDPGKVPARPFFDVDWALTTRELARMIKLAGIEIGHLP
EEDFDDPLGRSTGAATIFGTTGGVMEAALRTVYEIVEKKPLENIEFTQVRGFESIKSAEVVLGGSPV
RVAVAHGLSNARILLDEIRAGKSPYQFIEIMSCPGGCIGGGGQPVLADIEKKLARSKALYTEDRILPI
RKSHENPAVNTLYKDFLGKPLGHLSHELLHTSYRARVF*

SPBDM4_v1_40494|ID:27157799| FeFe Group A3 hydrogenase catalytic subunit [Uncultured spirochete bdmA 4]

MVNVKVNGIPVQVAEGSTMLEAAKKAHVKIPTLCYNPDLSPWAACGICVVKVEGSNKMLRSCCTP
VSEGMSIITNDADLVQTRRTVIELILSTHPDDCLFCPRNQSCELQTLAQEFGIREQPYKKMVRDIPT
DTSTNSLILNPSKCIRCGRCVEVCQEMQGVWAIEFLGRGESIRIAPAADVKLGDSPCIKCGQCSAH
CPVGAIYENDQTSLVWDALMKEGPDAKICAVQIAPAVRVALAESFGLPPGTDLTGKIYTALRRLGF
DAVFDTNFSADLTIMEEGTELVHRLTEALKGGMQQATADHKLPLITSCCPAWVDYMEKYYSDMIP
NFSTAKSPQQMMGVMIKTYWAAKAKVDPAKIYSVSIMPCTAKKFENGRDESMYSSGYKDVDVTLT
TRELARMIKQAGIDFLNLPDSQPDSPLGPYSGAGVIFGATGGVMEAALRTAYFLVTKEELKDVNFT

AVRGLSGIKEATVHINGIELRVAAAHQMGNIATVLEEVRKARAEGRETPWHFIEVMACRGGCIGGG
GQPYGATDEVRKLRMRSIYDHDEKSEYRCSHDNPYIKQIYAEFLEKPGSHRSHELLHTHYVEKPLY
LK*

SPBDM4_v1_40759|ID:27158064| FeFe Group C1 hydrogenase catalytic subunit [Uncultured spirochete bdmA 4]

VSFEPANQSPNIFQTFHSVLLDADLCVGCTTCIKFCPTKAIRVRNGKAKIFEDRCIDCGECIRRCPK
GAKKAVSDPLFMMDAYDIKVALPAPSLYAQFGTKYSQSDIFNAIHSAGFDEVFDVAWGALVVTTMT
RSILAQEALRPRISSACPVIVRLIQQRFPSLIPNLMPILPPSEIAAREARRRLGSLSQKVGIFFLSPCTA
KVTSVRTPLGYEQSAIDAVFSFGDIYASLKRALDPTPSSAPHIDAISSGNASTHHLLPIMNNLEPGM
GWARSDGELDALHIENAVSVDGISNVIELFEAIENGNIDSIQYIEALACPGGCVGGPMAVENPHIAR
STMRQRYQHPFSAYPGSKTAQDHHRTAKERSKSLSPESSTADKEYLAFKWTRPLPPNPVLVLDT
DLSKALQMAEKIEQIRNRLPGIDCGACGAPDCDAFAEDIVRGLSSIEDCRLLASPPPARNEEENPK*

JGI12104J13512_100111416 FeFe Group A3 hydrogenase catalytic subunit [Uncultured spirochete SA-8]

MINCKVNGIPVQVAEGATILEASKKANVKIPTLCYNPDLAPWAACGICVAKIEGSNKMLRACCTPVA
EGMNIITHDPDIVETRKTVIEMILSTHPDDCLACPRNQNCELQTLAQEFGIREQAFPKMLHDLPIDDT
TGSIVLNPEKCVRCGRCVTVCQQMQNVWAIEFLGRGETIRIAPAADAKLGESPCIKCGQCSAHCP
VGAIYENDQTKIVWDALRKTGDDAKTCVVQIAPAVRVALGEAFGLQPGTDLTGKIYTALKRLGFDV
VFDTNFAADLTIMEEGTEFVKRLTSALQNGLGTATREKSMPLITSCCPAWVDYMEKYFPDMIPNFS
TAKSPQQMMGAMIKTYWAEKANVRPDKIFSVSIMPCTAKKFETHRDETMCSSGYQDVDVSITTRE
LARMIKQAGIDLLNLPESEPDSPLGPYTGAGAIFGATGGVMEAALRTAYYLVTGNELKDVNFTAVR
GISGIKEASVHVNGVVLRVAVAHQMGNIEQVLNEVRKARDEGRDTPWHFIEVMACRGGCIGGGG
QPYGATDEVRKLRIRGIYDHDEGKEYRCSHQNPYIKKVYNEFLEKPGSHKAHELLHTHYTERPLFL
K*

JGI12104J13512_10045282 FeFe Group B hydrogenase catalytic subunit [Uncultured spirochete SA-8]

MAKENNAVRLKRRLICEVTSLVLEGKLADEIDSIPYAMTNENWETIQCCIHHDRANLRLRLMSLLGY
STEGMLDVDKPLRTYAQEALSGKKPDAFPLSLMSAACNGCTKSRYIVTNVCQGCLARPCKVNCPK
GAVSIINNQSHIDPELCVNCGLCEKSCPFHAIIKIPVPCEEVCPVGAIQKGEDGIAKIDESKCILCGKC
LSACPFGAPVEKSEIVHVLSALIHGKKLIAMVAPAAMVQFPFPPGKFIAALEHFGFSKVMEVAEAAD
RVAEAEAREFAERLHENNKVLATSCCPSWVRAAGSMGLEQILSDTPSPMLVAAKTAKAQDPDAFT
VFIGPCLAKRWEAHRASQNSPLVYAVLTSEEVGAMLMAAGIQVNEENEEDLATAGNASVYGRGFA
ATQGVTAAVKHALSPSAVEVNSCIVSGITKDTASQLKKVQESDKPLLIEVMACDGGCINGPCQLTN
PKVAGAFLERYKAAAEHTTALKSA*

JGI12104J13512_10009791 FeFe Group C1 hydrogenase catalytic subunit [Uncultured spirochete SA-8]

AAREAKKLVADLDPSLRVGMFFISPCTAKVTAIRMPLGYERSLVDAVFSFQDIFPALKKALSRPSET
PSRFAPLQERIARMRRGHGMDWARSDGEIDGLGIEQAVSVDGIQNVIALLEEIDNGKFSSVPYIEAL
ACPGGCVGGPMAVANPHVARAAMKHIAAAEKTAAAQSGQSEQPAQAGFGWERELQPKPVFVLD
RDMLKALQLAEQMELITSQLPGLDCGACGSPDCRALAEDIVKGKAVIEDCLVMMRKKTAFNLTNE*

JGI12104J13512_10045285 FeFe Group C3 hydrogenase catalytic subunit [Uncultured spirochete SA-8]

MDSAQVIYTELTECQDCYKCLRECPVKAIQIVRGHARVLEDRCIHCGNCVEICPQKAKKVRSDLER
AKILIRLRQKTVLSLAPSFIAEFSGIPMQKLIAGCKKLGFSHVSETSVGADAVSESVSKTIAEQQPPL
MLSSACPAVVQYVDKYLPEMSGFISTACSPMVAHARIIKQTLGPGTAVVFAGPCIAKKREADASEG
AVDVALTFQELRQWFCEEGIDPEDAAVRDEDSFFLNQAQDGILYPIEGGMVASIKHLKHSDAHCMT
YSGIHQIREAVRGIVDQYLENENNPGNQKTLFLEMLACEGGCVNGPMVQQSGGTVAKRLRVLSEK

EKRTERGRVLSEPVSVQDIAADLTMPQSIRQKPVAAVAVSEEDIKASLASIGKYSRKDELNCSGCG
YDSCQAFAAAMFLGKAEKTMCLSYTRKLAQKKANALLKAMPSAAVVVDASMHIVECNKPFAELLG
TDVMELYALKPSLEGADLRKLLPFWEAFEQVLMPESQDIVASDFQCNGKIVHGSVFSIEKGLLAGG
LFQDITAPWIQKDRVISQARKVMSQNLRTVQKIAYLLGENAAEAEAALTSIIESFQSERSGDSYKSN
KE*

DESUN47_v1_100151|ID:27211809| NiFe Group 1a hydrogenase catalytic subunit (fragment) [Uncultured Desulfobacterium sp N47]

MKVNLGPVTRIEGHLNIETTVENNKIVDARCMGEMFRGFEVFLQGRSPLDAQQITQRICGVCPYAH
AVASSYAQESVYKLNVPPNGRIMHNLIQGANHLYDYLLQFYQLAALDFVDITAILKYKG*

DESUN47_v1_100152|ID:27211810| NiFe Group 1b hydrogenase large subunit [Uncultured Desulfobacterium sp N47]

MAKRITIDPITRIEGHLRIEVEVADGKVVNAWSSGQMFRGIEMILKGRDPRDAPLFTQRSCGVCTYV
HYLASVRAIEAAVGVQIPENARILRNLLHGTQYQHDHIIHFYHLHALDWVDILSALKADPQKTAGLAE
NVCQARWGGTAYFKQVQDRIKTFVESGQLGPFNNAYWGHPAYVLSPEANLMAVSHYLEALRLQA
KAAQMHAVFGAKNPHLQSLVVGGVTCAMDLTPDRIAEFLYLWKETQTFVKNVYLPDVLAIGSFYK
DWGALGGTSNFLAWGDFPEGEREPDSLFMPRGLIMNRDISTVKQAEQDKITEHVAHSWYVGNAD
LHPFQGQTNPQHGDYNPDDRYSWIKAPRYEGEPCEVGPLARMLVAYGSGKSTARKLVDDTLTQL
SIPVTALFSTLGRTAARALETVLVGDAMEGWIMKLVENLKSGQDNTYQTWTMPDKAIGCGLNDVP
RGSLGHWIEIEDKKIKNYQYVVPSTWNLGPRCSNGKLGPVEQALIGTPVADPKRPLEVLRTVHSFD
PCIACAVHMIDPRSNEVYRIQVL*